Development of an Automated Mapping Technique for Monitoring and Managing Shellfish Distributions

A Final Report Submitted to:
The NOAA/UNH Cooperative Institute for Coastal and Estuarine Environmental Technology (CICEET)

Submitted by:

Dr. Steven R. Schill[*]
Dr. Dwayne E. Porter[+<]
Dr. Loren D. Coen[^]
Dr. Dave Bushek[#]
Jeffrey Vincent[+]

[*]**Mesoamerica & Caribbean Regional Science Team**
The Nature Conservancy

[+]**Baruch Institute for Marine and Coastal Sciences**
and the
[<]**Arnold School of Public Health**
University of South Carolina
Columbia, South Carolina, 29208

[^]**Marine Resources Research Institute**
South Carolina Department of Natural Resources
Charleston, SC 29412

[#]**Haskin Shellfish Research Lab**
Rutgers University

Port Norris, NJ 08349

February 24th, 2006

This project was funded by a grant from the NOAA/UNH Cooperative Institute for Coastal and Estuarine Environmental Technology, NOAA Grant Number NA17OZ2507

Abstract

There is a tremendous need to develop more accurate, large-scale, efficient, and timely methods for mapping intertidal shellfish resources and adjacent fringing marsh areas as urban pressures are continue to exert pressures on estuarine habitat. A majority of all baseline shellfish bed maps are currently produced through ground surveys and manual aerial photograph interpretation, a tedious process which is time-consuming and prone to human inconsistencies. The first objective of this research was to investigate and document the spatio-temporal variability of shellfish spectral properties by collecting and compiling monthly *in situ* spectral samples of oyster strata over the course of a year. The development of an oyster spectral library using consistent *in situ* spectroradiometer sampling over the course of 12 months is a significant contribution to the shellfish management community. These data are being used for identifying the optimal spectral and spatial characteristics that are required to map the distribution and condition of intertidal shellfish resources. The second objective was to assimilate the findings of the oyster spectral library in order to test and evaluate several new digital image processing methods that exploit the information in various remotely sensed data (e.g. hyperspectral imagery, high spatial resolution imagery, and Light Detection and Ranging (LiDAR).

As demonstrated in this research, scientists can use the spectral variation in hyperspectral imagery using Mixture Tuned Matched Filtering (MTMF) techniques, Automated Feature Extraction methods, and LiDAR, to perform a more automated, accurate, efficient and reliable method for mapping shellfish resources. Results suggest that the Automated Feature Extraction in conjunction with high spatial resolution imagery provided the highest accuracy and lowest time and cost expenditures as compared to spectral mixture analysis. The utility of a spectral library was shown to have mixed results. A high degree of spectral variability was found within the oyster habitat. Statistical analysis of the *in situ* data did show that the spectral profiles of triplicates varied with habitat complexity. Washed shells did not vary statistically as significantly as live healthy, vertically standing oysters.

LiDAR elevation data provided very little in the way of classification of oyster strata or health through the use of surface roughness, but the intensity returns provided a preliminary methodology for classifying oyster strata and mud surfaces based upon the last laser pulse returns. With projected exponential urban growth along our coastal waters, it is hoped that the mapping techniques developed throughout the course of this research will provide shellfish resource managers with up-to-date information on the condition of existing oyster reefs, compare changes from past surveys, and assimilate the data with other estuarine resource data to predict and manage using restorative science. The achievement of such mapping techniques will provide a more cost-effective (eventually), timely, and repeatable method for creating accurate baseline maps that are less subjective and will benefit the coastal community at national and international levels.

Keywords: Remote sensing, Shellfish mapping, Resource management, Mixture Tuned Matched Filtering (MTMF), Automated Feature Extraction, Classification and Regression Tree Analysis, Hyperspectral, LiDAR

Table of Contents

1. Introduction

Estuaries and their component habitats are recognized as some of the most productive and important ecosystems with component habitats, providing critical feeding, spawning, and nursery areas for species that include commercially and ecologically important finfish, shellfish, and waterfowl, to name a few. Many organisms found in estuaries are dependent on one or more specific habitat types (*e.g.,* mud flats, salt marshes, oyster reefs) that are increasingly threatened as a result of coastal population expansion and associated industrial, residential, and recreational development/utilization. Mollusks can have significant impacts on population, community and landscape level processes, due in large part to their ability to filter large quantities of water (e.g., Newell 2004, Grizzle et al. in prep.) and their ability to generate primary structure. For oysters and other species that perform these functions, they have been termed "ecosystem engineers" (e.g., see Jones et al. 1994, 1997, Coen et al. 1999b, Coen and Luckenbach). Data suggest that development expansion in coastal areas is already negatively impacting critical estuarine shellfish habitat (see Vernberg et al., 1992, 1999). This problem is manifesting itself in the form of increasing shellfish bed harvesting closures, declines in marsh habitat, runoff from impervious services and impaired functioning due to declining water quality conditions caused by increasing urban/suburban pressures (e.g., Daugomah 2000, Mallin et al. 2000, Holland et al. 2004, Mallin and Lewitus 2004, Mallin et al. 2004).

Estuaries in the southeastern U.S. are often dissected by shallow, expansive intertidal areas dominated by shallow tidal creeks fringed by salt marsh, with tides from 1-3 m (e.g., Kneib 1997, Dame et al. 2000, Holland et al. 2004). In recent years, intertidal estuarine habitats have largely been mapped through the use of remote sensing and related GIS datasets (Cracknell 1999). Current intertidal shellfish bed baseline maps were largely produced through the tedious process of ground surveys and manual aerial photograph interpretation, which is time-consuming and prone to human inconsistencies (DNR pub). With a projected 60% increase within the coastal zone by 2010, it is imperative that new methods be developed which employ a more automated approach and are easily transferred in a consistent manner across local, regional and national levels. New techniques are required to better understand and map the factors that enhance the persistence of oyster reefs. The development of such techniques will improve our restoration efforts on both a local, regional and national spatial scale. Rapid and cost effective methods for measuring and assessing shellfish status and change using successive surveys will allow resource managers to cover large areas in a rapid timeframe. These novel approaches will permit coastal managers to focus restoration and enhancement efforts in a more cost-effective manner.

1.1 Mapping the Eastern Oyster

The eastern oyster, *Crassostrea virginica,* forms extensive subtidal and intertidal reefs that are a dominant feature of many Atlantic and Gulf coast estuaries (e.g., Burrell 1986, 1997, Stanley and Sellers 1986). Besides the economic reasons for developing more efficient oyster reef mapping and management methods, these reefs provide numerous critical ecosystem functions (e.g., Coen et al. 1999b, Coen and Luckenbach 2000). In South Carolina estuaries, intertidal oyster reefs are often the only "live bottom" and appear to perform similar functions for fish as sea grasses do elsewhere, providing

refuge and nursery habitat for adult and juvenile fishes, shrimp and crabs (Coen and Luckenbach 1999a,b, Williams and Heck 2001, Luckenbach et al. 2005, Coen and Grizzle 2006; reviewed in Coen et al. 1999a,b). Previous Sea Grant-funded work has documented the presence of over 130 species, often reaching densities over 150/m^2 (see Coen et al. 2006, Walters and Coen 2005, Coen et al. in review). In the Southeast, where oysters occur primarily in the intertidal zone (Burrell 1986, Coen et al. 1999a, Coen and Walker 2005), oysters can provide a living bulkhead to reduce shoreline erosion and protect *Spartina* saltmarsh (Meyer 1996, 1997; Chose 1999, Coen and Fischer 2002, Coen and Bolton-Warberg 2005). As a part of its normal feeding activities, oysters filter large volumes (up to 50 gallons/ day/oyster) of water, removing both algae that they use as a food resource and suspended particles. Filtering by dense populations of oysters can significantly improve water clarity and remove suspended sediments (e.g., Dame et al. 2001, Nelson et al. 2004, Newell 2004).

There is a tremendous need to develop more accurate and cost-effective large-scale, methods for mapping intertidal habitats such as oysters and adjacent fringing marsh areas. As previously mentioned, these areas are highly threatened by significant development pressures in coastal areas (e.g., Jefferson et al. 1991). Traditional methods using ground-referencing and manual aerial photography interpretation are time consuming and inconsistent. This research was aimed at developing novel, cost-effective, and repeatable methods that take advantage of advanced remote sensing technologies to map and monitor intertidal oysters. Key temporal hyperspectral characteristics of oyster reefs were identified using spectral analysis techniques which are repeatable and less subject to human inconsistencies. The benefits and utility of high resolution LiDAR (Light Detection and Ranging) remotely sensed data for identifying shellfish habitat was also explored. An important benefit of this approach was the ability to combine or relate the distribution of different oyster 'strata' (i.e. oyster densities and reef bed quality) developed by SCDNR to other types of remotely sensed data being developed t for phytoplankton blooms and sediment loads in the water. While a significant contribution of this effort was directed towards the remote sensing and image processing communities, the more significant contribution will be to the shellfish and coastal management communities.

1.2 Past shellfish mapping research

Traditional methods used for mapping shellfish resources have proved problematic and challenging for coastal managers. These methods include time-consuming GPS and manual field surveys such as were used in SC in the 1980s (Jefferson et al. 1991), and the use of aerial photography interpretation (e.g., Grizzle 1990, Grizzle et al. 2002). The problems with these methods include: (a) the occurrence of water and mud between the observer and the resource; (b) the small dimension of the object being mapped; (c) changes in the spectral signature of habitat components with exposure and season (e.g., drying out, rewetting, benthic algal growth and species composition) and; (d) tidal influences such as varying water depth during imaging. Given such constraints and limitations, studies of shellfish structure and complexity have required extensive *in situ* sampling and evaluation through spatial and temporal sampling. Cores, profiles, nets, and sampling trays have been the tools of the researcher to obtain data on settlement patterns, surface roughness, and density (e.g., Commito and

Rusignuolo 2000; Coen and Luckenbach 2000, Luckenbach et al. 2005, Coen et al. 2006). In recent years, there have been several attempts to utilize new remote sensing techniques as an alternative to the expense, time and labor required in past management and research efforts. For example, Grizzle et al. (2002), used aerial photos as a general ground-referencing for to identify highly reflective, light-colored area adjacent to darker-colored live reefs that were used to detect the appearance of dead oyster reefs in historical aerials. Several other remote sensing methods have been employed in subtidal environments with varying degrees of success, including acoustic mapping, side scan sonar, and profiling systems (e.g., Powell et al. 1995, Pinn et al. 1998, Wilson et al. 1999, 2000, Smith et al. 2001, Coen and Grizzle 2006, Grizzle et al. in press). Smith et al. (2001, 2003) successfully employed an acoustic seabed classification system (ASCS) to distinguish between substrate types, with emphasis on oyster shell, in submerged areas of the Chesapeake Bay, TX and LA. The ASCS functions by emitting a sound wave through the water column. Objects on the bottom reflect the sound wave back to the instrument, which records time and intensity to create an image of the area mapped (Kracker, 1999). However, the techniques used in these submerged environments are poorly suited for mapping the intertidal zone of the turbid southeastern US coastal waters (but see http://marine.questertangent.com/qtc/pdf/hobcawreport03.pdf Quester Tangent pdf from workshop we sponsored).

The utility of high-resolution, multi- and hyperspectral imagery for coastal habitat mapping has been explored to some limited extent in other coastal ecosystems. Chauvaud et al. (1998) found that multispectral aerial photography at a resolution of 5 m or greater was effective for mapping and monitoring tropical ecosystems such as coral reefs. Tropical environments have the advantage of nearly transparent water for mapping submerged vegetation and structures. Even earth materials in subtidal locations, water transparency was derived as an endmember fraction as a function of depth for coral reef mapping in the tropics (Peddle, Holden and LeDrew 1995). In the intertidal zone, reefs are typically covered at high tide with cloudy, turbid water in depths ranging from a few centimeters to 2 or 3 meters. This necessitates image capture at low tide when the reefs are exposed. Previous attempts to classify oyster reefs using multispectral imagery have achieved limited success (Schmidt 2000). The primary problem was the misclassification of mud flats as oyster reefs due to the broad spectral bandwidths of the multispectral sensor. Demonstration oyster mapping projects using high-resolution digital frame multispectral imagery are currently underway with scientist from NOAA Coastal Services Center (CSC) and the South Carolina Department of Natural Resources (SCDNR) (CSC 2003). Hyperspectral remote sensing systems can acquire imagery at similar spatial resolution but these sensors offer increased spectral resolution that is necessary to differentiate between mud flats and oyster reefs. There is tremendous mapping potential and the authors recommend further research into applications of hyperspectral remote sensing in other coastal environments, including mangroves and mudflats.

Another promising remote sensing technology that has been recently applied to coastal mapping is LiDAR. When acquired under certain conditions, LiDAR has the ability to distinguish emergent features at spatial resolutions of approximately 10-15 cm. Most LiDAR applications have focused on terrestrial environments, particularly for

topographic mapping and forestry. However, the extreme precision of LiDAR for three-dimensional mapping is well-suited for many environments (Lefsky et al. 2002). Techniques for mapping submerged and intertidal resources vary in levels of accuracy, cost, and applicability. Many of the techniques suited for submerged environments are not useful in intertidal zones. This research is the first to evaluate LiDAR remote sensing of shellfish resources in the intertidal zone.

Shellfish habitats have typically been managed by individual states, each with its own distributional databases and management policies. The most information is available for species such as oysters that have been managed historically as a food resource, but now also as an ecological resource (e.g., Coen and Luckenbach 2000, Coen and Grizzle 2006). South Carolina has extensive information on oyster distributions, ranging from surveys completed in 1890-91 (e.g., Battle 1891) to maps based on recent aerial imagery (e.g., CSC 2003, Coen et al. 2005b, Schulte et al. 2005, Smith et al. 2005). SCDNR completed a statewide intertidal oyster resource assessment funded by SCDHEC, OCRM from 1980 to 1987, with periodic reassessments through the present day (see Jefferson et al. 1991). This intertidal oyster survey measured each oyster population using laser or split image rangefinders to determine a reef's dimensions. A GPS or map reading was taken in the center of each reef, the area digitized and later entered into the SCDNR's shellfish management Geographic Information System (GIS). Ancillary data, including temperature, salinity, shell matrix depth, reef elevation, adjacent water depth, dead vs. live oysters, etc. were collected and are currently utilized for management purposes (Jefferson et al. 1991). Oyster populations were categorized by characteristic spatial dispersions (densities) that allowed an estimate of each reefs' standing stock.

Currently, SCDNR is collaborating with NOAA's Coastal Services Center and several contractors to apply earlier developed methods (CSC 2003) using airborne multi-spectral digital imagery acquired by GeoVantage Inc.'s GeoScanner system. Photo Science (the SCDNR contractor) is deriving results including bed location, extent, and condition of intertidal oyster populations along intertidal areas of the South Carolina coast. Field assessments are being conducted in order to ground-truth these results and assist in development of extraction techniques. Extensive ground-referencing efforts are being conducted at or near MLW $\pm$2.0 h. The teams also collect GPS data as transects of intertidal oyster beds. Oyster density, reef size (or footprint) and location data are collected in the field, along with video. This information is available via the SCDNR's GIS Data Clearinghouse and Internet Map Server.

As summarized in Street et al. (2005), for North Carolina, the state's Shellfish Habitat and Abundance Mapping program began in 1988 with the creation of detailed bottom type maps using standard surveys from the South Carolina border through Core Sound, along the perimeter of Pamlico Sound, and in Croatan/Roanoke sounds (see pp. 203, Map 3.2). This mapping effort continues, delineating all bottom habitats, including shell bottom, with samples then collected of molluscan densities differentiating over 24 different bottom types based on combinations of depth, bottom firmness, vegetation density, and density of surface shells. They define shell habitat (or shell bottom) as >30% of bottom with living or dead shells.

Other states, such as New Hampshire, are mapping and managing shellfish species including oysters, mussels (*Mytilus*), and softshell clams (*Mya arenaria*). Distributional data are available for all three species, although historical information before the 1980s is meager. Ongoing shellfish mapping programs are research-oriented and include Grizzle et al. (in press) use of multibeam sonar, underwater videography, and extractive sampling methods (see Figure 4). Similar efforts have proven useful with other shellfish species (e.g., Goshimam and Fujiwara 1994, Powell et al. 1995, Smith et al. 2001, Carbines and Morrison in press). The utility of recent advances in remote sensing technologies for mapping intertidal and subtidal shellfish populations is just beginning to become apparent in the U.S., although they have been used more extensively in Canada and Europe with Roxanne and Quester-Tangent sonar instrumentation for mapping shellfish (Coen, Bushek and Grizzle 2004 Sea Grant supported Workshop on Remote Sensing of Shellfish, Marc Ouellette Fisheries Canada pers. comm.).

2. Objectives

The purpose of this research was to develop new and innovative shellfish mapping technologies for coastal resource managers to improve shellfish baseline mapping and monitoring methods. The first year objective was to identify the optimal spectral and spatial characteristics for mapping the distribution and condition of intertidal shellfish resources. The development of a shellfish reef spectral library was acquired monthly through extensive *in situ* field sampling over the course of twelve months. This represents a significant contribution to the shellfish management community and will serve future shellfish mapping efforts. The spectral library was used to compare the *in situ* spectral data with spectral data extracted from the imagery. Comparisons between the two spectral data sets were done using statistical methods as well as comparing accuracies of mapping products using remotely sensed techniques. In addition, the monthly library of shellfish reef spectral samples permitted the detection of seasonal changes in the reef habitat in order to determine the best sampling temporal range using remote sensing technology. This knowledge is a significant contribution to resource managers who previously could only guess the optimal season to acquire expensive remotely sensed imagery. Results of the first year objectives were used to determine the optimal spectral and spatial characteristics that are required in order to map the spatial distribution of shellfish and assessing reef condition. The second year objective was used to assess and compare the utility of a wide range of remote sensing and GIS methodologies to determine the most efficient method for mapping shellfish reefs. These methods can be used by resource managers to perform more automated, accurate, efficient and reliable shellfish mapping products. These methods include investigations into the utility of various types of remotely sensed data including hyperspectral imagery, Light Detection and Ranging (LiDAR), and high spatial resolution imagery for more cost efficient mapping solutions.

Identifying and mapping oyster reefs has been a high-priority issue facing shellfish resource managers. There has been a tremendous need to create accurate up-to-date maps of shellfish habitat as significant declines in the commercially important oyster have recently been reported. Oysters not only improve water quality and control eutrophication, they also serve as excellent places for recreational fishing. Current mapping methods using GPS surveys and extensive field surveys are man-power intensive and limit the ability of an agency to maintain and update oyster maps for large regional areas. Using these methods, reefs can only be mapped every 10-15 years, which is not adequate for identifying rapid die-offs, monitoring habitat changes, or directing enhancement/restoration efforts. The mapping of oyster reefs in a GIS environment provides resource managers with a means to assimilate and analyze estuarine resource data in relation to projected or potential environmental impacts (Jefferson, et al. 1991). The development of a new remote sensing / GIS mapping techniques, that exploit the unique spectral features found in oyster reefs, will promote the commercialization of innovative coastal and estuarine management tools and enhance coastal managers' access to up-to-date estuarine environmental data and information. The objectives of this project have been identified and coordinated through active communication with private sector, and academic and government institutions. Results of this project have met several CICEET goals including a) coastal management techniques for mapping oyster reefs that are integrated with leading GIS software; b) methods for developing oyster reef baseline

maps which can be used for future change detection studies; c) resource managers that are trained on the mapping techniques through a sponsored workshop and oral presentations at conferences; d) manuscripts in refereed journals (in progress); and e) sponsored graduate student research. The long-term goal is to provide managers with sufficient information to prevent further ecologically and economically valuable reef losses, and if appropriate, to restore the damaged reefs. This research has met the CICEET goals through a collaborative effort of private, government, and academia entities seeking to establish a timely, cost-effective, and repeatable method of mapping shellfish resources. Developed methodologies from this research have assisted in understanding shellfish spectral response dynamics within the natural environment and in return provide a more scientific-based approach for making critical management decisions.

3.0 Methods

3.1 Introduction

This section details the methods used to extract shellfish from multiple sets of remotely sensed imagery using spectral analysis and automated feature extraction. The remotely sensed data platforms vary in spectral and spatial resolutions, from 4 bands of 0.25 x 0.25m resolution GeoVantage imagery to 126 bands 4.0 x 4.0m resolution HyMAP imagery. The first section describes the study area, including a) locations of the field sample sites that were used for *in situ* spectroradiometer sampling; b) pictorial essay of the sample sites; c) classification of the sample sites using the South Carolina Department of Natural Resource shellfish classification system; d) establishment of *in situ* sampling points; and e) a description of the shellfish sample site data that were collected. Several datasets have been made available on-line as a resource for coastal resource managers. These include a) numerous digital images that were taken at several sample sites to depict the actual sample sites and associated environmental conditions; b) detailed documentation and cataloging of post-processing of the spectral files; c) a digital spectral library of monthly shellfish samples; d) the methods for spectral analysis mapping of the hyperspectral datasets using the developed *in situ* spectral library; and e) all raw data and aggregated spectral data files and associated global position system (GPS) point files in standard GIS compatible format.

3.2 Study Area

The North Inlet-Winyah Bay National Estuarine Research Reserve (NERR) covers about 80 km^2 of barrier islands, low-lying coastal forests, and intertidal salt marsh near Georgetown, South Carolina. It is an estuarine environment that is bordered on the east by the Atlantic Ocean and two rivers on the west-southwest: the Waccamaw and the Great Pee Dee that feed into Winyah Bay which is south of North Inlet. The 2,630 ha primary research area includes high salinity *Spartina alterniflora* marsh and 715 ha of tidal creeks with an average channel depth 3m, and a seasonal temperature range of 3-33° C, (Porter, et al.1996). Land cover composition at mean tide is *Spartina alterniflora* marsh is 73.0%, tidal creeks 20.6%, oyster reefs 1.0%, and exposed mud flats 5.4%, (Porter et al. 1996). There are a total of nine study sites located in two principal areas of North Inlet: Jones Creek/Bob Creek area and No Man Friend's Creek. Figure 3.1 shows an image of North Inlet with an inset image showing the point locations of the sample sites. Figure 3.2 is a pictorial essay of digital images showing the general characteristics of each of the sample sites. Each sample site was located using a Trimble ProXR GPS that was corrected using real-time differential correction and then corrected again in the lab using the Charleston, SC ground receiving station. Each sample site was identified by a four-foot section of PVC pipe that was hammered into the oyster bank and given a unique identification code.

Figure 3.1 - North Inlet Study Area with Sample Site Locations

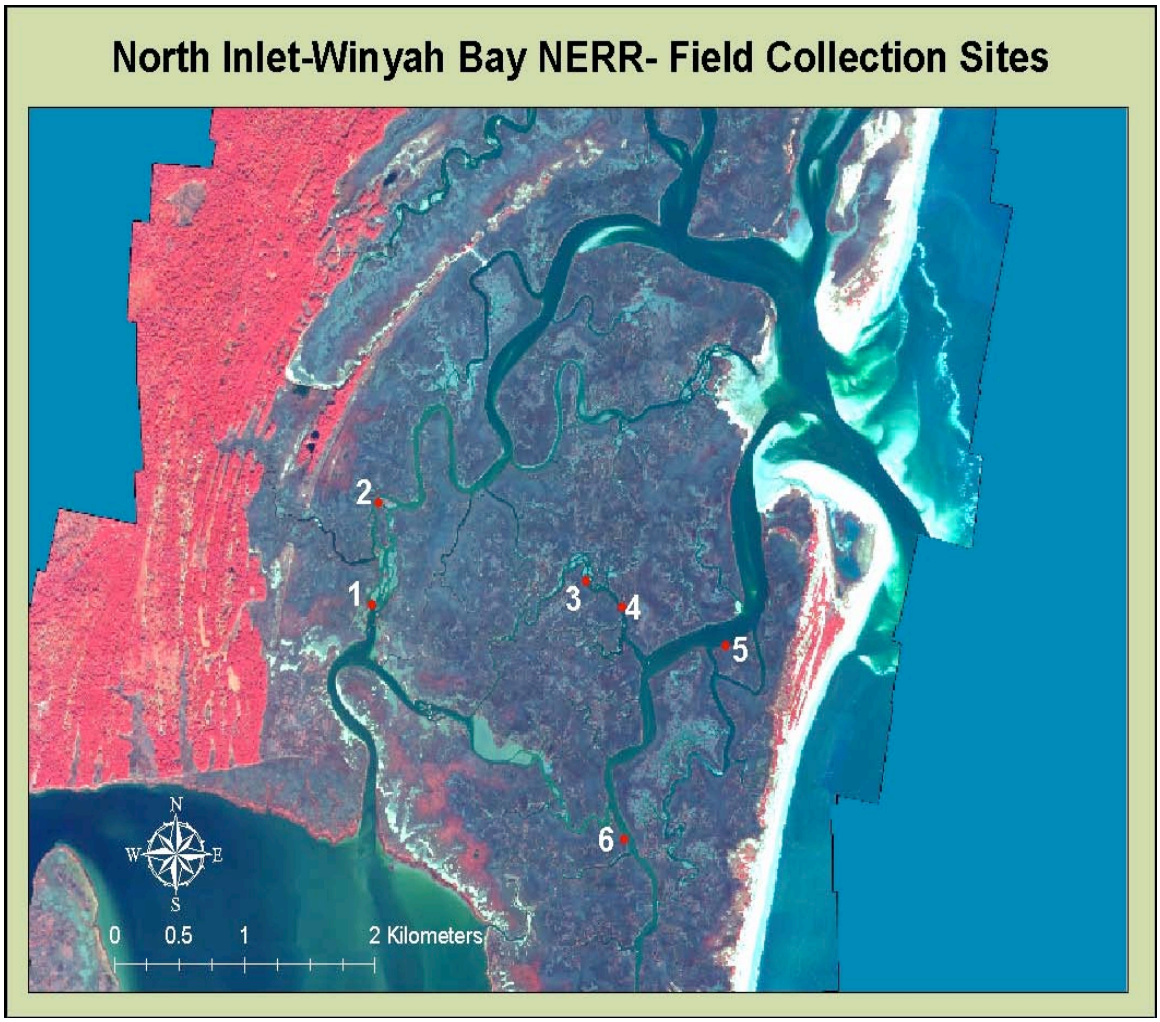

Figure 3.2 – North Inlet, South Carolina Sample *In situ* Sample Sites

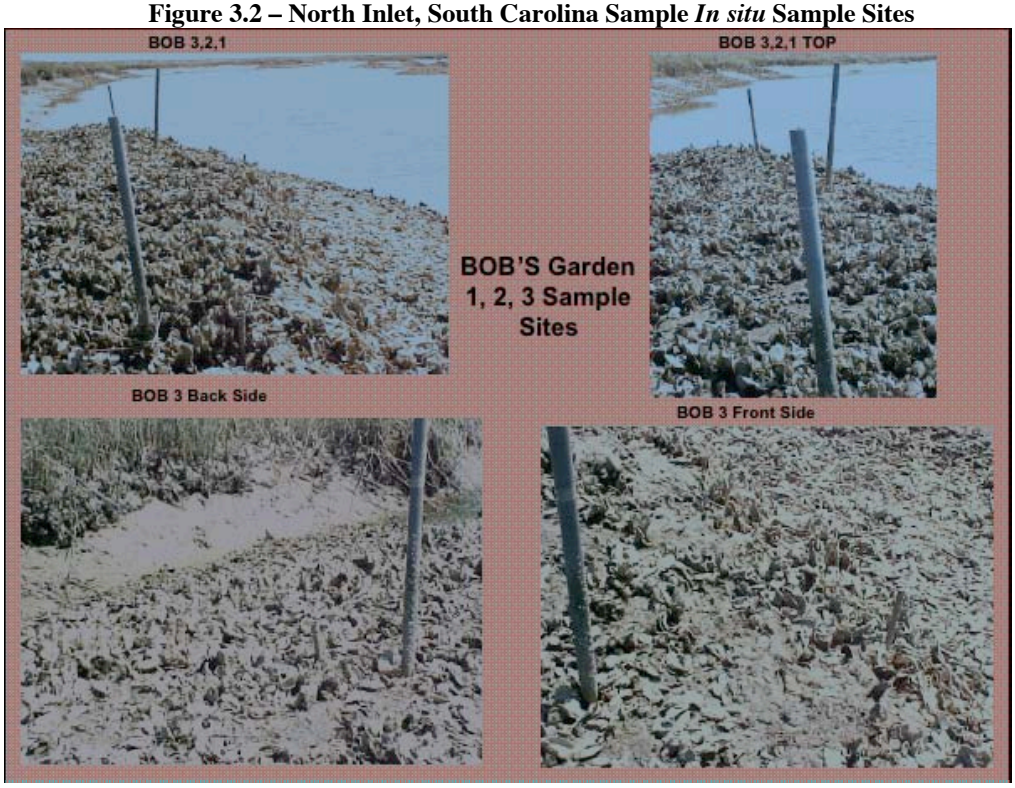

JC 1 – 1 Top Near Spartina

JC2 1 Thru 3

Jones Creek Sample Sites 1 Thru 3

JC3 – 1

Washed Shell

JC3 Looking North

Washed Shell

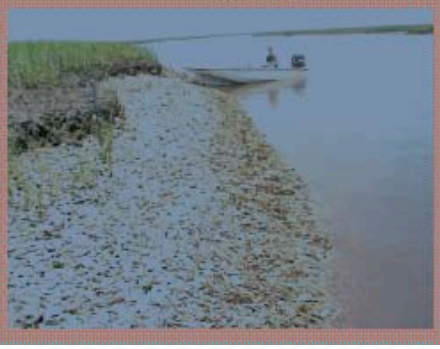

No Man's Friend 1 Sample Site

3.3 *In situ* Spectral Sampling

3.3.1 *In situ* Spectral Signature Collection and Aggregation

The study sites were selected and delineated for the gathering of spectral signatures of shellfish in a wide range of environmental conditions. These conditions include the: abundance of shellfish, positions (vertical and horizontal), and environmental state, (wet/dry, various amount of mud, algae, and detritus present). Site characterization of the oyster reefs were conducted using definitions from the Shellfish Management section of the South Carolina Department of Natural Resource's Intertidal Oyster Survey Field Data Sheet codes. The Oyster Survey describes the reef strata with respect to bushels of live oysters per acre, presence or absence of vertical clusters, proportion of live oysters to shells and amount of mud present. Each of the 10 listed strata or classifications are identified by a letter code. See Appendix 1 for a complete description of the Intertidal Oyster Strata descriptions and their letter designations. Table 3.1 lists the field study sites that were identified by their strata for spectral observations.

Table 3.1 - *In situ* Spectral Sampling Sites

Site	Description	Notes
JC 1	Jones Creek – "F1" Strata	Contains F1 and F strata. Linear feature along bank of creek with *Spartina a*. on top of bank.
JC 2	Jones Creek – "C" Strata	Island feature in creek
JC 3	Jones Creek – Washed Shell	Little to no live shellfish, all horizontal, some with inside of shell face up.
Bob 1	Bob Creek – "G" Strata	Island feature in creek
Bob 2	Bob Creek – "E" Strata	Island feature in creek
Bob 3	Bob Creek – "C" Strata	Island feature in creek
Bob 4	Bob Creek – "D" Strata	Island feature in creek
NMF 1	No Man's Friend Creek – "G" Strata overall	Large island feature with *Spartina A*. on west side of island. Also contains "D", F1", and "B" strata
NMF 2	No Man's Friend Creek – Mud	Control for mud endmember. No vegetation present. Also has enough vertical relief to obtain semidry and wet mud spectroradiometer readings.
60 Bass	60 Bass Creek – "E" like strata	Shellfish with sand filled interstitial spaces, tightly packed and completely covering the substrate.

Each field sampling point was aggregated into like shellfish classes. For each month, the triplicates for each sampling point within each shellfish class were averaged to obtain spectral curves for twenty classes.

Within the nine identified sampling locations, there were clusters of shellfish representative of "relatively" homogenous strata as well as a variety of mixed strata in and around each sampling locations. Transects were demarcated to represent vertical relief of the sampling reef from the waters edge, (below mean low tide) to the top of the oyster bank. No Man's Friend 1, Bob Creek 4, and Jones Creek 3 sample points have GPS point and distance measurement from the reference post to the sample point and demarcated using lengths of small diameter PVC pipe that was placed into the reef. Bob Creek 1 through 3 and Jones Creek 1 and 2, have their sample point distance measured only relative to the reference post. This is due to the relatively short distance to the reference post and a smaller sampling area. Spectroradiometer readings were taken in triplicate at the 3, 6, and 9 o'clock position relative to the sample point. Figure 3.3 shows the locations of the sample points for each of the sample sites which were color coded to indicate which group each sample point belonged to in the secondary level of

aggregation. In post-processing, the triplicates were normalized to apparent reflectance, and then averaged to obtain a single spectral curve for each sample point.

Figure 3.3 - Sample Sites North Inlet, South Carolina

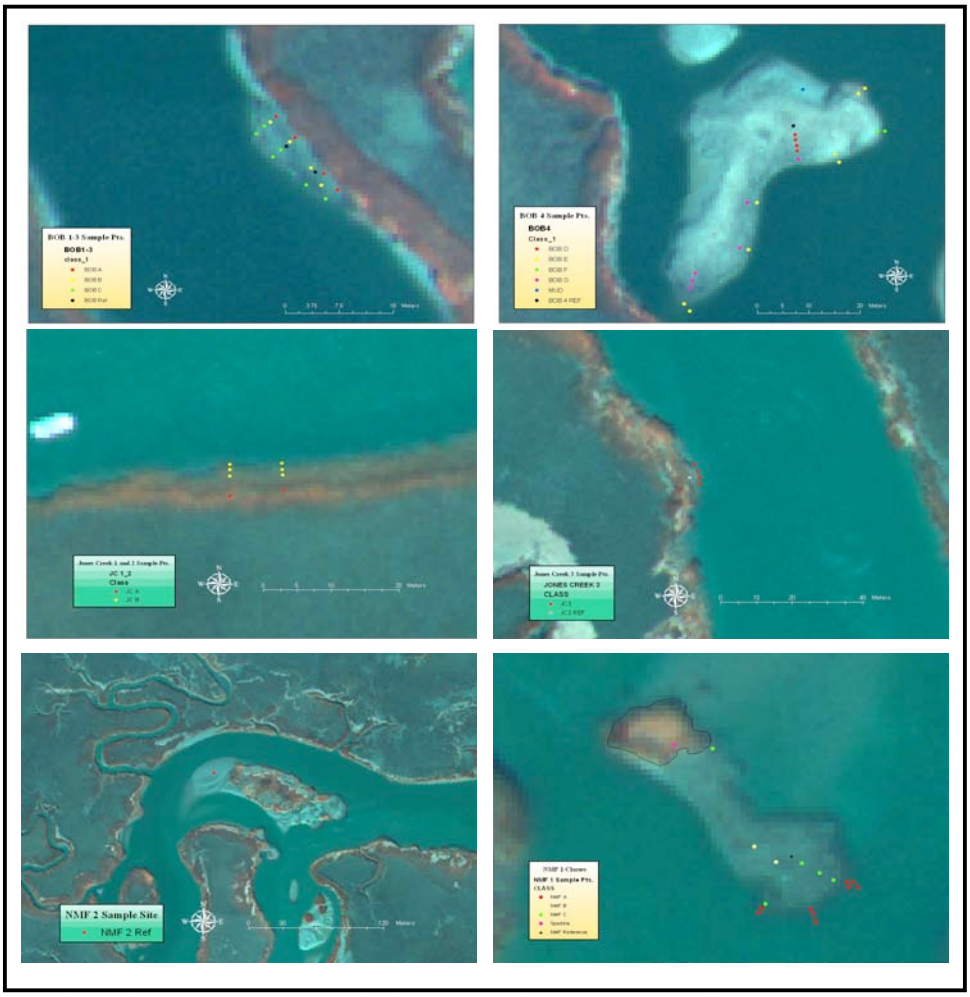

Sampling points or clusters were classified according to South Carolina Department of Natural Resources Field Data codes for Intertidal Oysters. We recognize there are some ambiguities in the DNR classification, but the intent is to use the DNR classification as a means to describe and differentiate between groups of shellfish.

All spectroradiometer measurements were taken using a GER 1500 (Geophysical & Environmental Research Corp (Millbrook, NY)) held at a stable height of ~ 1.5 meters above the sample point, (the height of holding the spectroradiometer at chest high, ~6 ft. tall). This height resulted in an IFOV of 1" x 1".. The spectroradiometer is calibrated from 350 nm to 1050 nm which roughly correlates with the long wave ultraviolet to the near infrared region (Jensen 2000). There are 512 bands with a spectral resolution of 3 nanometers at Full Width Half Maximum. The washed shellfish at the Jones Creek #3 site was sampled in dry and wet conditions. This was to document any changes in the spectral reflectance due to the presence of water. Relative terms were used to describe the wet/dry conditions included; dry (maximum dryness of the tidal cycle), semi-dry

(more dry than wet), semi-wet (more wet than dry), and wet (wet shellfish and pooling of water interstitially). Notes included descriptions of the amount of mud encrusting (heavy/medium/light/none), and any noted detritus, such as seaweed, leaves, grasses, etc. All spectroradiometer readings, descriptions, measurements, and records were documented in a bound field notebook and sample points were digitally photo documented. Endmembers of water, mud, vegetated areas such as *Spartina alterniflora,* and the concrete pad near Clambank Landing were used as controls.

As illustrated in Figure 3.4, monthly spectroradiometer files were organized according to strata and environmental condition (wet or dry). The files were then converted from an Excel spreadsheet format to ASCII text file for importing into Research Systems, Inc. (Boulder, CO) The Environment for Visualizing Images (ENVI) software version 4.1 Spectral Library. All monthly ASCII exported files for each stratum were aggregated into a single folder. At the end of the sampling period, each strata folder contains all spectroradiometer readings converted to reflectance. The spectroradiometer values were then averaged into a single spectral reflectance curve for each stratum. Appendix II contains sampling dates from June 2002 through July of 2003.

Figure 3.4 - Aggregations of Spectral Files

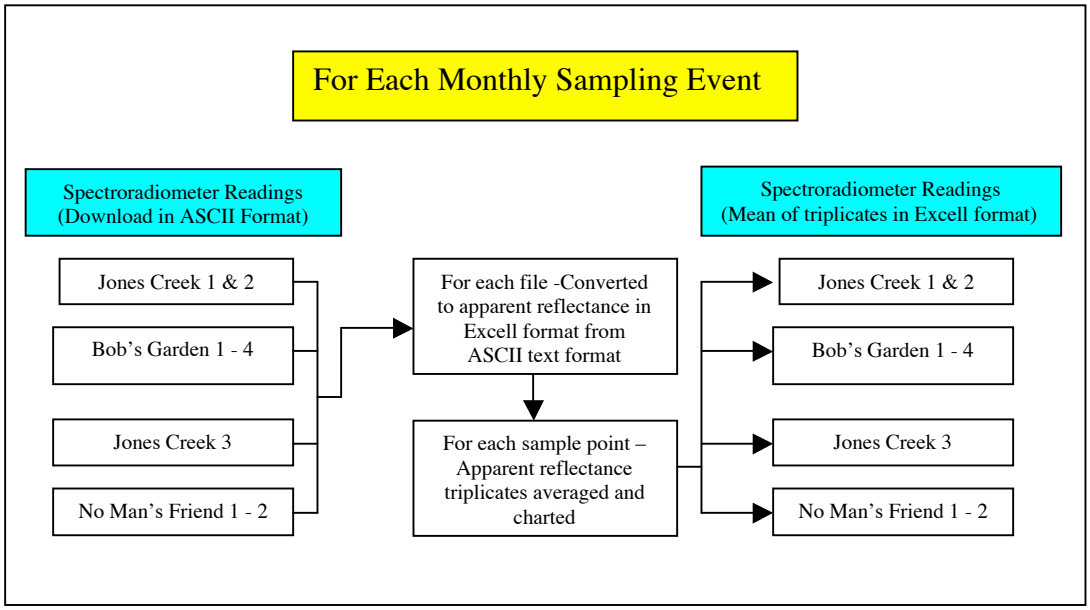

Primary aggregation was the importation of each spectral file into Microsoft Excel, conversion from radiance to reflectance, the averaging of the triplicates for an average signature of a particular sample point, and charting of the individual reflectance and average signatures. The file structure is by month and contains raw data, Excel format radiance and reflectance, and averaged triplicates. Further aggregation was necessary to have each strata represented and reduce the number of individual spectral signatures for mapping.

As shown above in Figure 3.3, the individual sample points were further aggregated by averaging the individual reflectance signatures at monthly intervals. Since each sampling point had a spectral reference signature recorded, it was not possible to

average individual radiance signatures and post-process into reflectance. Appendix 9.1 at the end of this document contains a table explaining which individual sample points were aggregated into secondary groupings.

A description of each sample point, including cluster type and secondary spectral signature aggregation, are listed in Table 9.1 in the Appendix. This table shows BOB A-C, aggregated from BOB 1-3 sample sites; and BOB D-G, aggregated from the BOB 4 sample site. Since these sample points are located within the same geographic proximity, they are differentiated by strata that align with the vertical rise of tide. Another aggregation from the averaged triplicates used all twelve months of spectral signatures by sample site. This is useful in looking at the annual phenological changes that may occur within the sample points. For example, sample point BOB4_12 is characterized by mostly washed bright shell but, in the winter months, there is a preponderance of marco-algae growth that obfuscates the washed shell. Spectral changes can be monitored using the aggregation of the monthly spectral data acquired on the concrete pad at Clambank. Figure 3.5 shows these monthly triplicate averaged spectral signatures. These data were acquired at precisely the same point on the concrete pad and were used as a de-facto control, showing subtle variations in the spectral response due to slight surface variations in the concrete pad.

Figure 3.5 - Concrete Pad Composite at Clambank Site, North Inlet, SC

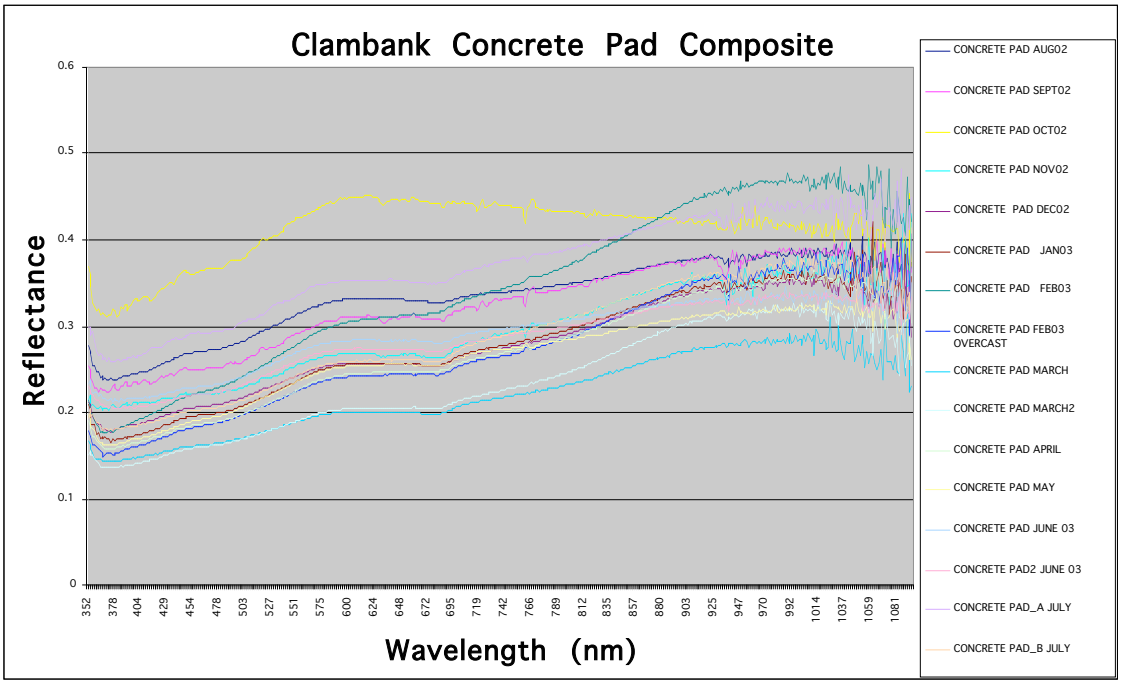

3.3.2 *In situ* Photo Documentation and Spectral Library

With each monthly sampling event, photos were collected at each site to document conditions or anomalies that influence spectral reflection. Changes in spectral characteristics were especially evident in the winter months when the presence of macro-algae growth was most significant. The on-line photo library is organized by month with an alternative index that places each photo with a specific sample point or description. .

Metadata for the spectral library has been organized in an intuitive order to view or download monthly spectral signatures as Excel files. Each monthly file contains the individual and the averaged triplicates in reflectance. At the root directory, there is a spectral folder that contains two files. The first file contains the Site Conditions file that describes the conditions of each sample site as being Wet U (submerged), Wet, Semi-Wet, Semi-Dry, or Dry. The second readme file contains the spectral metadata in XML file format. Currently, the web portal is in a "flat file" configuration allowing a user to download and view digital images, Excel formatted spectral files, raw spectral files, metadata, and the data catalogs. The data is housed at the following URL: http://carocoops.org/ciceet . Figure 3.6 graphically represents the schematic for web portal data delivery.

Figure 3.6 - Meta Data Schematic for Data Query, Retrieval, and Delivery

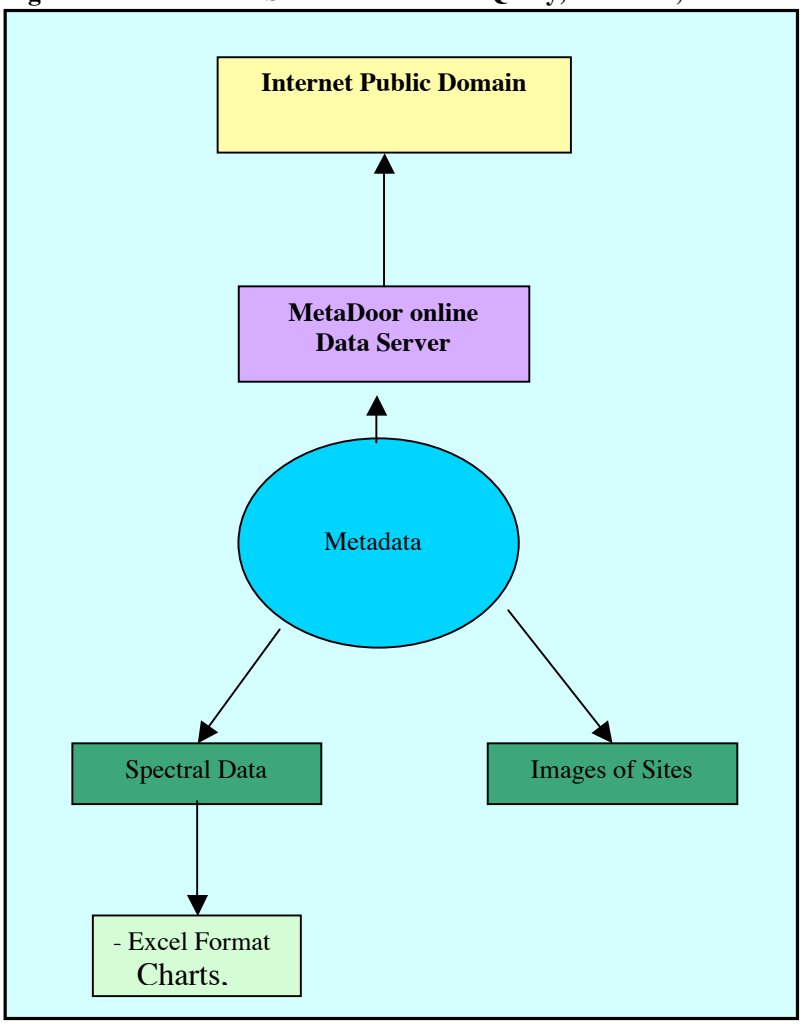

3.3.3 Statistical Analysis

The statistical analysis of the spectral signatures from the year-long *in situ* sampling resulted in the creation of a spectral library and spectral image endmembers that were derived from the HyMAP hyperspectral imagery. The HyMAP data were the

imagery of choice for statistical analysis owing to the greater number of contiguous bands (126 bands from ~450- 2400 nm) and narrower band widths than the AISA (7 bands from 498 nm – 819 nm). The pixels that were analyzed corresponded with areas where the *in situ* spectral signatures were collected. Selected spectral signatures contained in the pixels were analyzed both individually and averaged in order to represent the aggregated spectral and spatial characteristics of the *in situ* endmembers.

The statistical analysis addressed three primary questions:

1. With regard to *in situ* sample points, such as BOB4_1, there were three spectral readings taken at slightly different points around the sample point. If the earth material (shellfish) present within the sample points are considered to be of similar shellfish strata, how similar or statistically different are the three spectral readings? Does the type of oyster strata or material such as mud or the concrete pad make a statistical difference in the spectral signature of the triplicates?
2. The sample points were aggregated by similar strata in larger areal spectral representations by averaging the individual spectral reflectance signatures, but how different were the sample points that were aggregated together, i.e. does the average of triplicates from BOB4_1 differ from the average of the triplicates from BOB4_2?
3. With a sampling of pixels from the HyMAP imagery from locations of the *in situ* sampling as described above, do the spectral signatures from the HyMAP imagery differ from the *in situ* spectral signatures?

The process of selecting image endmembers was performed using the Pixel Purity Index and the N-Dimensional Visualizer in ENVI. This is a trial and error process that involves selection and aggregation of individual endmembers. The criterion for merging endmembers into "bundles" that represent the spectral variability of the earth material of interest was performed by implementing the Jeffries-Matusita Transformed Divergence algorithm. Transformed Divergence is computed using the mean and covariance matrices from the imagery and measures the degree of divergence or separability of two classes (Jensen 2000). This works well with image-derived endmembers, but this algorithm cannot be used on *in situ* endmembers independent of the imagery. Consequently there is not parity when comparing image-derived spectra with *in situ* spectra. As a compromise, image-derived endmembers utilized for the Mixture Tuned Matched Filtering (MTMF) mapping were exported as ASCII text and analyzed using the non-parametric Wilcoxon Signed-Rank test.

The Wilcoxon Signed-Rank test is the non-parametric version of the paired t-test that tests whether the median for a data set has a particular value. Using the two-sided, or signed rank of the Wilcoxon test, has the ability to test a null hypothesis that the two variables have equal centers of symmetry. It does not assume the data distribution is Gaussian in nature. The Wilcoxon Signed Rank test was used for the last objective as described above.

Although ANOVA is usually used with normally distributed data, an ANOVA 2-Factor analysis is used to test the hypothesis of no difference between triplicates of *in situ*

samples taken in three different spots at a single sample point, i.e. BOB4_1 triplicates (objective one from above). The ANOVA 2-Factor test was used for the first two statistical analysis objectives.

Not all sample point triplicates, or all possible combinations of aggregated *in situ* data were examined to determine differences or similarities between aggregated *in situ* or image endmembers. Given time and personnel constraints it was decided to use a smaller sample of data points within the BOB4 sample area, the No Man's Friend Sample sites and final image endmembers from the HyMAP imagery. In comparing the HyMAP image endmembers with the *in situ* endmembers, it should be noted that comparisons were done with *in situ* data that were convolved to match the HyMAP imagery which was subsetted to reflect the spectral range of the *in situ* data. This aspect is not central to the purpose and intent of the research, but should be the subject of future research using an intense and rigorous statistical analysis.

The ANOVA 2-Factor analysis of triplicates found results that were consistent with the type of material being analyzed. Triplicates from more homogeneous materials tended to have less overall variance. Mud from No Man's Friend 2, and bright sand from the beach fronting the ocean, are some of the materials that exhibited the least amount of overall variance. Conversely, variance was greatest with materials that exhibited the greatest heterogeneity such as live, vertical, densely clustered oysters on the west side of BOB4. Principally BOB4 sample points 14 through 16 and 19 through 22. Oyster strata such as "D", "B" or "F" stratums had mixed results for variances between triplicates.

Analyzing regions of the electromagnetic spectrum individually (blue, green, red and shortwave infrared regions) between triplicates, resulted in the smallest variances in the blue, green and red regions, and the greatest variance was found further out in the short wave infrared regions. Analysis of the spectral regions was carried out on sample points BOB4_1 through BOB4_4, and represents the "D" oyster strata class. These findings may not reflect results from more or less homogenous oyster strata.

Using the Wilcoxon test, it was found that the averages of triplicates are significantly different than the averages from another sample point within the same oyster strata. This analysis was performed between BOB4_1 and BOB4_2. In addition, averaged image spectral signatures were statistically different than averaged *in situ* spectral endmembers for the same area of BOB 4 sample site.

3.4 Mapping *In situ* and Image Derived Spectral Endmembers

3.4.1 Overview of Methodology

The primary methodology of this research compared image-derived spectral endmembers with *in situ* spectral signatures of shellfish strata. All image datasets were radiometrically and geometrically corrected to insure accurate GPS location and pixel registration agreement. The use of MTMF methods were first used to map shellfish distributions without the use of *in situ* referenced spectral endmembers. All field collected spectral signatures were first convolved to match the wavelength scale of the

remotely sensed images and Minimum Noise Factor Transformations (MNFT) were performed for inclusion in the MTMF mapping.

Figure 3.7 - Schematic of Shellfish Mapping Process

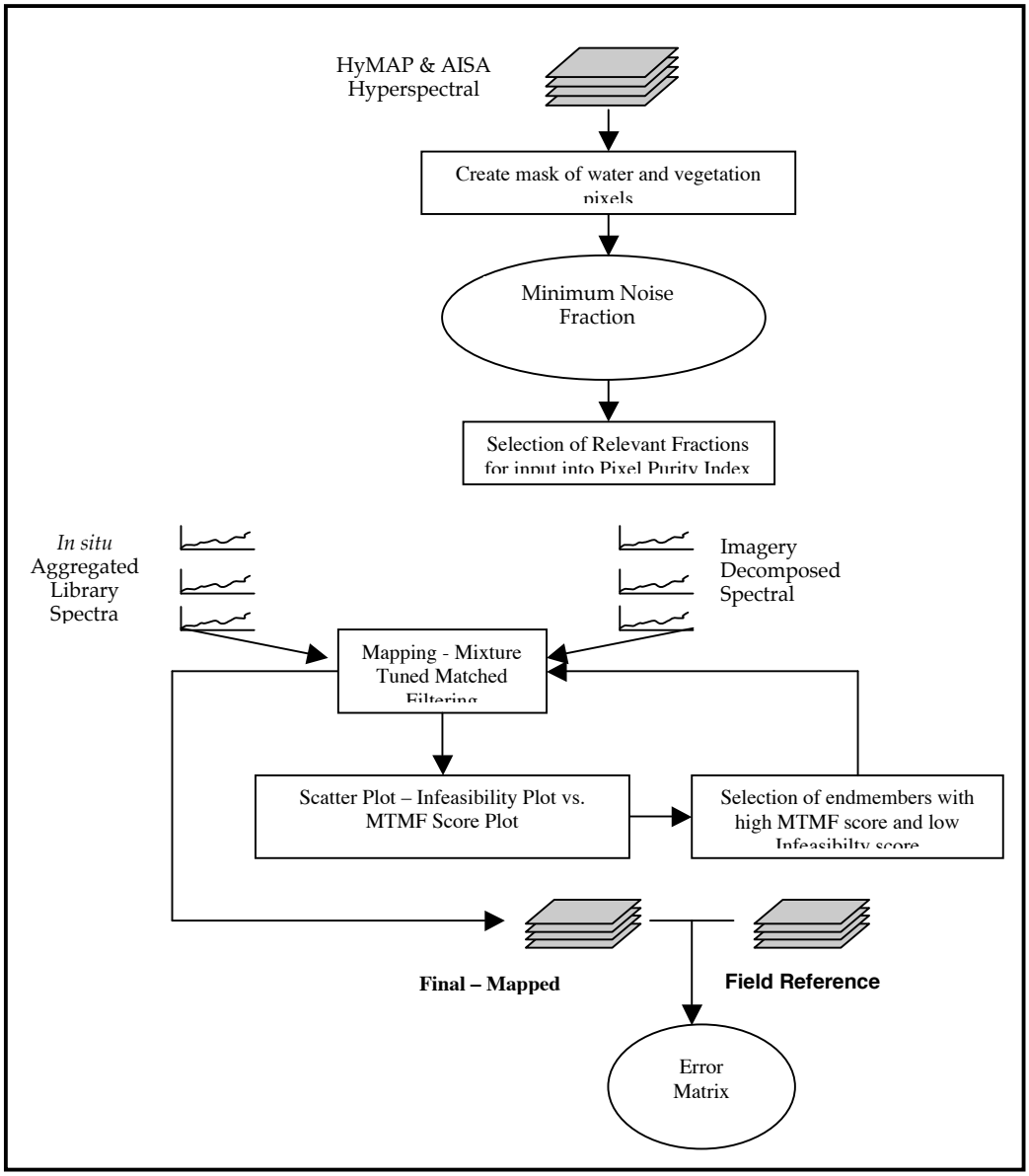

Mapping shellfish resources using *in situ* derived endmembers first required a decision regarding the level of aggregation of the *in situ* spectroradiometer signatures that would best yield a spectral signature corresponding to the same spectral dimensions found within the imagery. Since this represents a very small area of interest, the second level of aggregation as described above was used as inputs for spectral unmixing. The second level of aggregation of the *in situ* spectral endmembers was aggregated to represent the same patch type of shellfish aggregation and health. The *in situ* spectral reflectance sampling points that fell within an area of similar shellfish groups (i.e.

SCDNR strata class F or F1), were averaged. These averaged spectral signatures convolved to match the AISA wavelength (as described above) and a MNFT was applied to the spectra. They were then saved as a spectral library within the ENVI software to be utilized as inputs for mapping using the MTMF methodology. Figure 3.7 shows the steps that were followed to process the AISA and HyMAP imagery in order to spatially distinguish and map the shellfish and mud classes.

The targeted features to be mapped were patch or fringing reef structures. The first step in processing the hyperspectral data was to eliminate any unwanted earth materials within the imagery. This was accomplished by masking out the water and vegetation pixels. All shellfish are assumed to be near the waters edge or reposing on top of a patch reef. The process of masking was carried out by using the 2-dimensional feature space viewer within ENVI. The 2-dimensional feature space viewer places the pixel values of one band on the axis of a scatter plot and another band on the opposite axis. Typically, the chosen bands have one band that characterizes the material of interest, such as a band in the near infrared for vegetation, and the other acts as the contrasting band. The resulting "shape" of the data cloud is then density sliced to show areas of denser pixels. These areas represent features or materials within the imagery. When selected, the pixels are colored within the scatter-plot and appear within the imagery as colored pixels. In this way materials of interest within a scene are selected and placed into a class. Once all the pixels of unwanted materials are completed, a separate band of the imagery is derived and saved as a file.

The next treatment is to reduce the spectral dimensionality of the imagery. Hyperspectral imagery is usually defined as having many contiguous and discrete spectral bands (Jensen 2001). Many of these bands contain redundant information and the MNFT is designed to eliminate redundancy and segregate any noise in the image (Boardman and Kruse 1994). This is a process that uses two cascaded Principal Component transformations. The first Principal Component transformation is based upon the estimated noise covariance matrix, which then decorrelates and scales the noise within the data. This results in the elimination of band-to-band correlations. The second stage takes the noise-whitened data and performs basic Principal Component transformation. The associated images (often called 'eigenimages') and the eigenvalues (or eigenvectors) are used for further spectral processing. There is usually a parsing of the images and statistics into two groups, including a) those with the highest eigenvalues and coherent eigenimages; and b) those composed of the lower eigenvalues (with near-unity values) and eigenimages that are noise-dominated. By selecting the eigenimages that have the highest eigenvalues (and thus the most variance), the image dimensionality has been reduced to the bands with the most information, which are used for further processing.

The third treatment relates to the input of either *in situ* endmembers that have also been transformed via the above process, or endmembers of interest derived from the imagery through a process known as the Pixel Purity Index (PPI). The Pixel Purity Index is used to find the most spectrally pure pixels or extreme pixels. They are extreme in the sense that they are on the furthest edges of the pixel data cloud. The PPI is computed by

repeatedly projecting n-dimensional scatter plots onto a random unit vector (ENVI User's Guide 2005). Pixels at the end of the unit vector are counted as extreme and indexed as to the number of times they are marked as extreme. The output is a single band image with pixel brightness denoted as the count or number of times it was marked as extreme. Parameters the user can set are the threshold factor setting that determines the threshold for extreme pixels. A threshold factor setting of 5 marks all pixels at the end of a vector extreme that are within five digital numbers (high and low) of the extreme pixels as extreme. The higher the setting, the more pixels will be counted as extreme but are less likely to be spectrally pure. The other parameter that is set is the number of iterations that the algorithm will run. To know when all extreme pixels have been found and marked, a graph is displayed showing the number of iterations (x-axis) and the number of pixels marked as extreme (y-axis). When the curve flattens out at the top for a number of iterations then it is safe to assume that most of the significant extreme pixels have been marked and indexed.

If *in situ* endmembers are to be used to map an earth material within an image then the pixel purity index is not needed. To use *in situ* endmembers they must be in the same MNFT space as the image and placed into the ENVI spectral library for use in the MTMF algorithm.

The next treatment is the visualization of the PPI in *n*-dimensional space. This allows the user to view and refine the number of endmembers in multiple dimensions of space to visualize the PPI data cloud from as many different angles as necessary. This is useful for selecting the most spectrally pure endmembers. The user then has the options of exporting the endmembers to view the pixels within the image in geographic space and saving the bundles or collections of endmembers that represent a single class of earth material. Endmembers that are exported for viewing within the imagery are treated as ROI's (regions of interest) which can then be tested statistically using the Jeffries-Matusita Transformed Divergence test for endmember separability. Endmembers that are statistically similar can then be merged together into a single class. The selection and refinement of endmembers presents one of the most subjective portions of spectral analysis. The inclusion or exclusion of endmembers within a class is most problematical when trying to gather endmembers that represent the spectral variability of the earth material within the image.

The last treatment is the mapping of the endmembers using one of the available mapping algorithms. The two algorithms that were considered are Linear Spectral Unmixing and Mixture Tuned Matched Filtering (MTMF). MTMF was chosen over Linear Spectral Unmixing because in Linear Spectral Unmixing, all endmembers contained within the image must be derived. With both Linear Spectral Unmixing and MTMF, there is an inherent limitation in the number of endmembers that can be mapped. There can only be *n*-1 endmembers mapped, where *n* is the number of eigenimages used in the analysis. A limitation of the method becomes apparent when the image may contain more endmembers than there are available eigenimages. Since the object of the research was to map shellfish and not water or vegetation, it makes sense to mask these elements and not include them in the analysis. Additionally, when the MNFT is

performed on the image, the vegetation and water will usually encompass the majority of the variance within the image, and by comparison, the variances between mud and shellfish are much smaller. Thus when the eigenvalues are calculated, the higher values will be for the water and vegetation and the smaller eigenvalues relegated to mud and shellfish. These smaller eigenvalues may be lost within the noise dominated (near unity variance) eigenimages. MTMF is also called partial-unmixing because it considers only the endmembers of interest, while suppressing the remaining spectral signatures as background noise.

The results from MTMF include two gray-scaled images for each mapped endmember. The first is the MTMF Score image that shows the relative degree of match to the reference endmember scored on a scale of 0-1, with 1 being a perfect match. It is common to stretch the values in the right hand side of the histogram from just above zero to one to show pixels that are mapped correctly. The second gray-scaled image is the infeasibility image that shows values in noise-sigma units to indicate the feasibility result. Figure 3.8 shows a diagram of how noise-sigma units vary in digital number scale with matched filter values" (RSI ENVI 2004).

Figure 3.8. - Mixture Tuned Matched Filtering (MTMF) Methodology

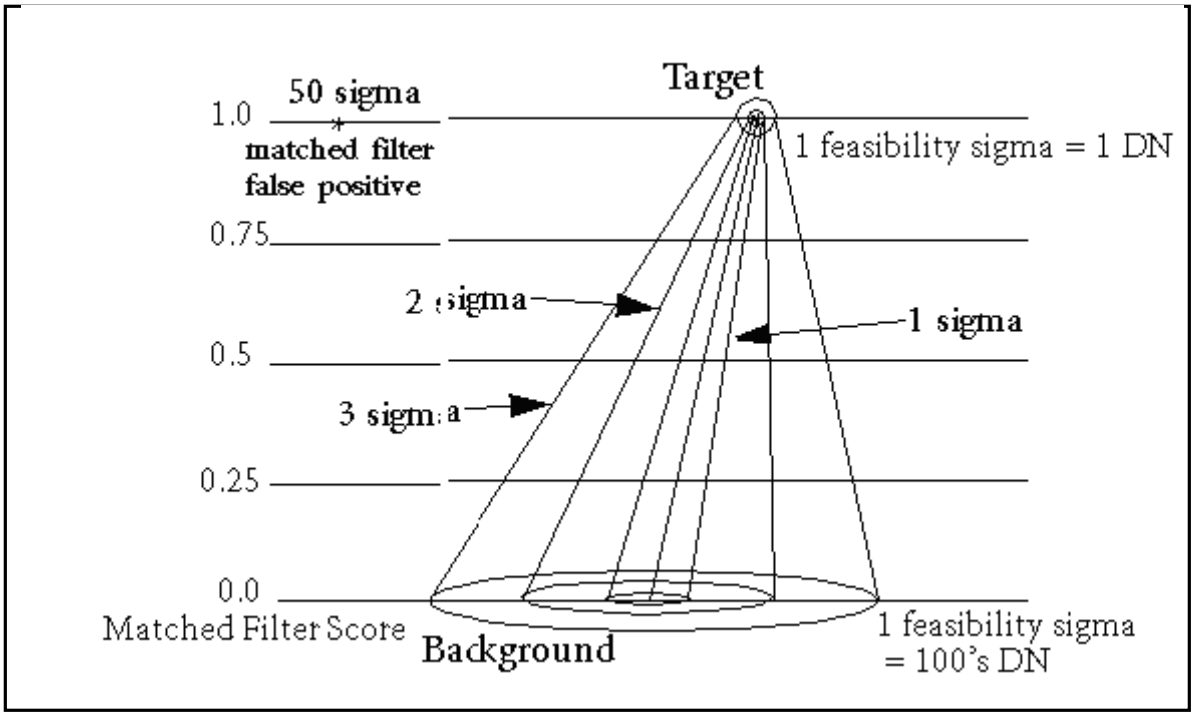

Pixels that are correctly mapped will have a high MTMF value and a low infeasibility value. Pixels that have a high MTMF value and a high infeasibility value, are "false positive". To refine mapped endmembers and correctly identify mapped pixels, the two-dimensional viewer is used to show the MTMF score on one axis and the infeasibility scores on the other. Pixels that are identified as correctly mapped can be exported as ROIs and treated as inputs into additional rounds of mapping.

3.4.2 AISA Imagery

The first of two hyperspectral remote sensing data that will be discussed is the Airborne Imaging Spectrometer for Applications (AISA) sensor (Specim Corporation) that was acquired onboard an aircraft managed by the University of Nebraska's Center for Advanced Land Management Information Technologies (CALMIT) remote sensing center. AISA is a push-broom imaging spectrometer with spectral and spatial resolutions that are pre-determined according to research needs. The AISA imagery acquired for this research has a spectral resolution of seven bands within a range of 498 nm – 819 nm. The spatial resolution is 0.5 x 0.5m which is adequate for visually discerning shellfish aggregates on a patch reef but is less adequate for discerning fringing reef structures. The AISA Plus sensor that was used for the North Inlet-Winyah Bay NERR overflight has seven bands between 498 and 819 nanometers (~6 nm wide) and a spatial resolution of 0.5 x 0.5 m. Spectral analysis was done using the photogrammetric and remote sensing software, The Environment for Visualizing Images (ENVI) version 3.5, SP1 and 4.1, by Research Systems Inc. (Boulder, CO).

Before analysis of the imagery could be initiated, a mask of the study area was constructed. Figure 3.9 shows the AISA image of the BOB4 study site showing bands 6, 4, and 2 (RGB). This study site was selected due to its large patch reef with a variety of shellfish strata types present both on the reef and on patch reefs surrounding the study site. The mask is used to negate water and vegetation pixels for the MNFT and subsequent analysis. Using the 2-dimensional feature space viewer in ENVI, clusters of water and vegetation were classified and used in construction of the mask. Pixels not classified using the above method were hand-selected and classed. Figure 3.10 shows the mask that was constructed and utilized for the MNFT.

Figure 3.9 - AISA Flight Lines and Image Subset in North Inlet, South Carolina

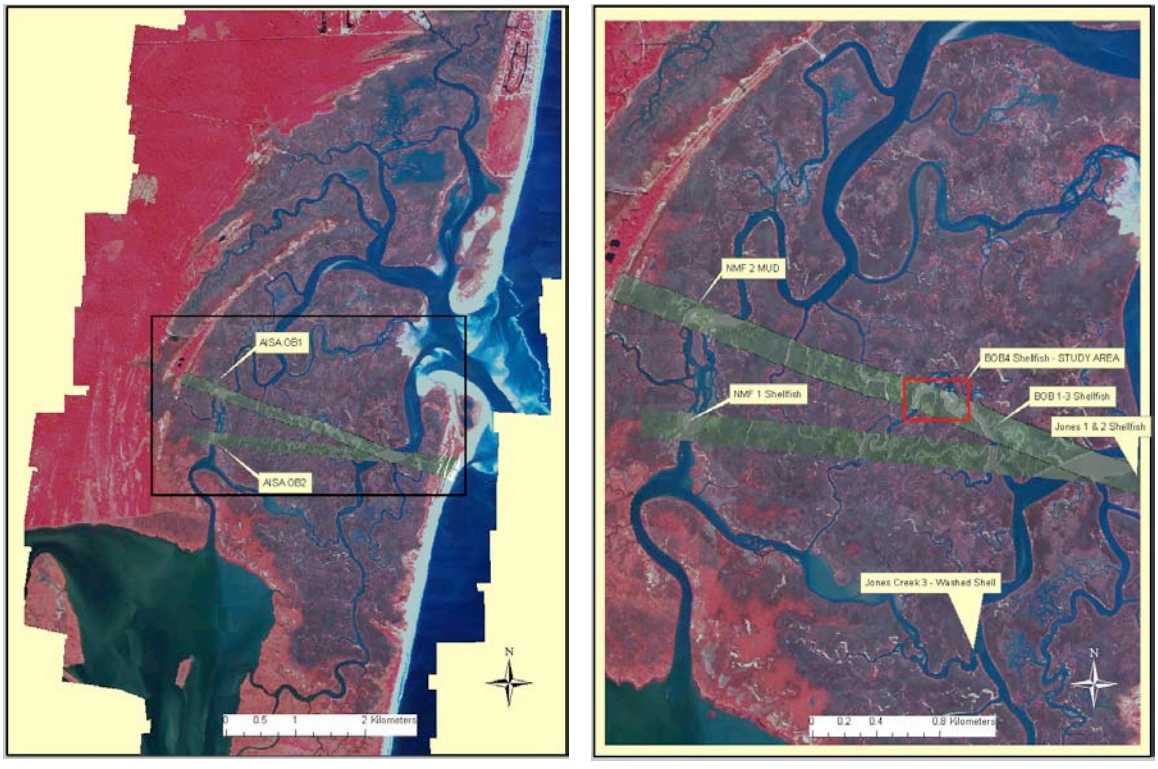

Figure 3.10 – AISA image Study Site and Mask indicating vegetation, water, and sunglint/shadow.

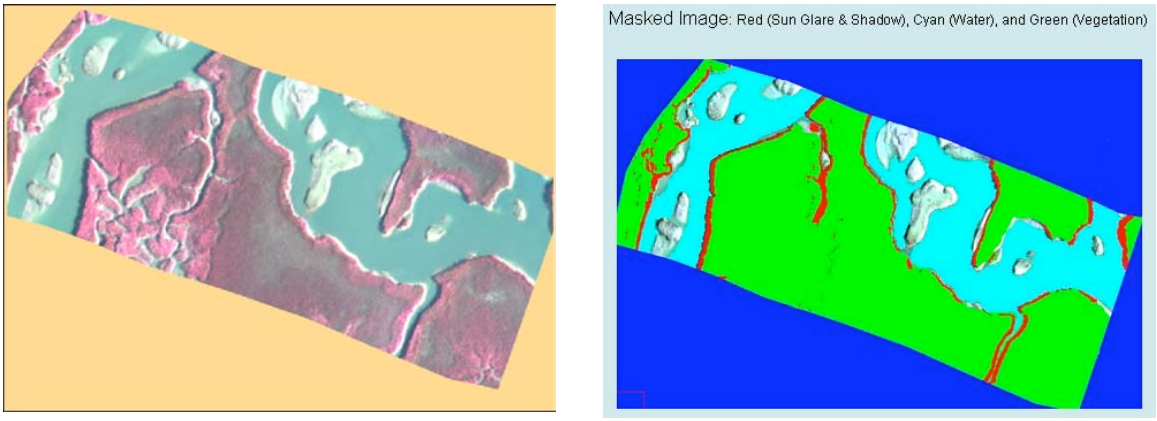

The mask was constructed using the feature space viewer within ENVI where larger groups of dense pixels or classes of pixels can be isolated and marked for masking purposes. Figure 3.10 shows the original AISA image and the three different classes of pixels that were isolated: a) vegetation; b) water; and c) sun glint and shadow. The sun glint and shadow is an artifact within the data and not representative of the earth materials typically found in these areas. This issue is explored in more detail in the Discussion section of this report.

3.4.3 HyMAP Imagery Spectral Mapping

The HyMAP data set required no instrument radiometric correction as evidenced in a Fast Forward Fourier Transform performed in ENVI. Atmospheric correction of the HyMAP data set was accomplished using the radiative transfer model algorithm Atmospheric Correction Now (ACORN) prior to spectral analysis. Prior to spectral analysis, all derived images were geometrically corrected using the georeference input geometry files that are supplied in the HyMAP dataset. Using the Input Geometry file (IGM) that is supplied with the HyMAP Dataset, a super Geographic Look-up Table (GLT) is derived. The IGM file contains the geolocation information for each original raw pixel. The derived images are then georeferenced using the super Geographic Look-up Table. A HyMAP image that is not spectrally unmixed will be geometrically corrected and the two flight lines can be mosaiced to produce a geometrically corrected reference image. This image can then be used for image-to-image geometric correction.

The HyMAP sample site around the BOB4 sample site did not capture the same area as the AISA image due to the spatial arrangement of the flight lines. The HyMAP Region of Interest (ROI) was spatially subset from the larger HyMAP flight line. The resulting HyMAP image subset dimensions were 258 columns by 189 rows. HyMAP has 126 bands covering the spectral range from 452.9nm to 2482.2 nm, effectively covering from the visible (VIS) to the short wave infrared (SWIR) regions of the electromagnetic spectrum. The spatial subset of the HyMAP image was then spectrally subset into two ROIs to ease computational loads and isolate more nuanced differences in spectral responses. Subset 1 (ROI_1_Bands2_44) and subset 2 (ROI_1_Bands45_126) include 452.9nm to 1078.8nm and 1.093.8nm to 248.2nm respectively. All bands are used in the

analysis with the exception of a few water absorption bands that occur at bands 63-65 (1.4044 – 1.4328 nm), 94-97 (1.8034-1.9877 nm), and band 126 (2.4822 nm) due to image cohesion.

Similar to the AISA region of interest, a mask was constructed of the water and vegetation using the 2-dimensional feature space viewer. Figure 3.11 shows the georectified HyMAP flight lines within North Inlet and Figure 3.12 depicts a masked subset of the HyMAP imagery. The masked subset was the same mask applied to the both the two spectral subsets, ROI_1_Bands2_44 and ROI_1_Bands45_126.

Figure 3.11 - HyMAP Remotely Sensed Imagery of North Inlet, SC

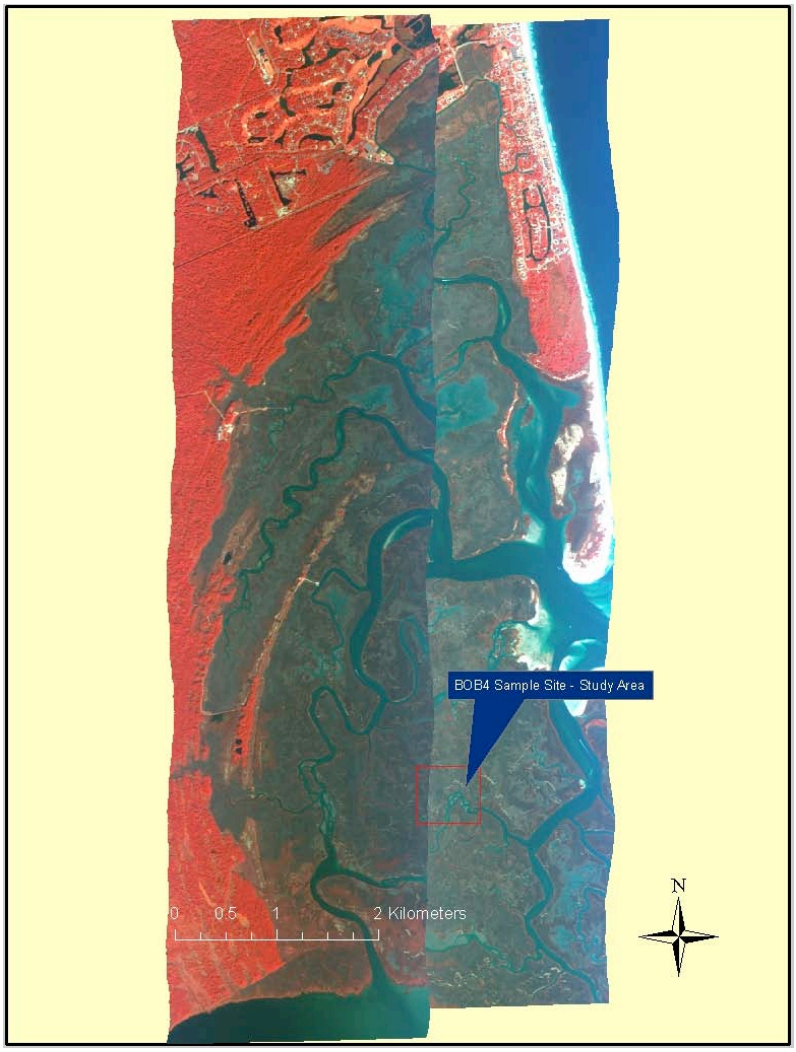

Both flight lines were atmospherically corrected using the ACORN (Atmospheric Correction Now) algorithm and georectified using the GLT (Geographic Look-Up Table) using the nearest neighbor approach that preserves the original pixel location. No color balancing was performed on the imagery or histogram

normalization procedures to maintain the integrity of the digital number (DN) values.

Figure 3.12 - HyMAP BOB4 Study Area and Mask image

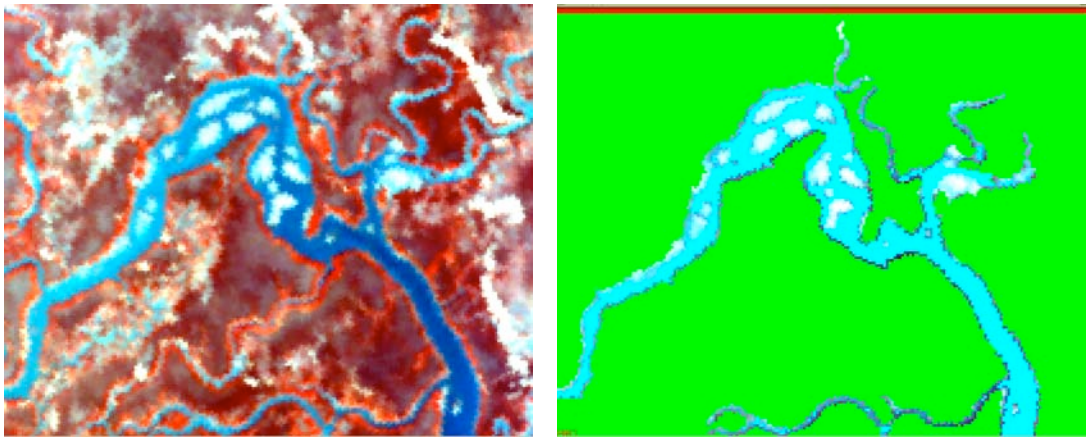

The HyMAP imagery was initially subset into two areas for ease of computation and to isolate any smaller variances in the mid-infrared region that would not be apparent if the visible region was analyzed in the same subset. An additional consideration was the subset of bands 2-44, which corresponded to the same spectral range as the hand-held GER field spectroradiometer. In order to map *in situ* derived endmembers, it was necessary that the subset matched the same spectral range as the *in situ* endmembers. Additionally, the *in situ* spectral library endmember were then convolved to match the spectral range of the HyMAP imagery and a MNFT was performed for inclusion in mapping with the *in situ* endmember.

3.5 Mapping Using Visual Learning System's Feature Analyst®

Feature Analyst (Visual Learning Systems, Inc. Missoula, MT), is a GIS-based, machine-learning system which was designed to improve poor classification accuracy often associated with high-resolution imagery. One of the premises behind Feature Analyst is the ability to reach out to GIS users in a timely and cost effective manner (Opitz 1999). The software provides a paradigm shift to automated feature extraction since it: (a) utilizes spectral, spatial, temporal, and ancillary information to model the feature extraction process, (b) provides the ability to remove clutter, (c) incorporates advanced machine learning techniques to provide unparalleled levels of accuracy, and (d) provides an exceedingly simple interface for feature extraction (O'Brien 2002). The benefits of using this software include automation (reducing labor costs of updating GIS databases), improved accuracy (compared to hand-digitizing), simplicity (user-friendly and easy-to-use), and innovation in the use of spatial context, clutter removal, and intelligent agent.

Feature Analyst is similar to a standard supervised classification in that the users supply training sites for each feature of interest. The difference is that along with collecting training sites with a wide array of spectral signature for each class, the user must takes care that the training sites represent examples of the class' shape. In short, the analyst hand digitizes representative samples of the feature target, allows the software to

search for like features, and then interactively "teaches" the system which resulting polygons correctly capture the desired feature and which do not (NOAA 2003). The software uses a hierarchical approach that iteratively allows the analyst to refine the classification. After an initial classification, Feature Analyst allows the user a chance to look at the new shapefiles and define them as "correct", "incorrect" or "missed". Running a series of iterations whereby a pixel value is assigned to a class, the user can define the level of correct results for each polygon. The workflow used in Feature Analyst is shown in Figure 3.13.

An important variable to consider when using Feature Analyst is computer processing speed. Each iteration may take considerable time (+3 hours, depending on the size of the input data), but usually two to three passes through the image is enough to come up with a final classification. The software also includes a contextual classifier, allowing the user to input a pattern that captures the spatial structure of the feature that is to be extracted. For example, a star pattern might best represent a tree stand. Although this is a useful feature of Feature Analyst, it can be perfected only with trial and error.

Figure 3.13 - Work flow used in Feature Analyst which includes the creation of training sites, preparing the input layers, setting up the learning parameters, and refining the and combining features.

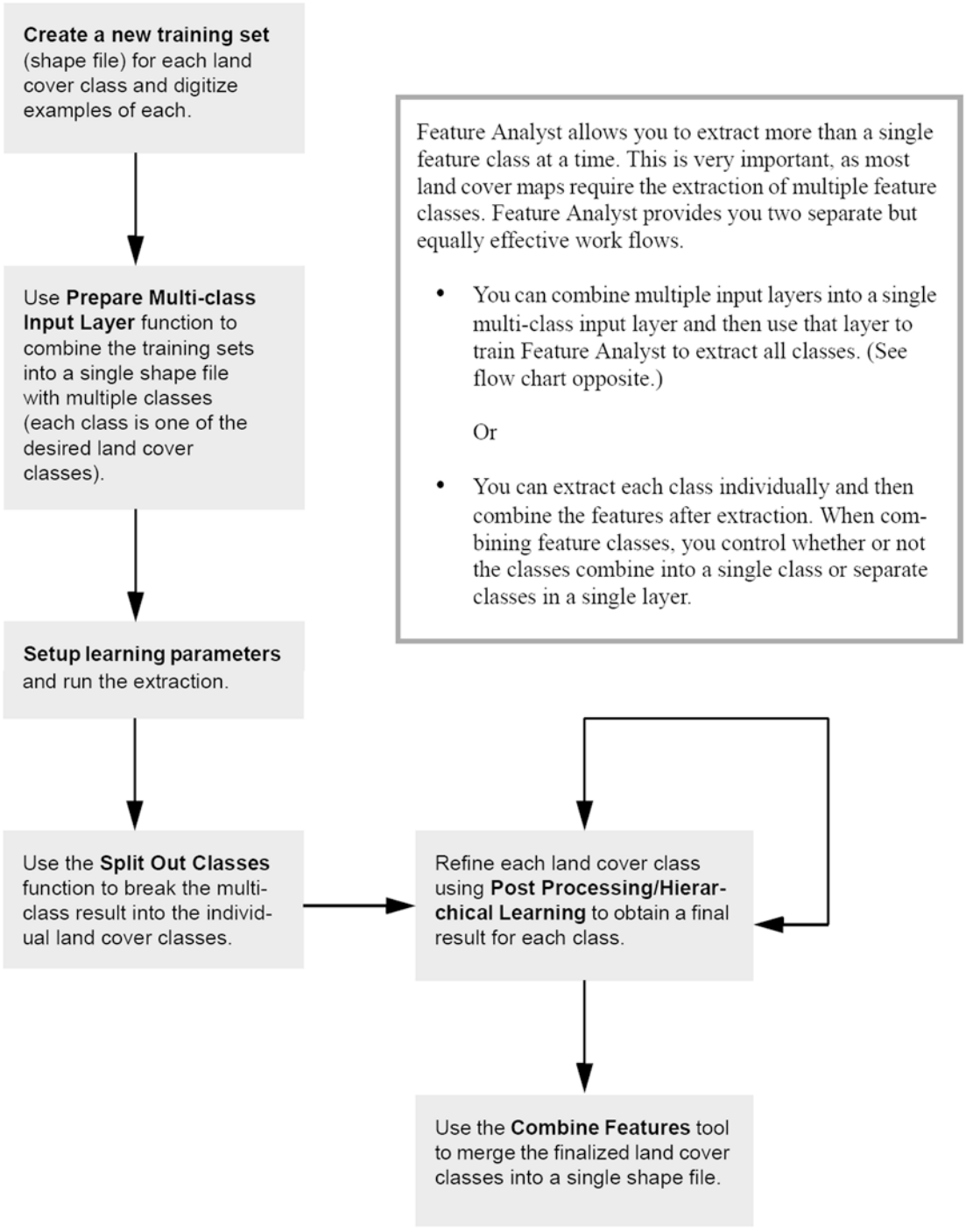

3.6 LiDAR Data

LiDAR data were acquired by Airborne 1 Corporation (Los Angeles, CA) on January 16th, 2003 in the North Inlet study area. Two low-altitude flight line swaths were acquired at a nominal posting of 0.25 meters. Figure 3.14 shows the acquired flight swaths superimposed over the 1990 ADAR imagery. A more detailed view of the No Man's Friend sample site is shown in Figure 3.15 and shows the 10th LiDAR tile from the extracted files which was converted to a TIN and superimposed over the 1999 ADAR imagery. Due to cost constraints and the very low post spacing of the LiDAR system that was required, the data collection mission was strategically designed to incorporate as many of the field sampling sites as possible (Figure 3.15). One of the research objectives was an attempt to incorporate LiDAR-derived elevation and laser return intensity values into the shellfish classification process. Both Feature Analyst and the SEE5 algorithm within the Classification and Regression Tree (CART) made for ERDAS Imagine software were used to investigate the utility of high-resolution LiDAR for classifying shellfish resources.

Figure 3.14 - LiDAR Flightlines in North Inlet, SC

Figure 3.15 - LiDAR Tile 10 Converted to TIN

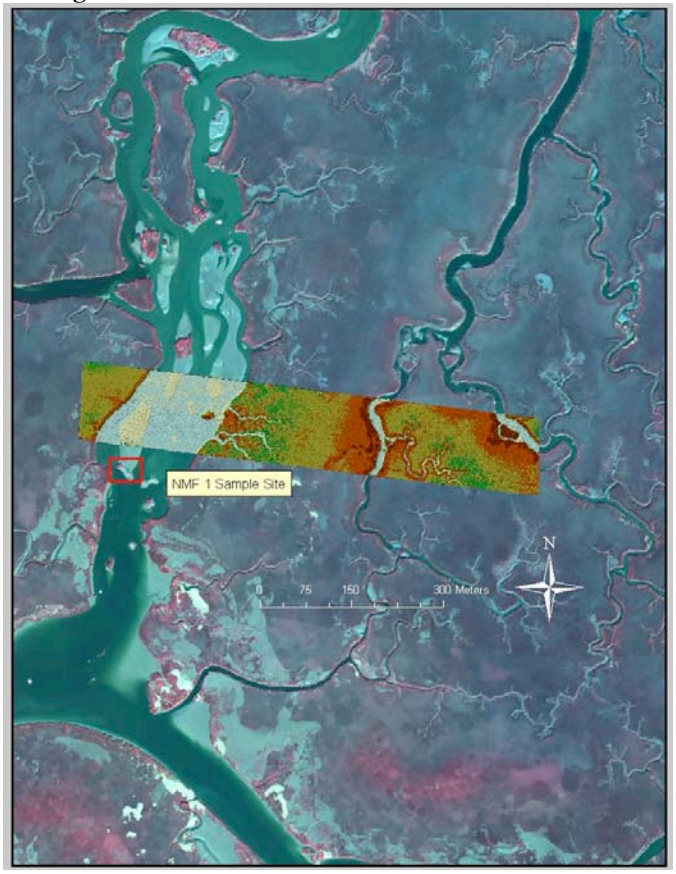

This Figure shows good elevation features but the imagery was acquired approximately 60 meters north of the No Man's Friend 1 sample site.

Data received from Airborne 1 included ten ASCII files for each of five categories: a) bald earth; b) extracted features; c) first pulse; d) last pulse; and e) model key points. Each category measured both elevation and intensity of the returning laser pulse. Both the LiDAR-derived elevation and intensity were evaluated as potential surrogates for classifying or discerning "health" of the shellfish reefs. The utility of elevation is first described, followed by a discussion on the results of the intensity value mapping.

A 'bald earth' elevation model constitutes LiDAR points that represent terrain topography without the influence of trees, buildings, or artifacts that do not represent the natural topography. This product is created by statistically culling LiDAR points that are modeled as having returned to the system before they reached the ground. Oftentimes, this algorithm and the process by which they derive the bald earth, is proprietary. The extracted features folder typically has the terrain topography as well as the natural and anthropogenic features mapped by the first returns of the system. Such features at North Inlet include trees, buildings, sand/mud bars, streams and shrub tussocks. Since North Inlet is predominately a natural estuarine ecosystem, the difference between the extracted features and bare earth is nominal. Within a natural setting, single LiDAR laser pulses

have the potential to create multiple returns as light is scattered from objects such as trees or buildings. When these light pulses are returned, they are classified as being either the first or last return. Since Airborne 1's bald earth algorithm is proprietary, it is assumed that the first of the last returns were statistically extracted for the calculation of the 'bald earth' model.

Figure 3.16 - TINs of First Pulse and Second Pulse with Statistics

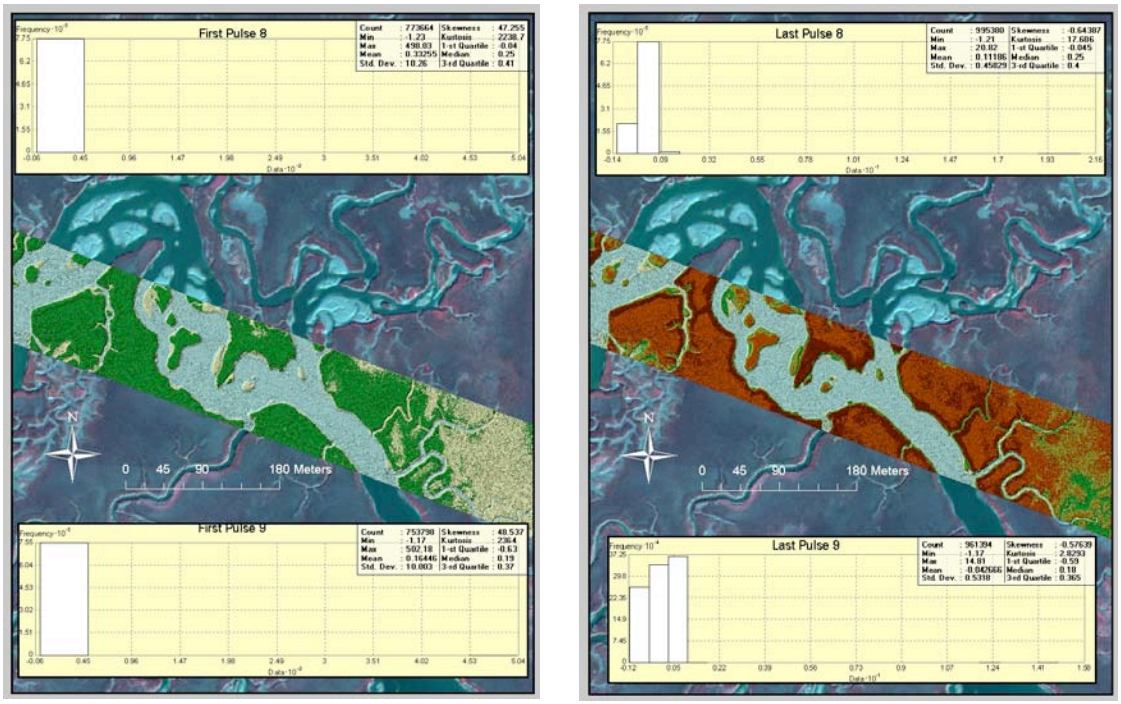

The first returns histogram reveals a highly skewed and kurtosis in the data. Examining the TINs (Triangulated Irregular Network) of the first and last returns, there is a greater level of detail in the last returns than in the first returns. This is most likely due to the skewness of the data in the last returns. Figure 3.16 demonstrates this point by showing the corresponding area of BOB 4 with the first and last LiDAR returns which have been converted to a TIN. Intensity of LiDAR data is not normally used due to calibration issues of the laser. In practice, calibration is usually accomplished by flying the targeted area first, then calibrating the laser intensity to the range of values from the initial overpass. Problems with comparing different areas arise due to the inability of not being able to compare different over-flights. There is some utility when examining the relative intensities of the returning laser pulses. Due to data skewness, the data were log transformed to approximate a normal distribution.

Rather than transforming the larger scene for patch reef delineation, these reefs were manually digitized using the 1999 ADAR imagery. These areas were pre-selected based on field surveys and consisted of mostly shellfish, part shellfish / mud, and mud reefs. The LiDAR point files were then subset from the digitized study areas to produce a file of LiDAR points representing the last returns that contained elevation and intensity values. These intensity values were then log transformed and converted into a continuous

raster surface via interpolation using both Kriging and radial basis function algorithms. As previously mentioned, a Log transformation was done on the data due to the high level of data skewness, and to approximate a more normal distribution of the data. Kriging was used because it represents a more robust method of deterministic interpolation than the more popular Inverse Distance Weighed interpolation method. Deterministic interpolation relies on the values of the points around it to determine the value of a central point and the further away from this point, the less "weight" is assigned to distant points. A criticism of this approach is in establishing what the appropriate weights should be. When using Kriging, the weights are assigned from the semivariogram which is a statistical relationship based on autocorrelation. The Radial Basis Function is an exact interpolator and does not use a weighting scheme. The methodology used in the Radial Basis Function uses splines that are fitted through each point (ESRI 2005).

Several patch reefs were identified at sample site BOB4, and were used for investigating the utility of LiDAR intensity data based on a computed raster continuous surface derived using the Radial Basis Function and Kriging. These classified structures were then used as inputs into the SEE5 Classification and Regression Tree Analysis that is implemented through the Leica Geosystems ERDAS Imagine, version 8.7.

4. Results

4.1 Introduction

The results presented in this section first show the most recent effort of mapping using the 2-dimensional scatter plot to review and select endmembers. The second effort involved using the last two mapping trials to a) illustrate the technique of using the scatter-plot to isolate and refine endmember bundles; and b) demonstrate changes in the results showing the before and after effect of using this technique. This section presents the results of the *in situ* spectral libraries that were collected and constructed through the course of a year and applied to the AISA and HyMAP imagery. The principal study sites used to map the *in situ* and image derived endmembers were BOB4, No Man's Friend 1 and No Man's Friend 2 (mud) field sampling sites. The process of deriving the spectral shellfish endmembers from the AISA and HyMAP data sets are shown and the results are then applied to mapping the shellfish distributions from the study sites in both the AISA and HyMAP datasets.

Mapping shellfish using field-derived spectral endmembers first entailed adjusting the bandwidth of the spectral endmembers of the GER 1500 Spectroradiometer to mimic the number of bands and spectral range of the remotely sensed data. Specifically, the GER spectroradiometer that was used to collect the *in situ* shellfish spectral signatures has 512 bands (spectral range of 350nm – 940 nm), AISA has 7 bands (spectral range 498nm – 819 nm) and HyMAP has126 bands (spectral range 0.4529 – 2.4822 nm). Depending upon the spectral range and number of bands, each remotely sensed dataset required having the *in situ* spectral signatures convolved to match the specific remotely sensed imagery platform. The *in situ* spectral signatures were then processed through a MNFT in the same manner as the imagery. The last step in processing the *in situ* spectral data is to compile then into a convolved spectral library that was then used as input into a mapping process such as the MTMF mapping.

The analysis of the LiDAR data was exploratory in nature, and used to investigate if high spatial resolution elevation data was helpful in classifying shellfish reefs. One question we initially posed was whether LiDAR be utilized to differentiate textural differences between shellfish classes, mud and vegetation? A secondary question was the ability to incorporate classified LiDAR data into a neural network approach to classify remotely sensed imagery? This last question posed difficulty in answering due to spatial misalignment between the LiDAR data set and the other geospatial data products.

4.2 Mapping Remotely Sensed Imagery From *In situ* Derived Endmembers

4.2.1 Mapping *In situ* Endmembers Using AISA Imagery

The mapping of the AISA remotely sensed imagery, as described in the Methodology section, started with masking and executing an MNFT to reduce the dimensionality of the data and any band-to-band correlations. This aspect of the methodology was the same for all the datasets analyzed. Before the MTMF is executed, the user must decide on which endmember to use as inputs. If the user chooses to utilize *in situ* endmembers then the implementation of the Pixel Purity Index is skipped and the *in situ* endmembers are convolved to match the specific bandwidths of the imagery. A MNF

transformation is then implemented on the *in situ* endmembers prior to inclusion into the MTMF algorithm.

4.2.1.1 MNF Rotation of Imagery and *In situ* Endmembers

In order for *in situ* derived spectral endmembers to be utilized for spectral analysis, they must first be convolved to match the specific bandwidths of the imagery that was used for mapping. Because the remotely sensed images were transformed using the MNF rotation algorithm, the spectral signatures were also transformed. Figure 4.1 shows image-derived endmembers from the BOB 4 sample site and aggregated *in situ* spectral signatures. This figure shows that for the most part, the endmembers and *in situ* curves line up spectrally with little error. The red/infrared shift for both the shorter AISA derived endmembers and the *in situ* spectral signatures all co-inside. The AISA derived endmembers do not match the spectral range of the *in situ* endmembers due to the *in situ* spectral endmembers not having been convolved to match the AISA spectral range. Figure 4.2 shows after the *in situ* spectral endmembers have been convolved to match the AISA spectral bandwidth and range. The spectral signatures in red are *in situ* endmembers that have been aggregated and convolved to match the AISA imagery bandwidth and spectral range. The black spectral signatures are the AISA spectral endmembers that were derived from imagery at the BOB 4 sample site.

Figure 4.1 - Spectral curves of *in situ* and AISA imagery shellfish

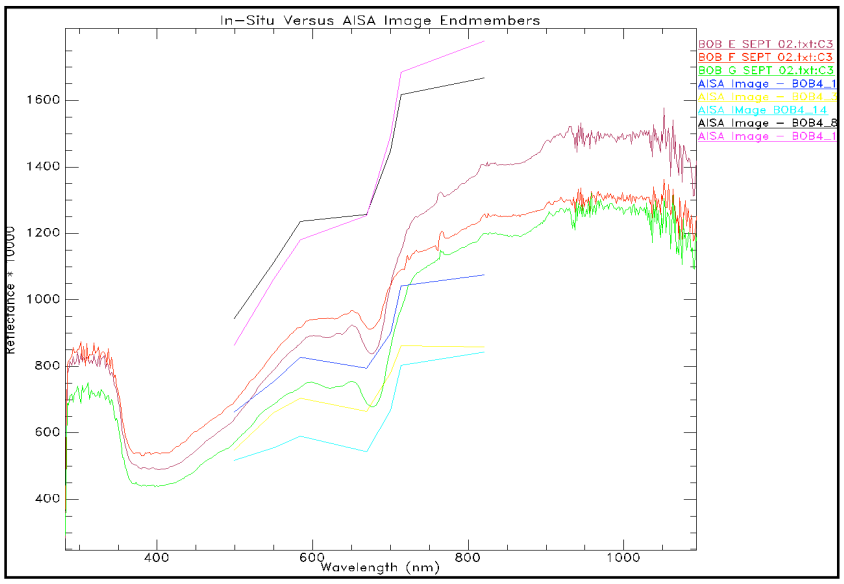

The *in situ* endmembers align very closely with the image endmembers, the exception being that it appears the image-derived endmembers (black) have a lower reflectance than the *in situ* endmembers. This may be the result of image and *in situ* endmembers acquired on different dates or differences in radiometric corrections. This underscores a concern that is expressed in the literature on the accuracy of using *in situ* derived versus image-derived endmembers for mapping. The literature supports this contention that better results are obtained using imaged derived endmembers for the reasons stated above (Elmore, et al. 2000)

Figure 4.2 - Convolved *In situ* Endmembers and AISA Image Endmembers

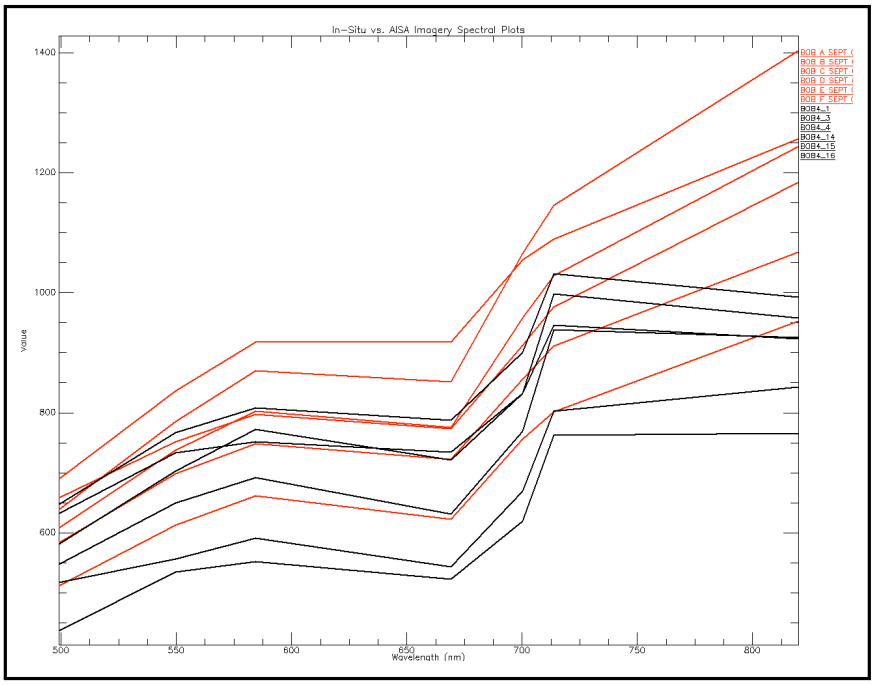

4.2.1.2 AISA Mixture Tuned Matched Filter (MTMF)

Using the convolved *in situ* endmembers, we mapped the endmembers in two parts using the AISA imagery. The first part used the *in situ* endmembers aggregated from BOB 1 through 3, (aggregated clusters BOB A through C). The second part utilized *in situ* endmembers from BOB 4, (aggregated clusters D through G). One reason for this is due to using the first five transformed AISA eigenimages and mapping one endmember less than the number of eigenimages used. Additionally, the first set of endmembers were not native to the study area of interest but the sample sites BOB 1-3 are the closest to BOB 4 than any other sample site. Endmembers needed to be tested to see if those that were derived from the study site had the same level of mapping accuracy as endmembers derived from the area of interest. Figure 4.3 shows the last two revisions of mapping using BOB A through C *in situ* endmembers.

Figure 4.3. - BOB A through C *In situ* Mapping

BOB A MTMF Score

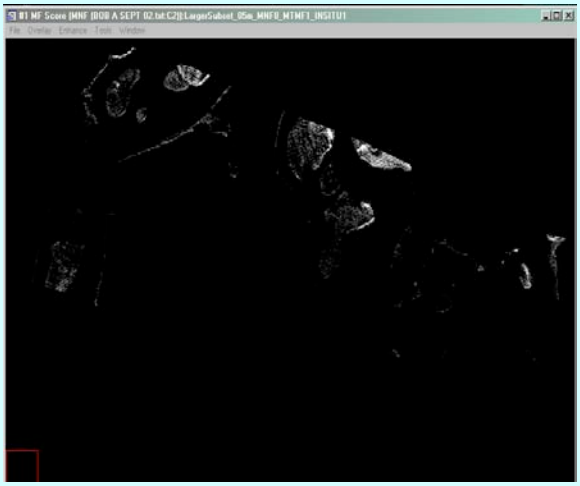

Infeasibility (y) vs. MTMF Score (x)

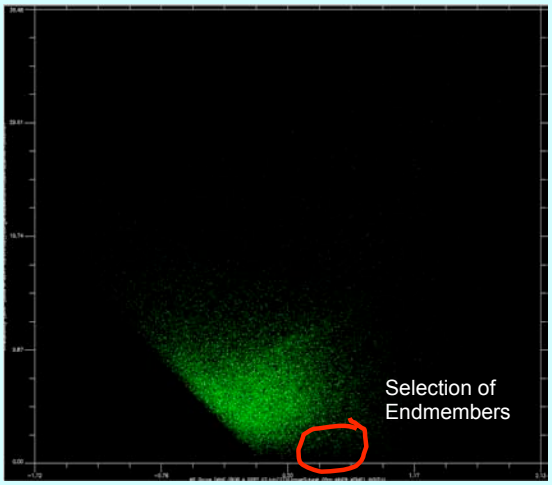

BOB B MTMF Score

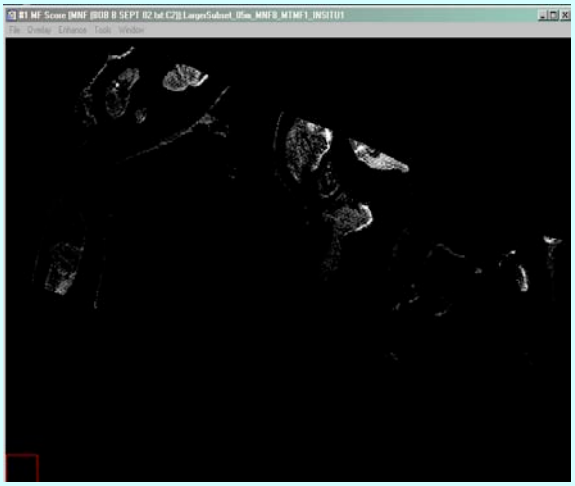

Infeasibility (y) vs. MTMF Score (x)

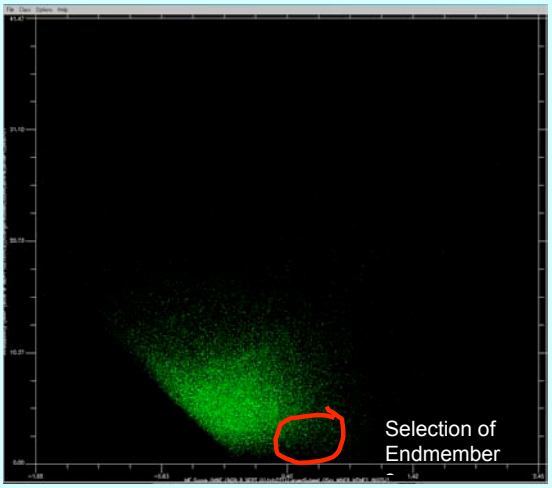

BOB C MTMF Score

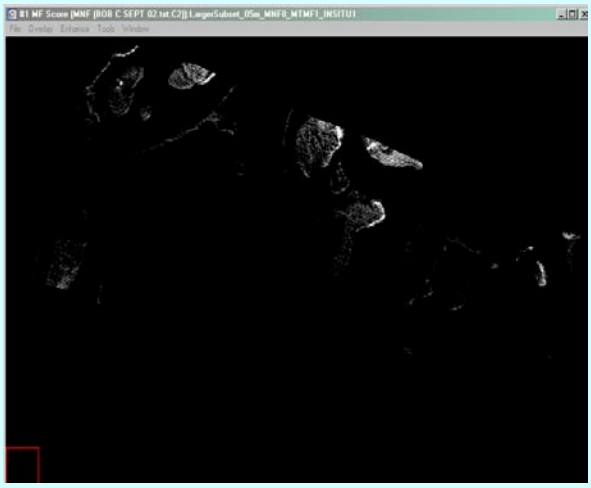

Infeasibility (y) vs. MTMF Score (x)

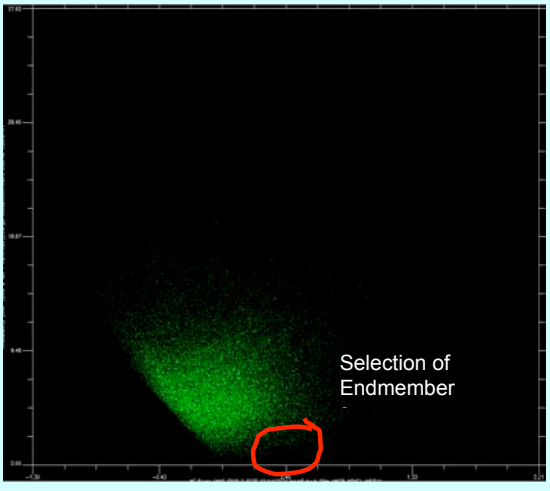

The MTMF results were very similar between BOB A, BOB B, and BOB C *in situ* endmembers. The endmembers from the scatter-plots that were collected using the scatter plots were unique as measured by the Jeffries-Matusita Transformed Divergence test (scores greater than 1.8). When *in situ* endmembers BOB D through F were utilized for mapping the AISA imagery and the subsequent endmember revisions were made using the 2-dimensional scatter plots, it was found that the revised endmembers were not unique and were combined into a single class of endmembers. Figure 4.3 shows the result from mapping these single class endmembers.

Figure 4.4 - BOB D through F (combined) Revision 1 Endmembers with AISA Imagery

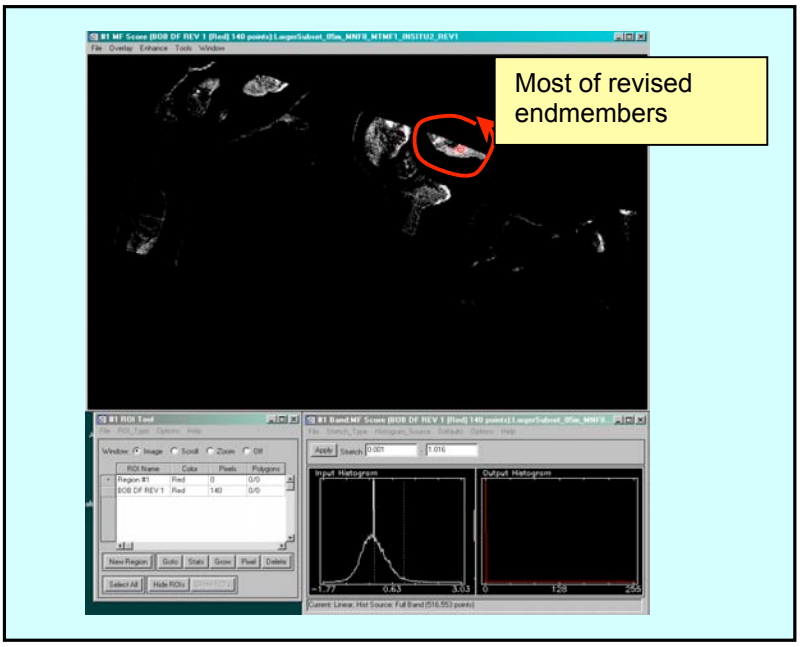

It is interesting to note that when the revised endmembers are shown on the MTMF score, their location is geographically different than where they were sampled in the field, but they are located in an area that contains dead brightly reflective shells, few live shellfish and a similar type of strata as found on top of BOB4 (BOB D through G were field sampled from BOB 4).

4.2.2 *In situ* Spectral Mapping Using HyMAP Imagery

The use of the 4.0 x 4.0 m HyMAP imagery with *in situ* endmembers follows the same analysis flow schema as described in Figure 3.7 in the Methodology section. The spectral image analysis was performed using a subset of HyMAP bands 2 - 44. One limitation of using the *in situ* spectral imagery is the GER 1500 spectroradiometer is calibrated from 350- 1050 nm while the HyMAP imagery has a spectral range of 439.0 – 2482.2 nm. To utilize the *in situ* endmembers, the HyMAP imagery had to be subset to the same relative spectral range of the *in situ* data. Consequently, the HyMAP subset that was utilized for the purpose of mapping the *in situ* endmembers were bands 2 through 44 (452.9 – 1078.8 nm). The *in situ* endmember sets were derived from BOB A through Bob G sample sites (see Table 4.5 – Shellfish Secondary Aggregation for specific sample points used) which were convolved to match the HyMAP band widths and spectral range. Figure 4.5 shows the convolved *in situ* endmembers with HyMAP endmembers of shellfish from the BOB 4 sample site.

Figure 4.5 - Comparison Between HyMAP and *In situ* Endmembers

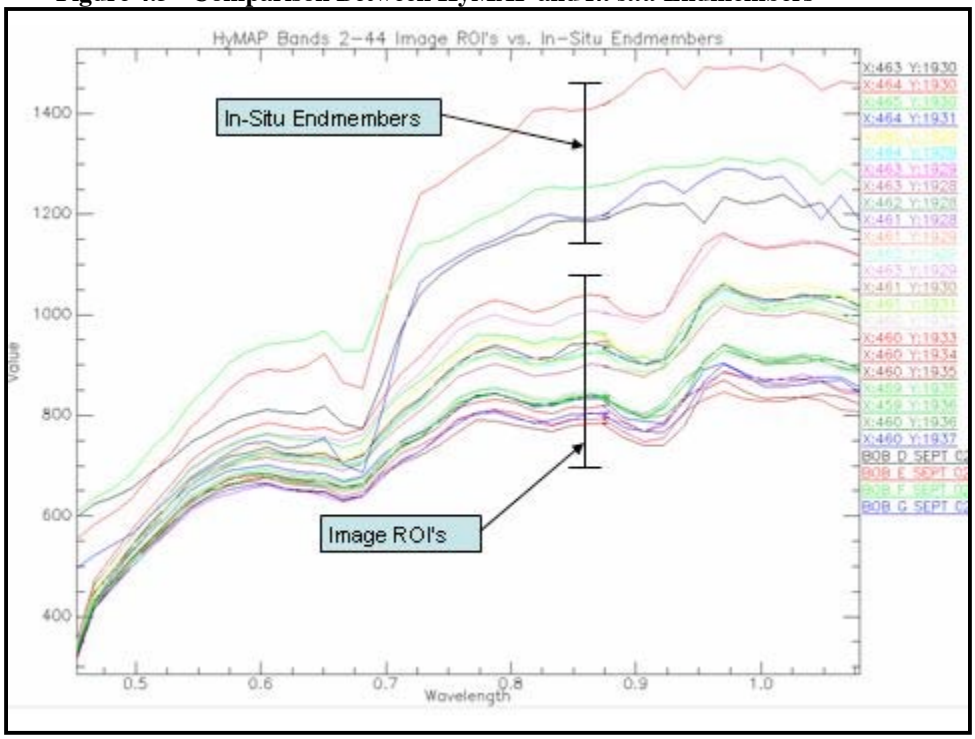

The overall alignment between the HyMAP and *in situ* endmembers is very good but it is also interesting to see there is a greater slope increase in the red to infrared between the *in situ* and image endmembers. At approximately 700 nm, the *in situ* endmembers exhibit a greater overall reflectance than the *in situ* endmembers.

4.2.2.1 MAP Masking and Minimum Noise Factor Trans. (MNFT)

The HyMAP image with a spectral and spatial subset showing bands 2-44 of the area around the BOB4 sample site is shown in Figure 4.6 (first image). The second image in Figure 4.6 shows the HyMAP subset with vegetation and water masked. Only shoreline

and patch reefs were not masked since our principal areas of investigation were patch and fringing reefs. The MNFT of the HyMAP subset bands 2 - 44 is shown in Figure 4.7

Figure 4.6 - HyMAP Sunset and Mask Image

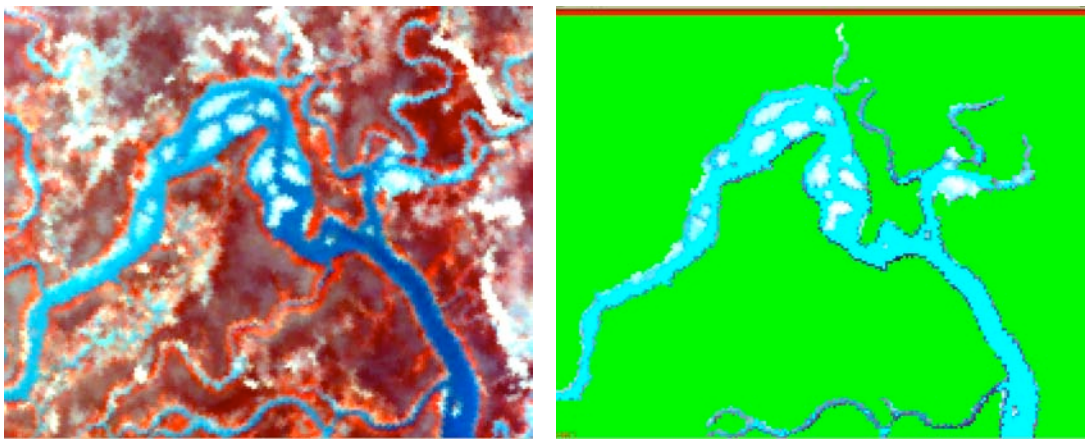

Figure 4.7 - Eigenvalues of ACORN HyMAP 2_44

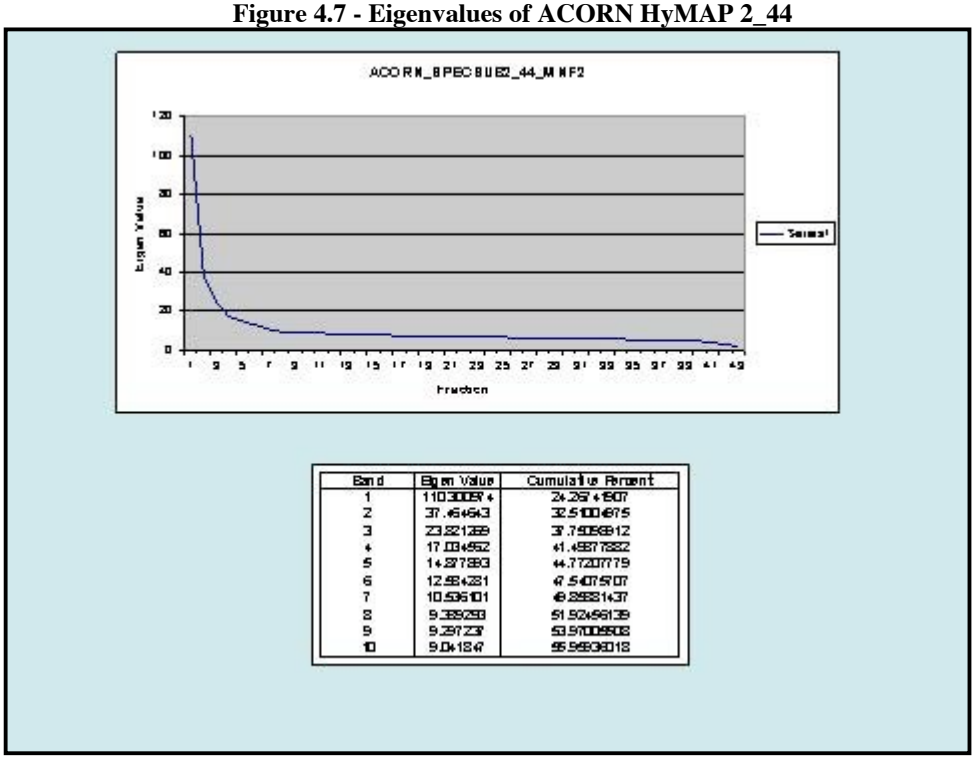

The chart in Figure 4.7 shows a dramatic leveling out of the slope beginning at eigenimage 7 and flattening out by eigenimage 10. The cumulative percent for the first ten images explains almost 56% of the variance. This is an unexpected low value but is consistent with the amount of variance explained with the other subsets that were analyzed for the same image. A visual inspection of the first 10 eigenimages shows by the tenth eigenimage the image cohesion is starting

to be compromised and by the eleventh eigenimage there is no discernable pattern. Figure 4.8 shows the MNF rotation of the HyMAP image.

Figure 4.8 - MNF HyMAP Subset 2-44 Eigenimages 1-6.

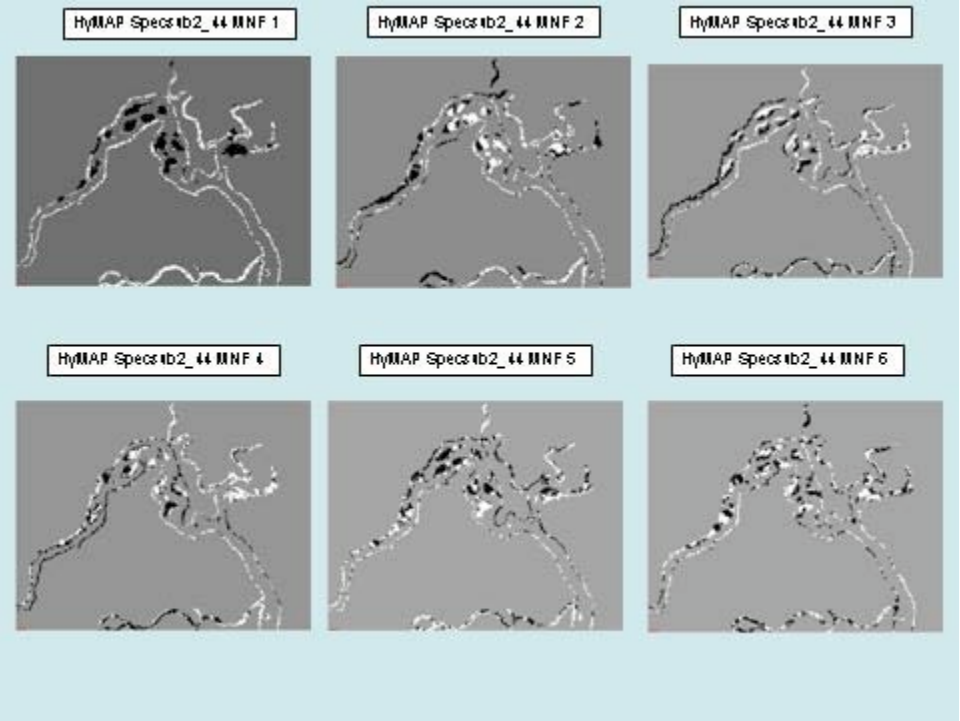

Figure 4.8- Continued Eigenimages 7- 10 HyMAP Subset 2-44

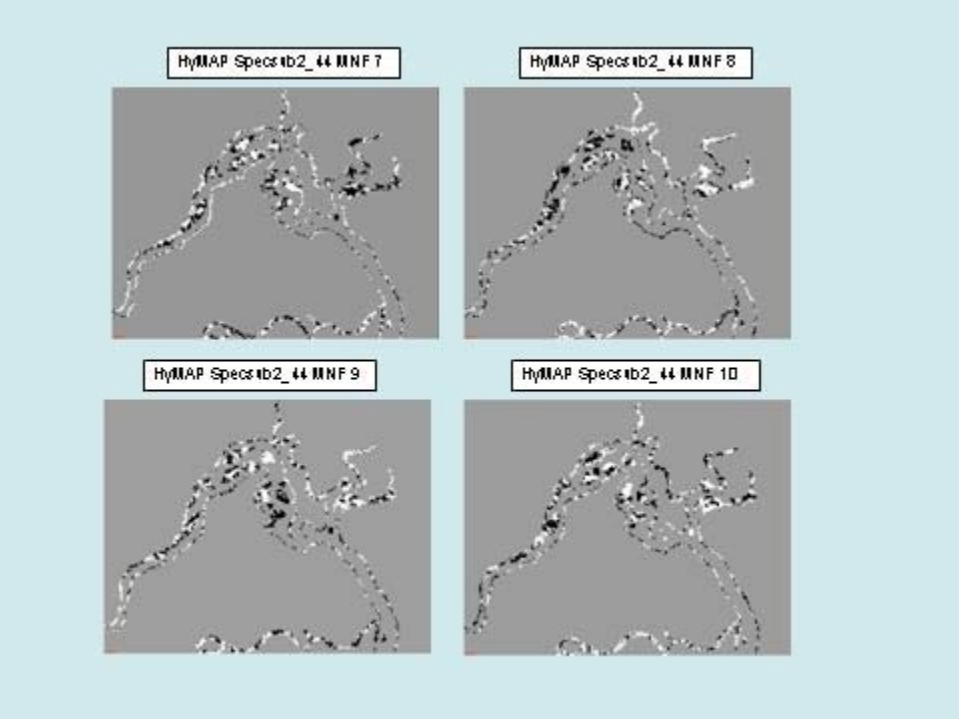

The ten eigenimages displayed show various images that have higher values within the patch reefs but limited information can be deduced from fringing reefs along the shore due to the larger 4.0 x 4.0 m pixel size. Eigenimage 1 highlights the shore, eigenimage 2 appears to highlight the shellfish portions of the patch reefs, and eigenimage 3 being the opposite and highlighting mud. It appears the remaining images highlight various combinations of mud, standing water and shellfish. For the MTMF mapping process the first ten eigenimages were used as inputs.

4.2.2.2 HyMAP Mixture Tuned Matched Filter (MTMF)

The initial runs used the convolved *in situ* spectral endmembers from BOB A through G and the endmembers from a shellfish patch reef located within the subset image. The success of using *in situ* endmembers for identifying patch reef was marginal. This set contained seven shellfish endmembers from the aggregated *in situ* endmembers with all but one resulting in the data range being extremely narrow (the data being centered on zero, representing the suppressed background data). Figure 4.9 shows the endmember BOB E, which is an aggregate of dead shellfish that have higher over-all brightness.

Subsequent mapping efforts centered on BOB G endmembers and refining the selection of endmembers using the 2-dimensional scatter plot with the Infeasibility image. After three more successive rounds of mapping and refining endmembers Figure 4.10 shows the results with a density slice over lay to identify pixels that are highest scoring for shellfish.

Figure 4.9 - MTMF Result for BOB E *In situ* Endmembers

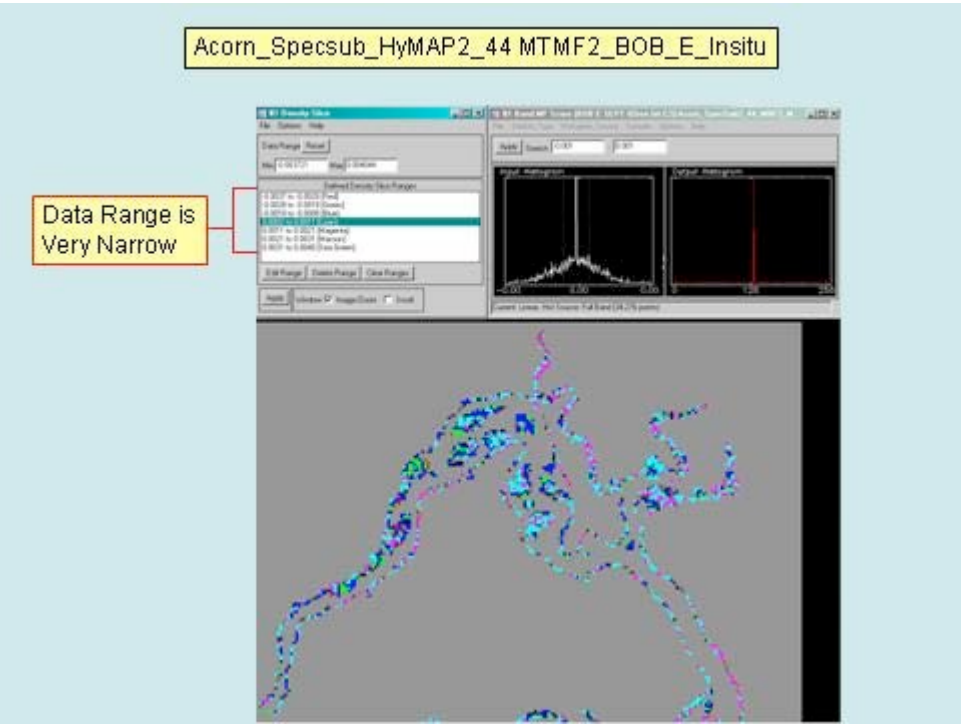

Figure 4.10 - MTMF 5 BOB "G" *In situ* Endmembers

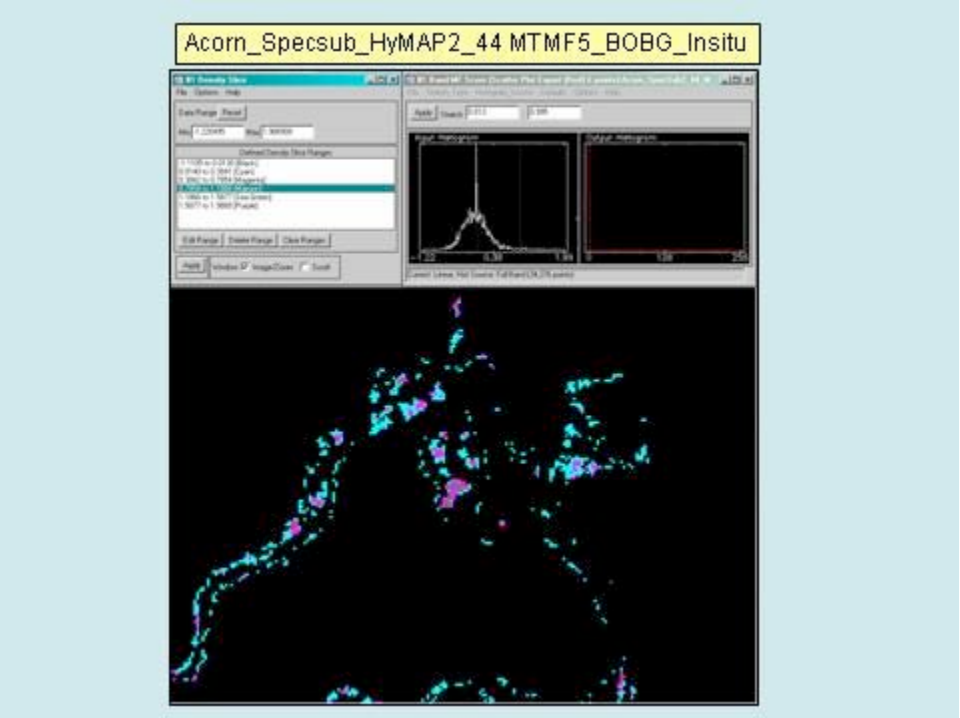

These runs were more promising, resulting in wide data range with values from -1.22 to 1.98. The image in Figure 4.10 was stretched between 0.013 and 0.995 to show pixels that have the highest probability of being shellfish. Of interest is BOB G which is primarily composed of shellfish from BOB 4. This sample site contains live vertical clustered shellfish, not dead washed shells that exhibit higher spectral reflectance. Since the *in situ* endmembers originated from BOB 4 (larger patch reef), it was expected these features would map with a higher probability. This assumption proved correct. In addition, there were additional pixels mapped that showed higher probabilities of being correctly mapped as shellfish on the left side of the image and to the north. Pixels colored cyan indicate a lower probability of being correctly mapped than the sea green and magenta pixels.

4.3 Mapping Image Derived Endmembers From Remotely Sensed Imagery

4.3.1 AISA Imagery Spectral Mapping

The study area for the AISA imagery included the BOB4 study site since this area contained the largest patch reef within the sample sites as well as additional surrounding patch reefs. Figure 4.11 shows both the study site and surrounding patch reefs and the AISA study area with the spectral mask applied.

Figure 4.11 - BOB4 AISA Study Area and Image Mask

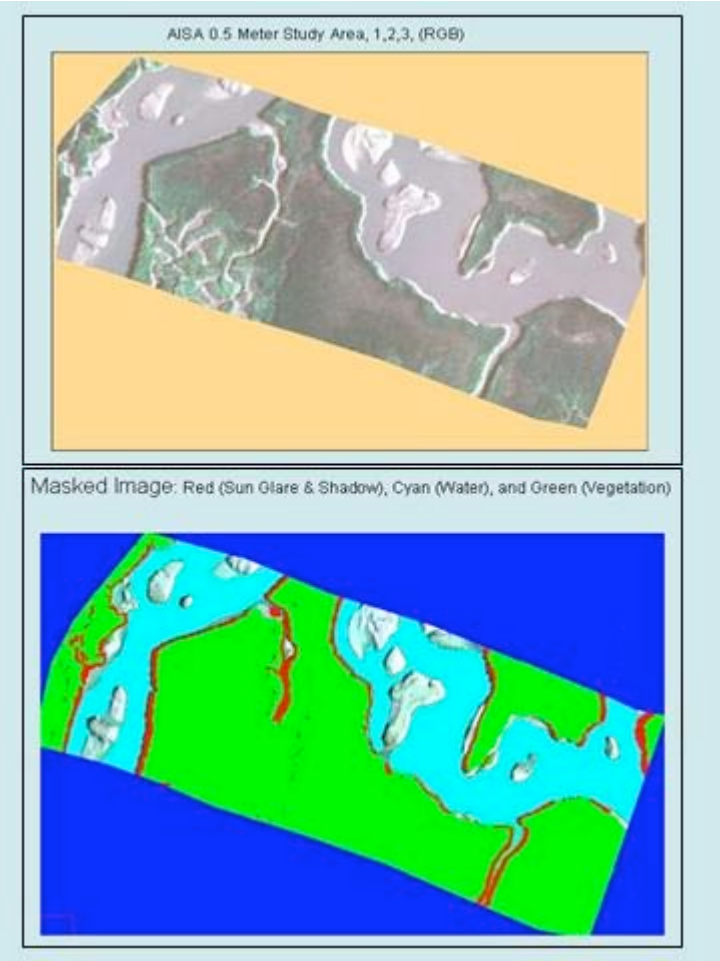

4.3.1.1 ASIA Minimum Noise Factor Transformation (MNFT)

Seven bands of the AISA imagery, with the mask band applied, were used to derive the MNFT. Figure 4.12 shows the graph of the eigenvalues, band weightings, and cumulative percents of eigenvalues. Upon examination of the MNF transformation statistics, it appears that the variance between eigenvectors 6 and 7 show the least amount of change. The first six eigenvectors account for more than 98% of the total variance and looking at the band weightings shows band 7 in eigenvector 2 as having the highest weighting with band 3 in eigenvector 5 and band 4 in eigenvector 3 second and third respectively.

Visual inspection of the eigenimages shows image cohesion starts to be compromised in eigenimage 6 with eigenimage 7 showing no discernable patterns. Eigenimage 5 appears to show the remaining sun glint and shadows that was not masked out of the image. Of interest is eigenimage 1, which shows the higher value areas of mud and higher density live shellfish. Eigenimage 2 represents areas of bright shellfish that are dead on top of the patch reef but in eigenimage 3, it becomes more difficult to interpret as

mud is highlighted with areas of known mud not highlighted. Eigenimage 4 and 5 tend to be more ambiguous and not as readily interpretable but with eigenimage 6 and 7 image cohesion breaks down with very little to interpret within the image. Using the statistics and visual interpretation as described above it was decided to use the first four eigenimages for further processing in the Pixel Purity Index to derive the endmembers for mapping shellfish.

Figure 4.12 - AISA MNF Transformation Statistics

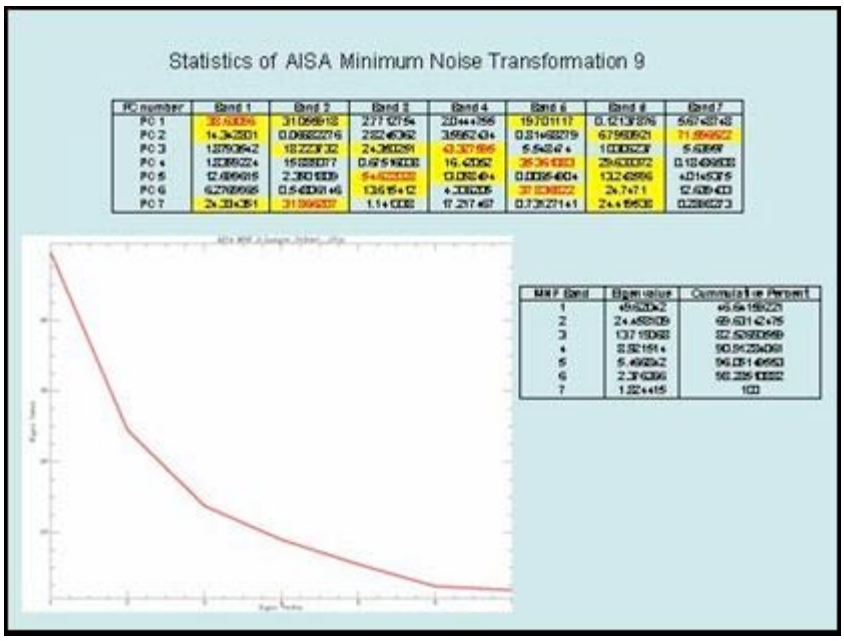

Figure 4.13 - Minimum Noise Fraction Transformation of AISA Imagery

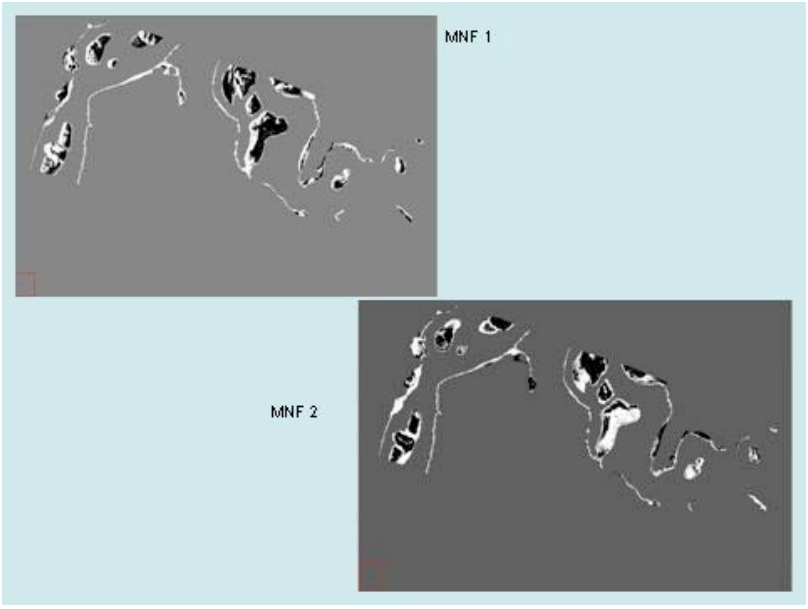

Figure 4.13 - Continued MNF Eigenimages

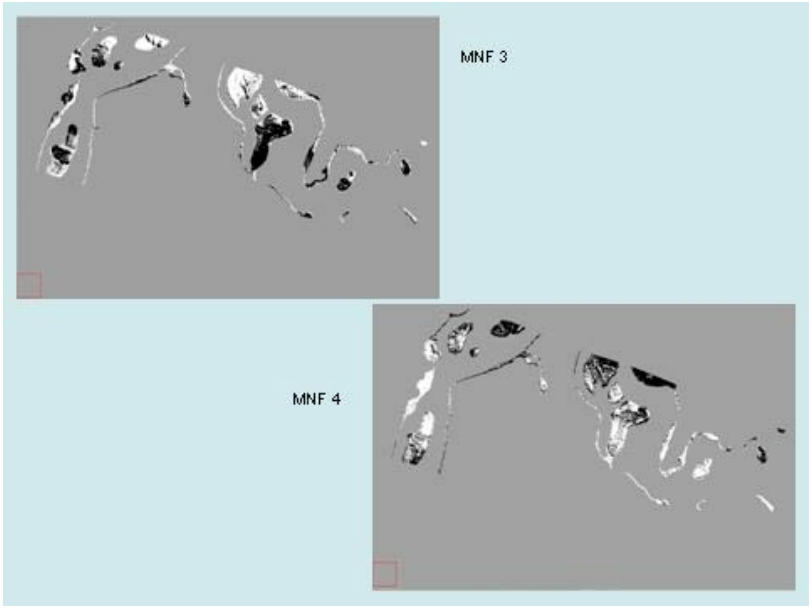

Figure 4.13 - Continued MNF Eigenimages

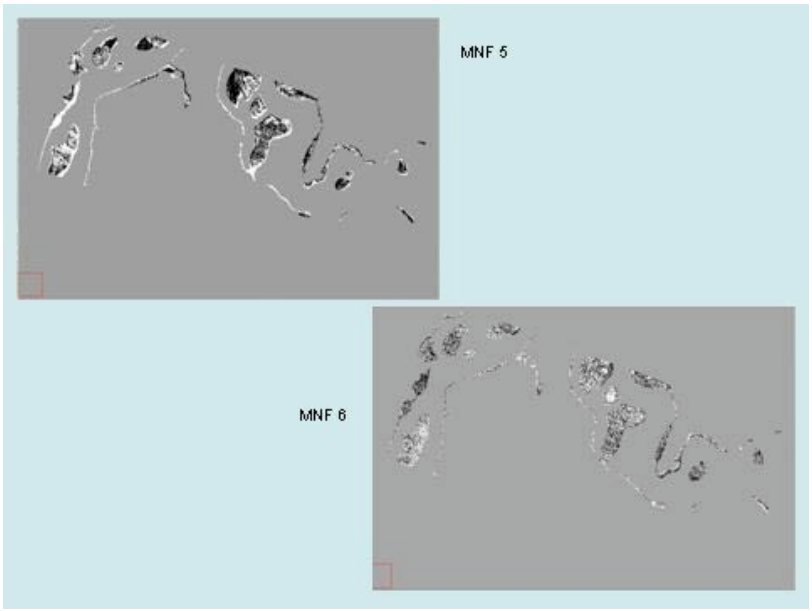

Figure 4.13 - Continued MNF Eigenimages

4.3.1.2 AISA Pixel Purity Index (PPI)

The parameters used for the Pixel Purity Index was a threshold factor of 2 and 10, 000 iterations. The curve describing the number of spectrally pure pixels was relatively flat after the initial round after finding 1853 pixels that were designated as spectrally pure. Figure 4.14 shows the image produced from the process over-laid on the AISA image and density sliced by value for better viewing.

Figure 4.14 - MNF Iteration 9 Pixel Purity Index

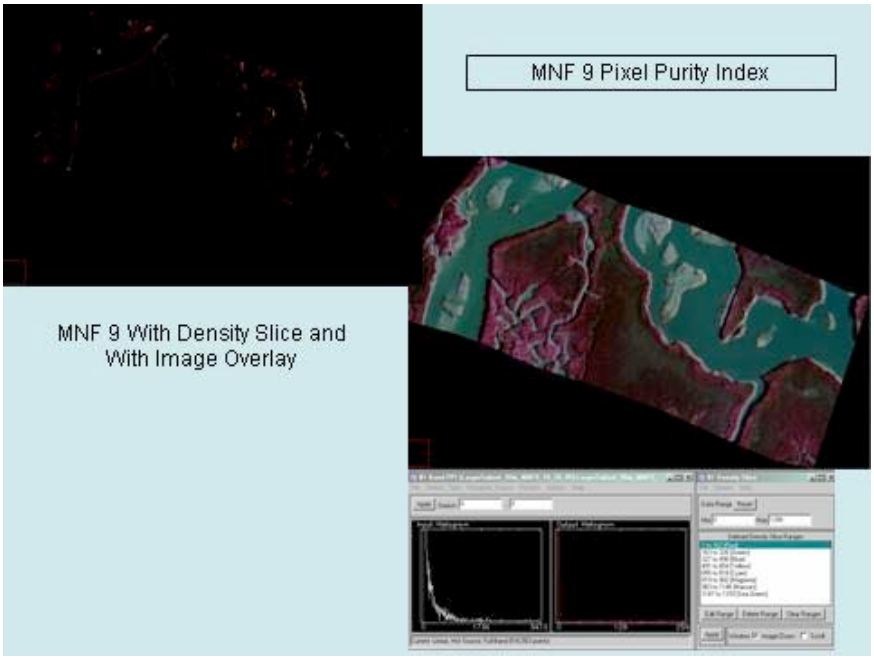

From the pixels that were marked as spectrally pure, these were then processed in the *n*-Dimensional Visualizer within ENVI. The *n*-Dimensional Visualizer assigns the pixels to classes and displays the results of the colored classes visually in a multiple dimensional viewer. The user can manipulate these classes in various dimensional axis' as well as rotate and turn to inspect the data cloud. The user has the option of including additional endmembers within the class or endmember bundle, delete classes or add more classes. The user also has the option of exporting a class of pixels to the Region of Interest (ROI) viewer to view the pixels within the image. This is helpful in deciding if a certain class of endmembers correlates with *a priori* knowledge the user may posses of the image. This inspection of the data is the most subjective portion of the analysis and is discussed in greater detail in the Discussion section. Figure 4.15 illustrates the two classes of endmembers that were collected using this technique. There were 20 endmembers that were collected to represent the shellfish. This was to ensure enough spectral variability to adequately map most or all of the shellfish found within the study area. Only six endmembers were selected to represent the mud class. Fewer mud endmembers were found but this may reflect the narrower spectral variability of mud within the scene. Figure 4.15 illustrates graphically the two classes with the Pixel Purity Index image overlaid on the AISA image for two sample sites within the study area. A final proof of separability between the two classes is the use of a statistical test named the Jeffries-Matusita Transformed Divergence test. The two classes are termed separate if the score is above 1.8; a score below this value indicates they should be merged into a single class. The results of this test yielded a score of 1.895, which indicates these two classes (shellfish and mud) are distinct and separable.

Figure 4.15 - Regions of Interest (ROI) for Image Derived Endmembers - AISA

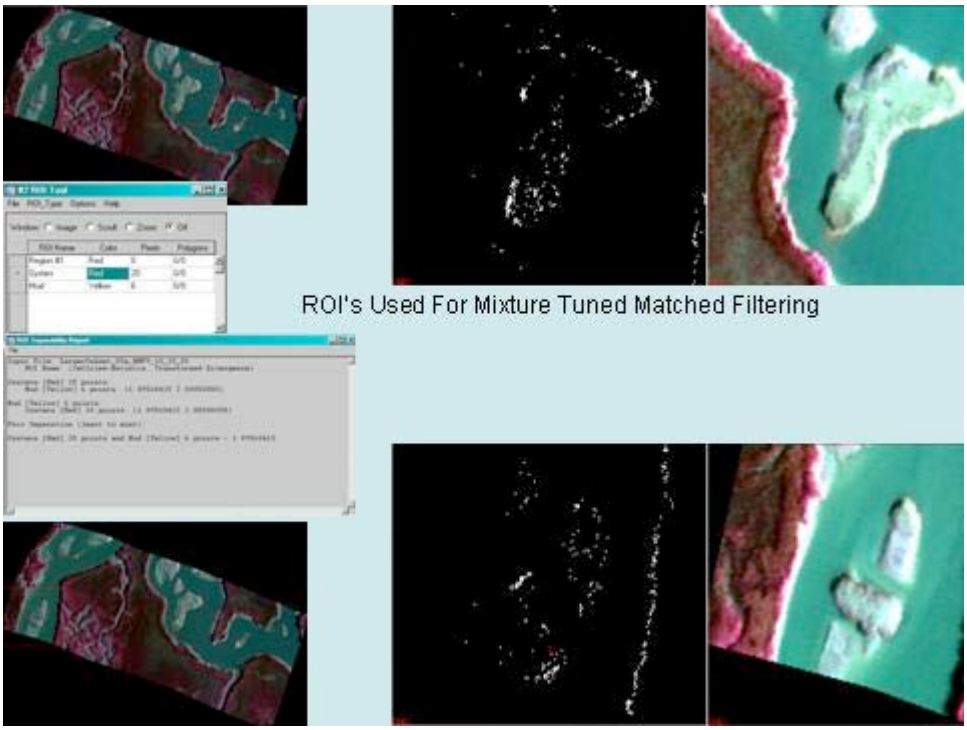

4.3.1.3 AISA Mixture Tuned Matched Filtering (MTMF) Mapping

An MTMF and Infeasibility Score (two images for each endmember) was calculated using the endmembers from the BOB4 study site as input into the MTMF. Results of several MTMF runs are shown in Figure 4.16. This figure shows the pixels mapped as shellfish with values linearly stretched between just above zero (the background pixels) to one. Also displayed is the 2-dimensional scatter plot of the MTMF Score (x-axis) and Infeasibility Score (y-axis) showing most of the pixel values residing between zero and one with a relatively low score on the infeasibility axis.

Figure 4.16 – MTMF Results for Shellfish AISA Imagery BOB4 Study Site.

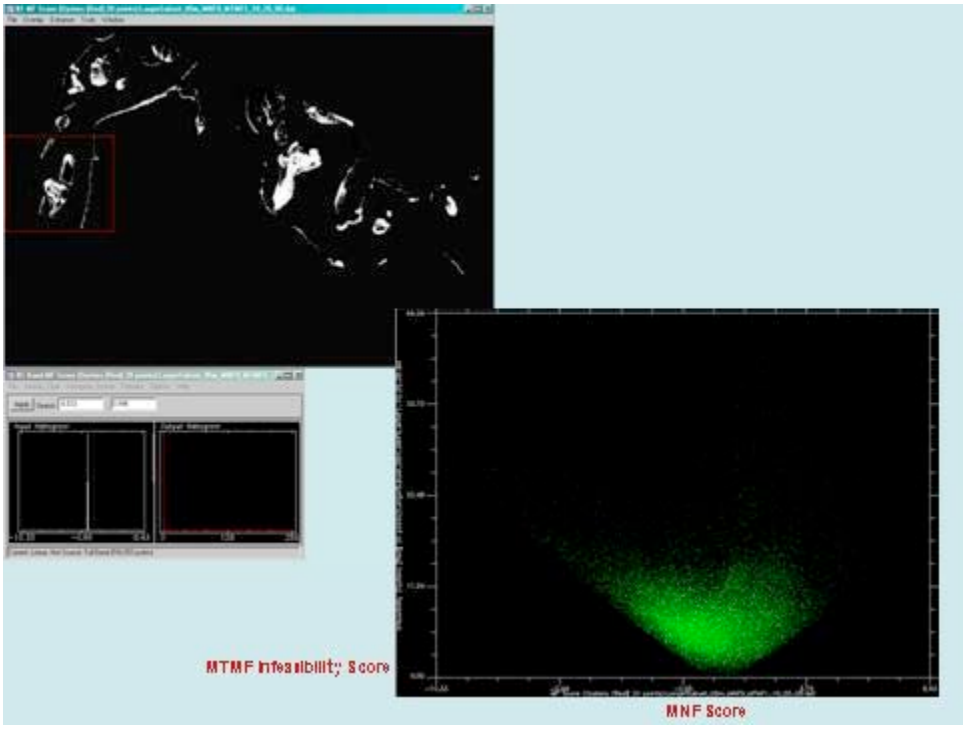

Interactive stretching uses set minimum and maximum values (0.0 to 1.015) and "stretches" those values over the whole range of values that can be displayed. Figure 4.17 shows the results obtained for mud using the MTMF process and stretching the pixel values from zero to one. This image represents mud features, and has values from -0.014 to 0.968 stretched to isolate and map the mud pixels. Notable is the scatter plot showing most of the pixels with the lowest infeasibility values centered near zero to one, thus illustrating a successful endmember mapping process.

Figure 4.17- MTMF Result for Mud Endmember AISA Image BOB4 Study Site

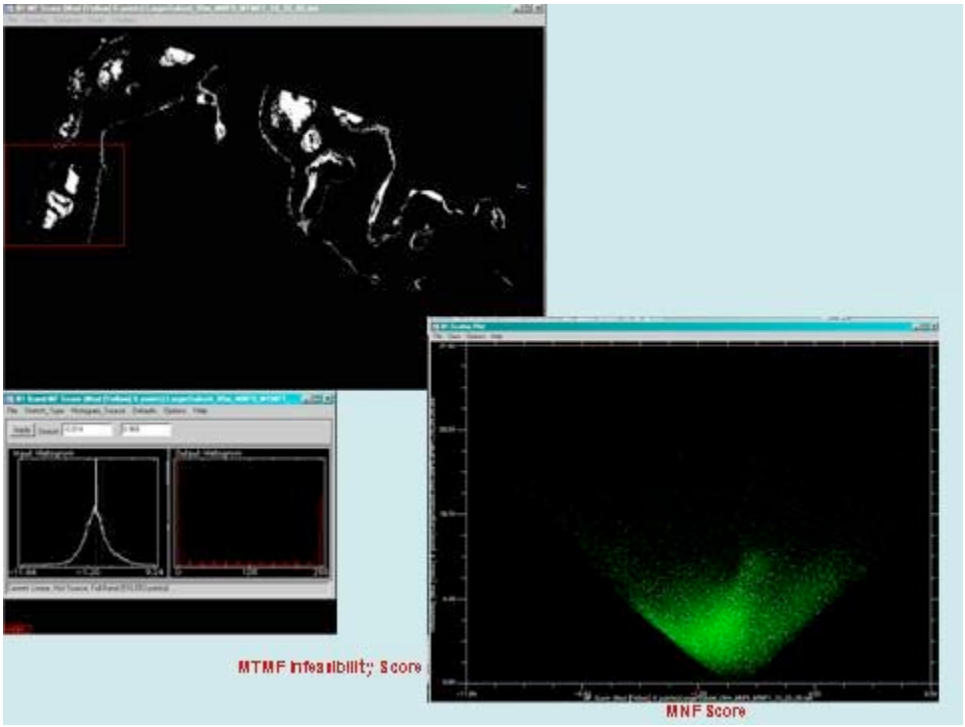

4.3.2 HyMAP Imagery Spectral Mapping

4.3.2.1 HyMAP Minimum Noise Factor Transformation (MNFT)

It was determined that the best subset of the 126-band HyMAP imagery was bands 2 - 61, unlike bands 2-44 that were used for the *in situ* mapping. This difference may be explained by the optimal use of bands and the limitations imposed by using the GER *in situ* data. For example, bands 61 - 126 contribute very little to the weights of the MNFT when bands 41 - 126 or bands 2 - 126 are subjected to the MNFT. This report shows the results from using bands 2-61. Band 1 was not considered due to the prevalence of noise within this band. Since the targeted features were shellfish and mud, a mask was applied that effectively negated water, vegetation and areas outside of the image that would otherwise be considered in the MNF transformation. As previously described, the inclusion of water and vegetation in the MNF transformation skews the eigenimages to favor the water and vegetation, effectively relegating mud and shellfish to the lowest end of the eigenvalues. Any of the subtle variances within mud and shellfish are lost within the larger variances of the vegetation and water. The same mask was applied to the image endmember analysis as was used in the MNF transformation.

All bands between 2 and 61 were utilized in conjunction with the mask band for use in the 2-dimensional feature space viewer. This process resulted in the transformation of each band and the creation of 60 eigenimages, including standard statistics of each of the eigenvalues and transformed bands. Figure 4.18 shows the graph of the eigenvalues versus eigenvectors, indicating the typical steep descent of the curve, followed by a longer flatter curve.

Figure 4.18 - Eigenvalues of ACORN_SPECSUB2_61_MNF1

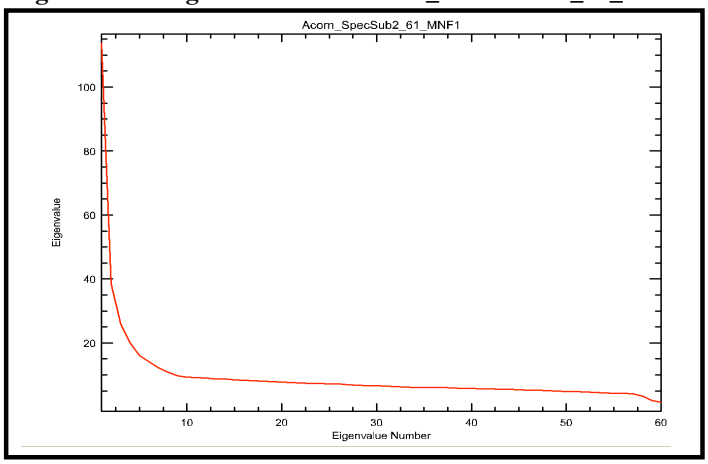

In Figure 4.18, the curve starts to flatten out around the 6th eigenvector and is flat by the 10th eigenvector. When significance between eigenvectors diminishes, very little information is contributed to the explained variance. The ability to reduce the dimensionality of a hyperspectral image is a key component in the analysis of hyperspectral imagery. Since many of the bands within a hyperspectral image have a high degree of colinearity, the ability to eliminate redundant information or information that is of no use, is an important step. The next step was to visually and statistically examine the eigenimages to select the eigenimages that represent shellfish; and eliminate eigenimages that represent noise. Table 4.1 shows the top three bands for each eigenvector that contributed the most to each eigenvector.

Table 4.1 - ACORN_SPECSUB2_61_MNF1 Weights

Band Contributions and Weightings:

Principal Component Analysis for Acorn_SpecSub2_61_MNF1

PC Number	BANDS			WEIGHTS		
PC 1	Band 6	Band 2	Band 3	11.987379	9.2760573	8.5539724
PC 2	Band 8	Band 6	Band 16	29.277465	18.890562	7.220803
PC 3	Band 5	Band 4	Band 12	41.006034	7.734877	6.4461721
PC 4	Band 15	Band 13	Band 19	15.454924	14.655724	9.3147558
PC 5	Band 2	Band 15	Band 26	10.631192	10.335425	8.0594018
PC 6	Band 16	Band 17	Band 35	16.724908	4.6216271	8.6137405
PC 7	Band 28	Band 18	Band 16	8.4118245	7.4878084	6.9099657
PC 8	Band 39	Band 31	Band 20	11.9482	11.251051	9.9917252
PC 9	Band 47	Band 22	Band 16	7.5668694	6.7345066	6.6067521
PC 10	Band 16	Band 50	Band 31	15.394009	8.2520497	7.0312418

Upon reviewing the individual MNFT eigenimages (Figure 4.19), the images become grainy around fraction 9 or 10, because there is no pattern to the light / dark pixels that would correspond to either mud or shellfish. Taking all the pertinent information together, MNFT eigenimages 1 - 10 were more suitable for further refining of the pixels via the pixel purity index. How much of the total variance is accounted for when utilizing just 10 out of a possible 59 eigenimages? Table 4.2 shows the cumulative variance that is associated with each successive eigenimage. With 60 bands and a masked portion of the imagery, the first 8 eigenimages account for 46% of the total variance. This was an unexpectedly low value but could be caused by a number of

factors. Most prominent is the large number of bands used as input. One also must consider that none of the single or group of bands carries a disproportionate amount of the variance in the scene. Hence the variance may be spread out evenly over all the bands. Table 4.2 shows the highest three weights and bands within each of the first ten MNFT eigenvectors. It is difficult to pinpoint at this stage of the analysis, a single band or bands that discriminate shellfish from mud easily. It is safe to conclude that the most optimal bands for identifying mud and oysters are the visible bands (blue, green and red). Although the highest weighted principal component is in component 3 and band 5 (0.4972 μm) is listed as having the highest weighting, with component 2 and band 8 (0.5439 μm) having the second highest weighting. Band 5 is in the blue region of the electromagnetic spectrum and band 8 is in the green region. Although the two bands are relatively close to the lower limit, band 5 is around the maximum transmittance of clear water while band 8 is in the lower area for the detection of chlorophyll. In this case, the presence of diatoms may be influencing the reflectance patterns.

MNF Band	Eigenvalue	Cumulative Percent
Band 1	113.715216	19.68291099
Band 2	38.496547	26.34625944
Band 3	25.867514	30.82365476
Band 4	20.076597	34.29870309
Band 5	16.016936	37.07106669
Band 6	14.004451	39.49509025
Band 7	12.275391	41.61983166
Band 8	10.877002	43.5025266
Band 9	9.760726	45.19200588
Band 10	9.31478	46.80429659

Table 4.2 – Cumulative Percent ACORN_SpecSub2_61_MNF2

Figure 4.19 - Minimum Noise Factor Transformation (MNFT) for ACORN_SPECSUB2_61_MNF1 BOB4 sample site

a. MNF1

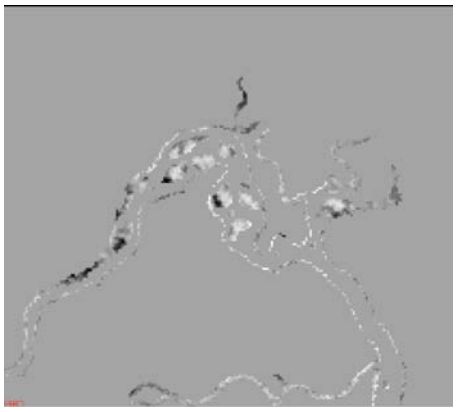

b. MNF2

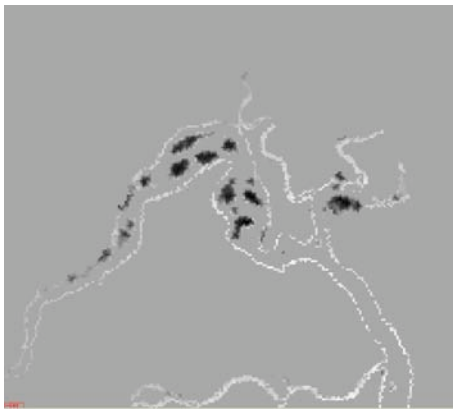

c. MNF3

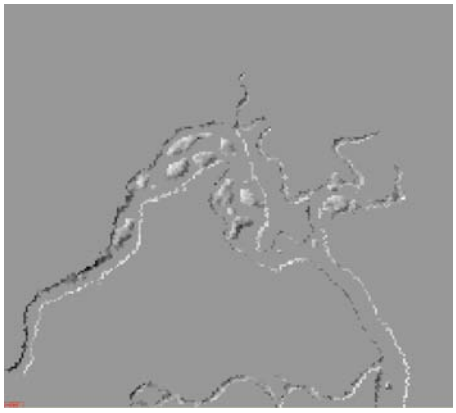

d. MNF4

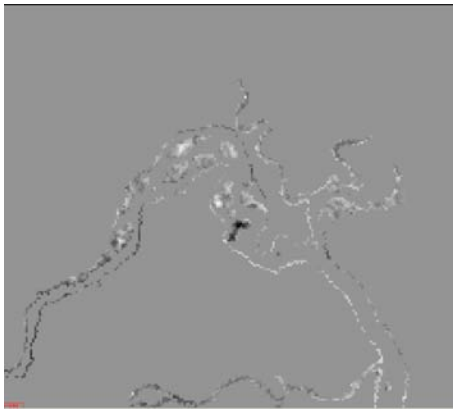

e. MNF5

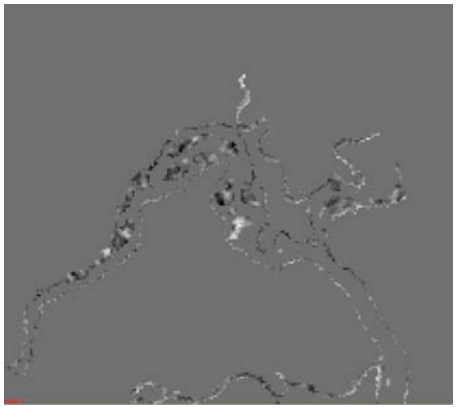

f. MNF6

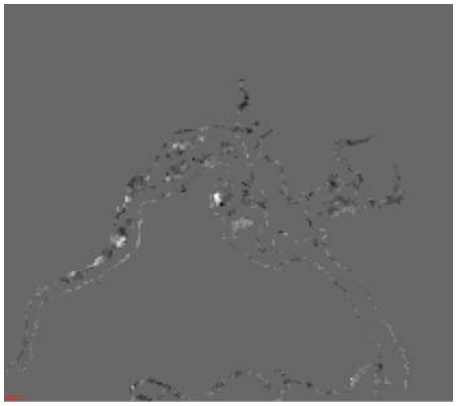

g. MNF7

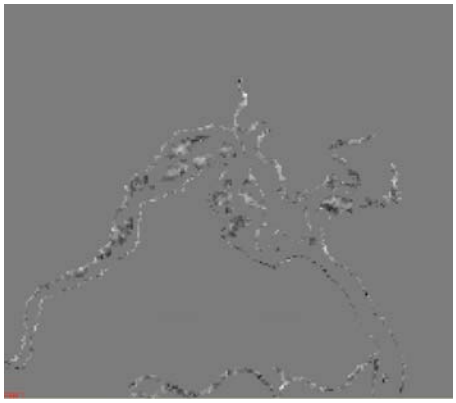

h. MNF8

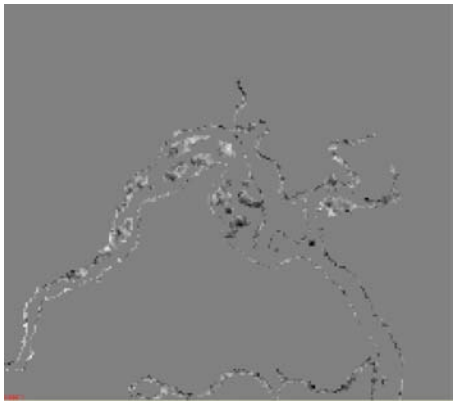

i. MNF9 j. MNF10

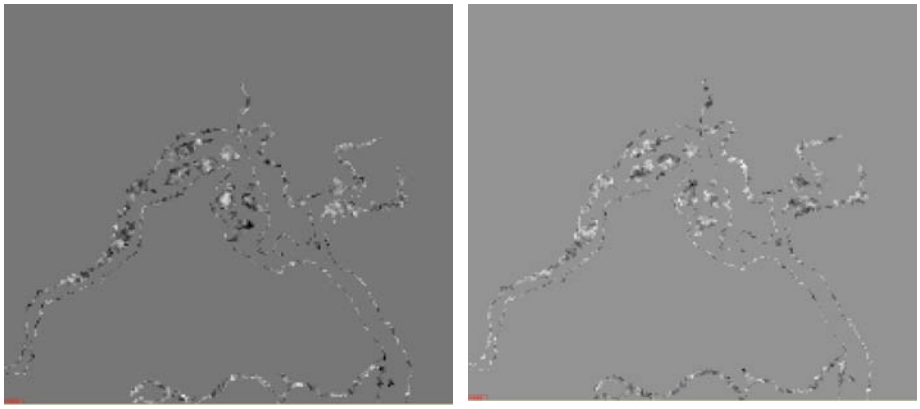

4.3.2.2 HyMAP Pixel Purity Index (PPI)

The Pixel Purity Index for the ARCORN-processed HyMAP image subset was derived using ENVI software. As stated above, the purpose of the Pixel Purity Index (PPI) is to transpose the pixels from the MNFT image into multiple dimensions and rotate the data cloud, then mark the number of times certain pixels on the extreme edge of the data cloud are captured. This technique was derived from the convex hull geometry concept (Boardman, 1993). The purpose is to compile a list of pixels that are the most extreme and thus the most spectrally pure. These pixels are then utilized to map the image for a specific earth material or endmember. There is a large degree of relative objectivity injected by the analyst in the sense that many endmembers have the ability to be selected with varying degrees of pureness. It is up to the analyst to determine which ones are of most utility and represent the material of interest. Additionally, one spectra or endmember may not adequately reflect the full range of spectral variability found *in situ*. To counter this endmember "bundles" with multiple endmembers have been produced to try to encompass the spectral variability. This has limitations since you can only have *n* -1 number of endmembers compared to the number of input eigenimages used in the mapping (Bateson, Asner, and Wessman, 1998).

In the course of this research there was dozens of permutations of the imagery and parameters computed. For purposes of this report, only the results from the most successful runs of the endmember selection and mapping are discussed. The first ten eigenvectors were used with five thousand iterations with a threshold factor of 1.0 resulted in finding 999 spectrally pure endmembers within the image subset. In Figure 4.20, the Pixel Purity results show the full range of the pixel values in a density slice. As a matter of reference, pixels with a higher score are considered more "spectrally pure" than pixels with a lower score (the number represents the number of times the pixel is marked as extreme). Only one pixel had a score greater than 754 (the most spectrally pure) and two pixels were in the 646 - 753 range. From *a priori* knowledge, both of these sets were located within the shellfish reef areas. These sets were utilized as input into the MTMF mapping method and then subsequently refined to obtain more accurate shellfish mapping

Viewing the results, most of the pixels are low scoring and thus do not represent spectrally pure pixels. To isolate the higher scoring pixels, subsequent density slices

were preformed on the threshold values. Figures 4.21 exclusively show the higher scoring pixels as many of the lower scoring and less pure pixels have been eliminated. Figure 4.22 shows the higher threshold and the most spectrally pure endmembers from the PPI process overlaid upon the HyMAP imagery study area (scores labeled). After further refinement of the shellfish and mud endmembers by successive iterations of mapping, the Figure 4.23 shows the endmember results that were used for the final MTMF mapping.

Figure 4.20 – PPI Image showing Full Range of Pixel Values

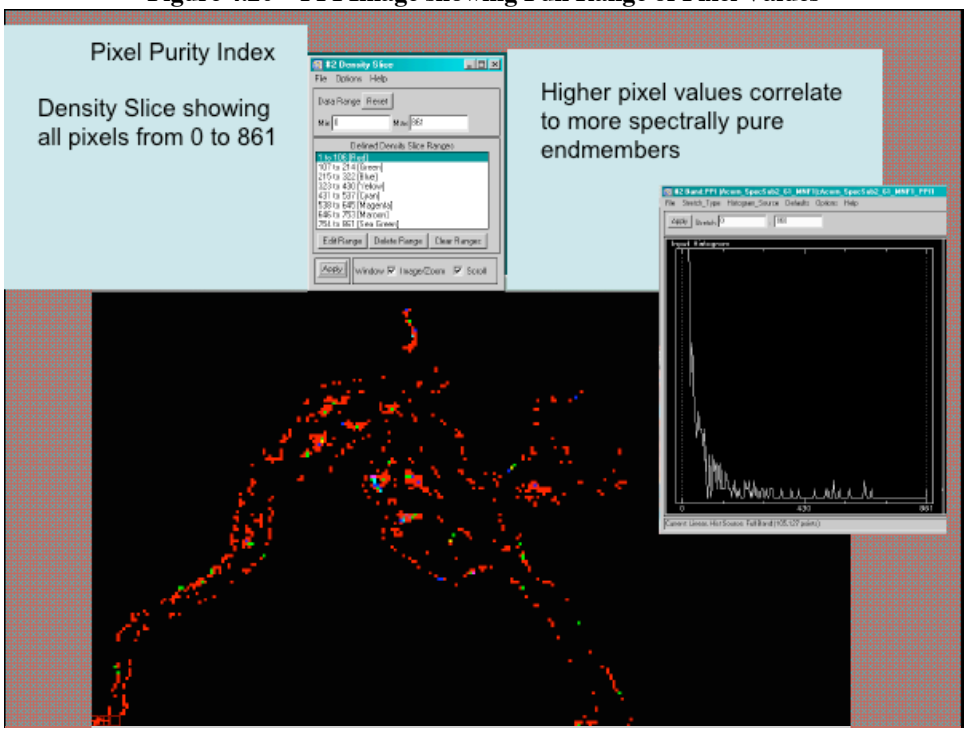

Figure 4.21 - Pixel Purity Index Showing Values From 154-861

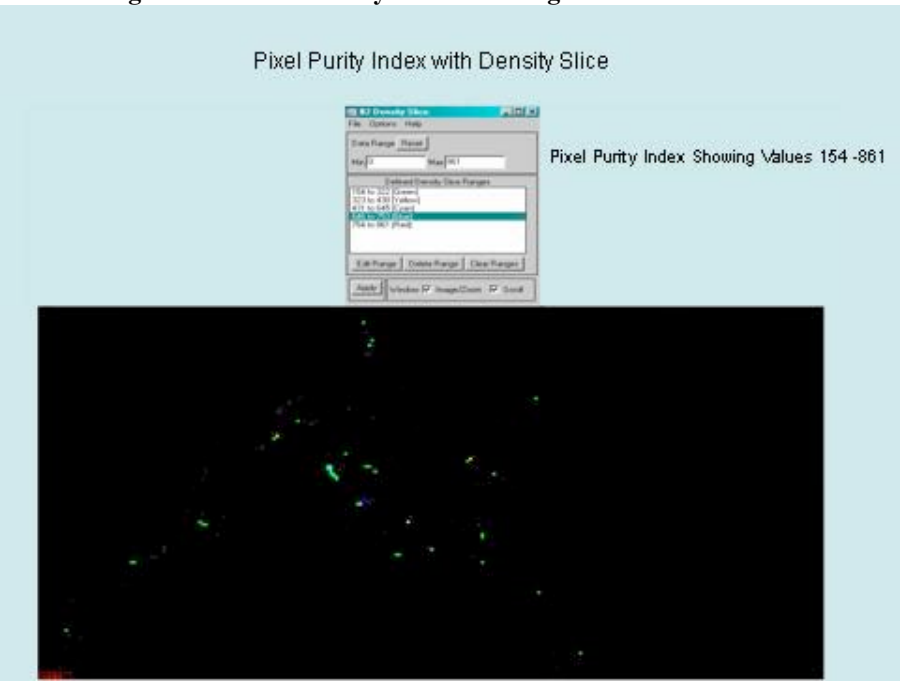

Figure 4.22 - Pixel Purity Index Showing Values From 154-861

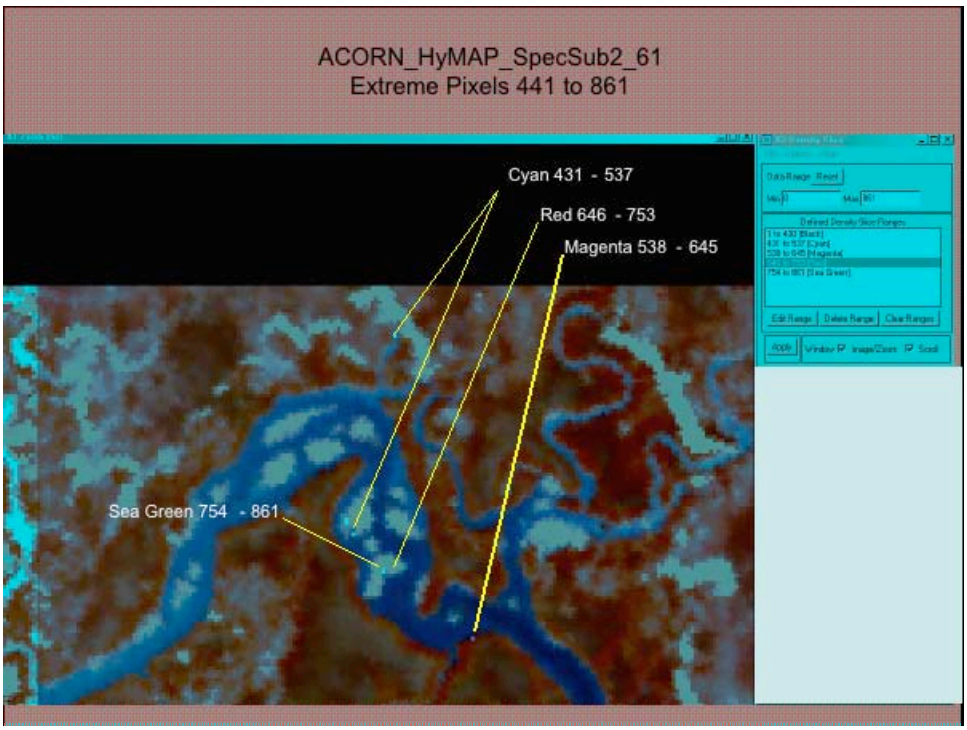

Figure 4.23 Shellfish and Mud Endmembers

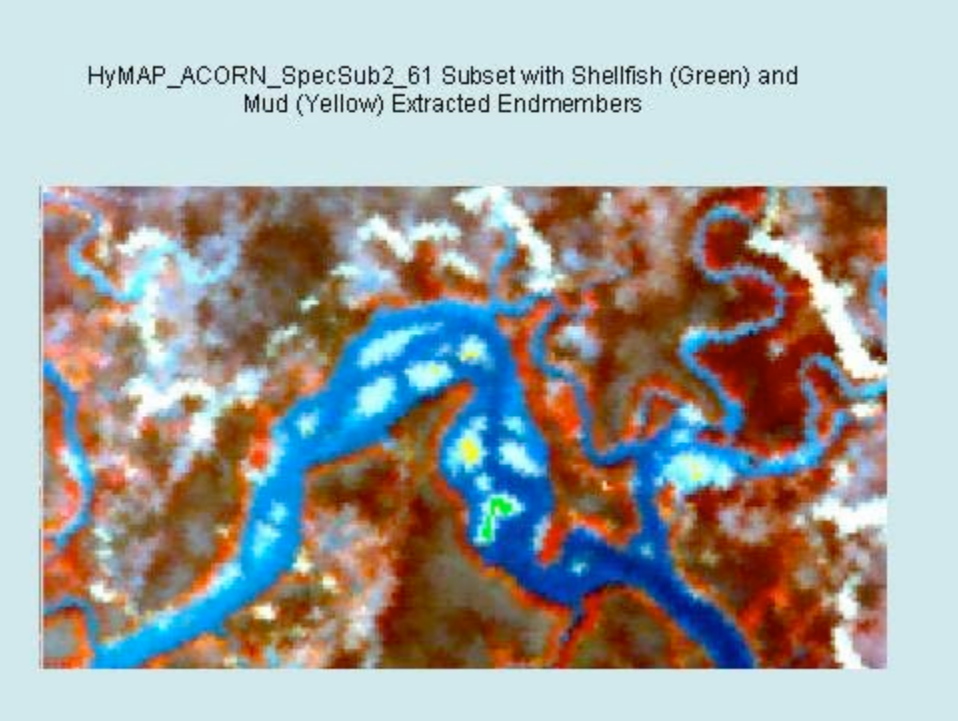

Figure 4.23 shows all the endmembers selected from the field sampling site BOB4 which has a higher spectral reflectance than the surrounding mud patch reef. There are 23 green pixels which are shellfish and 25 yellow pixels represent mud.

4.3.2.3 HyMAP Mixture Tuned Matched Filtering (MTMF) Mapping

The same endmembers were used as input into the MTMF algorithm along with the first ten MNFT eigenimages produced four images, two MTMF Score images and two Infeasibility images (one for each endmember). To aid in visual interpretation, the results are density sliced and color added to the categories. As expected, pixels that were from the location of the endmembers scored the highest and the areas immediately next to and around the endmember locations scored the next highest. Pronounced distance decay is observed with pixels that are further away from the locations where the endmembers were chosen.

Endmember spectra used for input were obtained from the Pixel Purity index rather from the n-Dimensional Visualizer. Since familiarity with the area allowed *a priori* knowledge of the study site, specific endmembers are known to be shellfish or mud. The endmembers are designated for analysis by simply dragging-and-dropping the endmember on to the endmember collection dialog box. Since these endmembers were collected from an image that already had under-gone the MNF rotation there was no need to convert the endmembers into MNF rotated endmembers.

Each endmember that is used as input produces two images: 1) the Mixture Tuned Matched Filter Score image shows the mapped pixels with their DN designating the probability of the pixel matching the reference endmember, 2) an Improbability Score shows the degree of probability of a pixel being not correctly identified. Figures 4.24 and 4.25 show the MTMF Score for shellfish and mud overlaid on the HyMAP subset image

with the values stretched between 0-1 with a density slice. What is interesting to note is that mud is found in the same locations as shellfish although the values of mud indicate a lower probability of correctness where shellfish have a higher degree of correctness.

Figure 4.24– MTMF Oyster Result With HyMAP Image

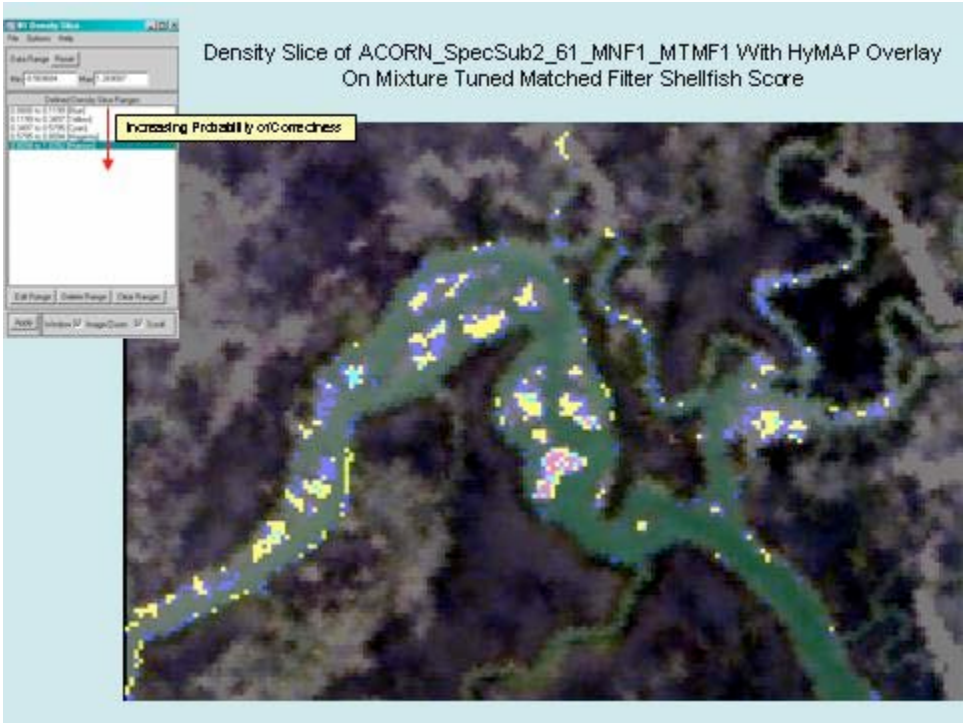

Mud was also found to have a greater areal extent than shellfish, as you would expect. From *a priori* field work, there are areas known to have shellfish that are not scored as having shellfish, there should exhibit some refinement of endmember mapping is subsequent rounds of mapping. Using the 2-dimensional scatter plot of the MTMF Score versus the Infeasibility Scores, we can select endmembers with a high MTMF score and low Infeasibility Score. Figure 4.26 shows the 2-dimensional scatter plot and selected endmembers. The Y-axis is the MTMF Infeasibility score and the x-axis shows the MTMF score. Selection of the endmembers that have a low infeasibility and high MTMF score are shown in the figure.

Figure 4.25 - MTMF Mud Result with HyMAP Image

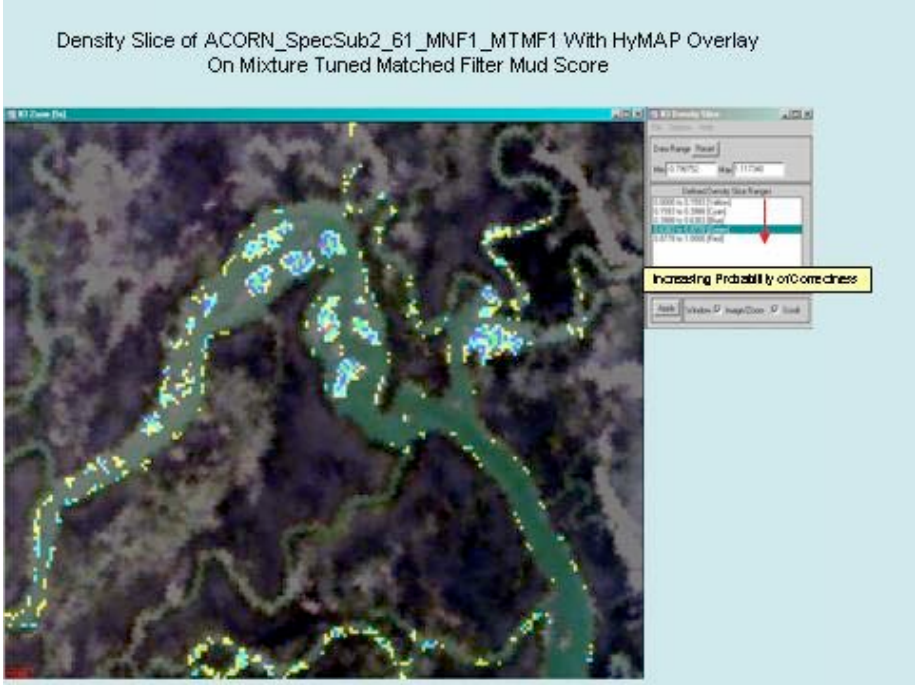

Figure 4.26 - Scatter Plot of MTMF Scores Versus Infeasibility

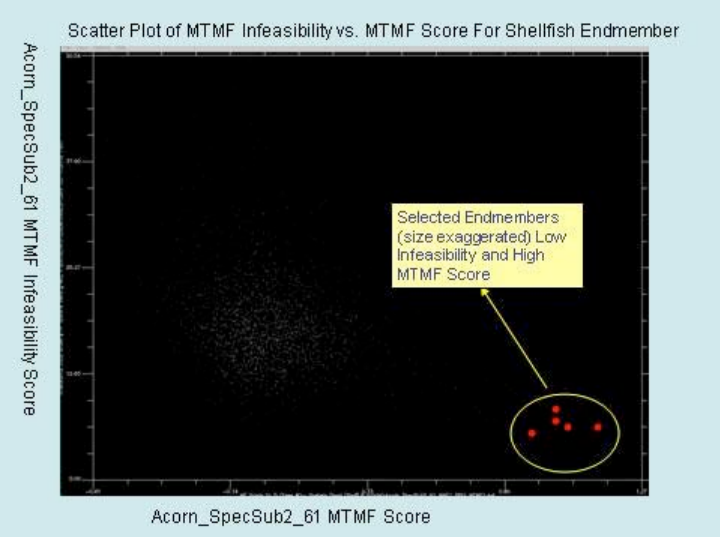

Collection of these endmembers is accomplished by exporting the endmembers and then saving them as library spectra. Once they have been exported they are viewable within the HyMAP subset image. Figure 4.23 above, shows the mud and shellfish endmembers that were exported and saved as library spectra. In the figure showing the location of the mud and shellfish endmembers, the green pixels represent shellfish and yellow pixels represent mud. These endmembers are then stored as a spectral library and used as input into the next round of mixture tuned matched filtering. In the first round of mapping the endmember values of the mapped shellfish pixels were from -0.55697 to 1.2690 and there was a greater amount of fringing reefs.

Second round of mapping produced results that were more focused where the endmembers were located and showed an increase in the range of pixel values. Figures 4.27 through 4.29 shows the mapped results of the second round of mixture tuned matched filtering for shellfish and mud.

Figure 4.27 – MTMF Second Round Mapping of Shellfish

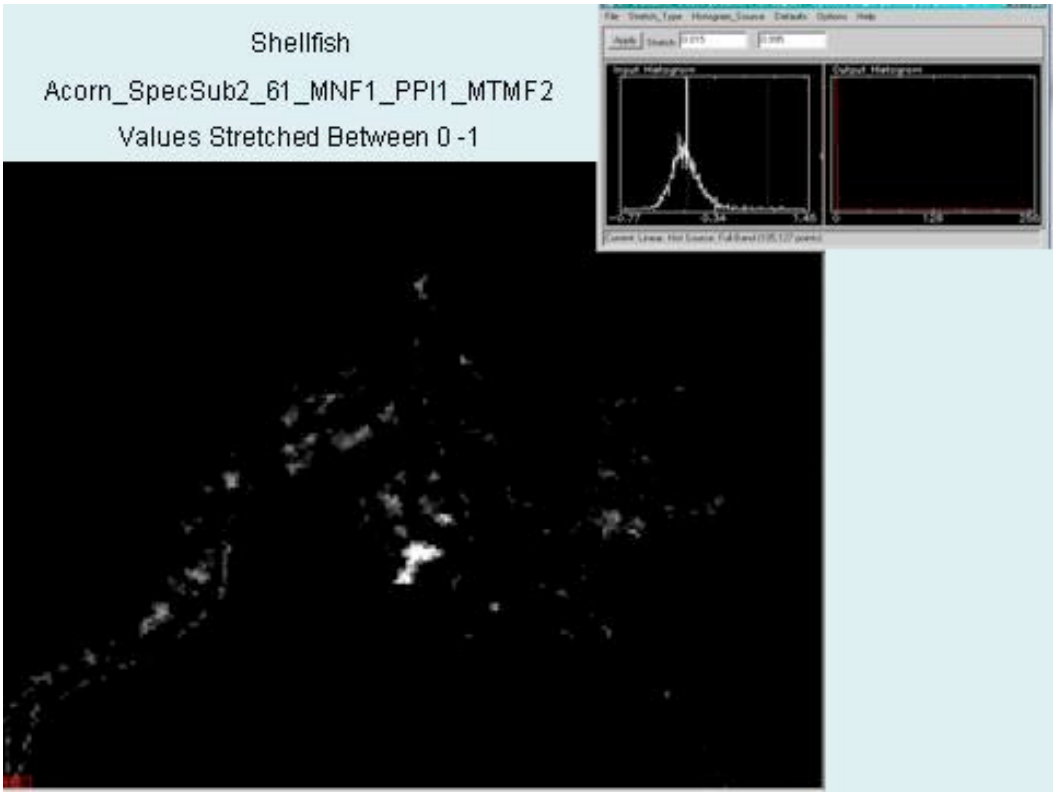

Figure 4.28 – MTMF Second Round Mapping of Shellfish Overlay with HyMAP Image

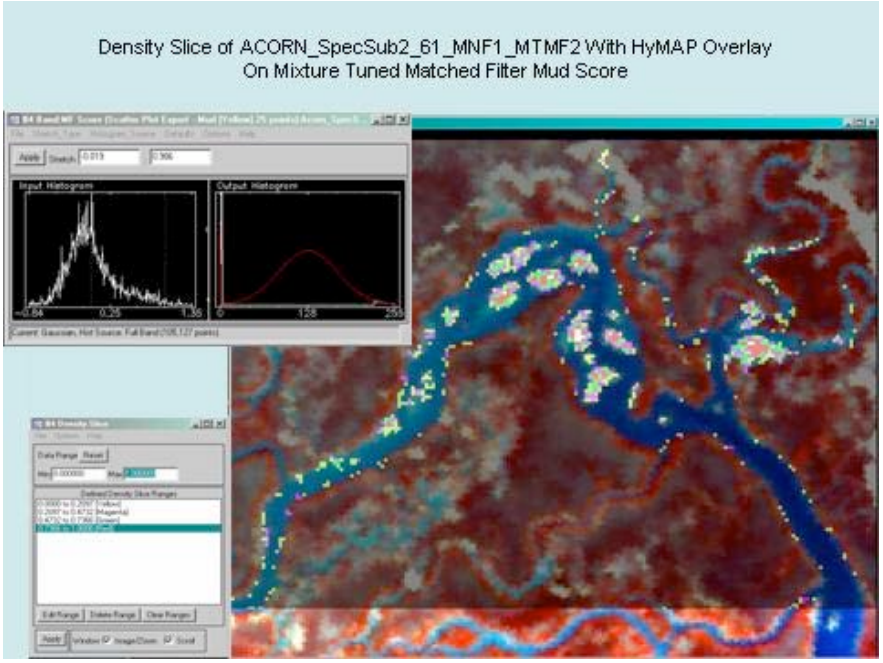

Figure 4.29 – MTMF Second Round Mapping of Mud

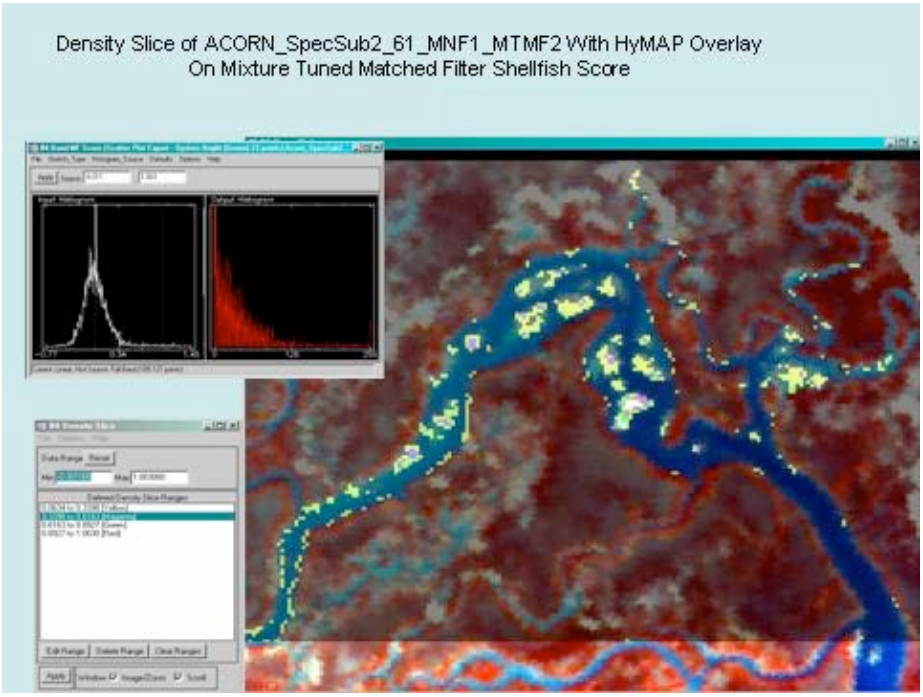

4.4 Mapping Using Visual Learning System's Feature Analyst®

Previous studies conducted by NOAA's Coastal Services Center indicated that Feature Analyst had difficulty discriminating oyster from textured mud, sparse *Spartina* and other marsh plants and their shadows which can be confused with low-profile oyster

with mud (KAPPA = 63.3%) (NOAA, 2003). In this project, both fringing and patch reefs were adequately captured using Feature Analyst although superior results can be achieved in several iterations through testing of input data layers and input representation (Figure 4.30). The extraction of oyster strata could be improved with additional ancillary data (i.e. shoreline) and better ground-referencing polygons of varying classes of oyster strata. Additional field surveys with high levels of detail would help to increase the accuracy of the delineation of the strata through improved training site input.

In summary, Feature Analyst provides:

- Spectral and spatial context in imagery
- Easy-to-use software
- Operation on widely used-GIS platforms (ArcGIS, ArcView, and ERDAS Imagine)
- Hierarchical learning approach to achieve the best results possible

Figure 4.30 Examples of fringing and patch reefs captured using Feature Analyst.

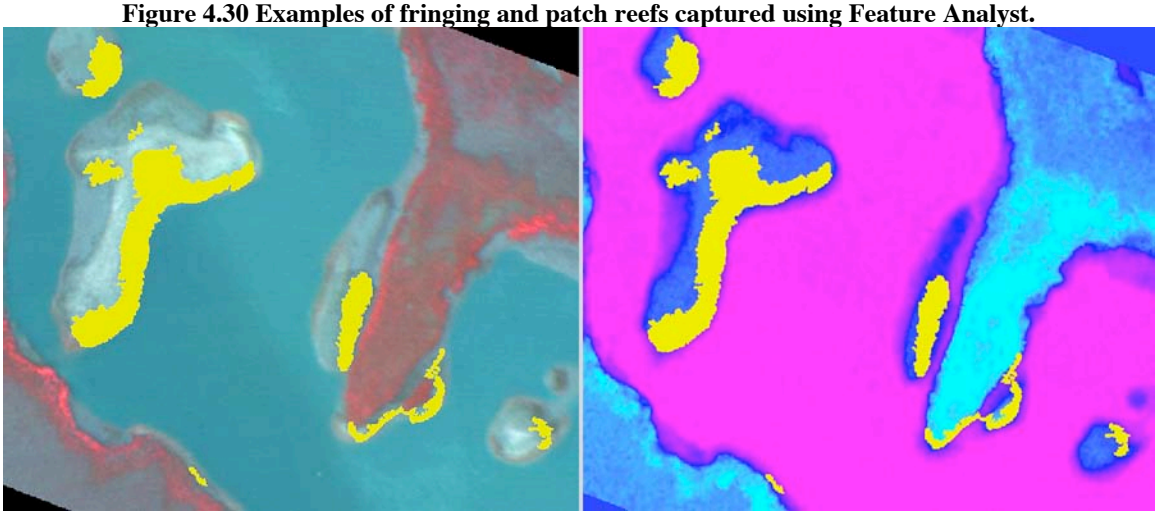

4.5 LiDAR Imagery

The Light Detection and Ranging (LiDAR) imagery was flown by Airborne 1, a commercial data provider, in North Inlet, SC on January 16th, 2003. Two flight lines were run to collect elevation and intensity information of the first and last returns of the laser beam. The flight paths collected data from Jones Creek 1 and 2, BOB's Garden 1 through 4, No Man's Friend Creek 2. LiDAR data were not collected for Jones Creek 3 and No Man's Friend Creek 1. This very dense point coverage, even by LiDAR standards, collected 6,638,640 points with average post spacing of 0.25 meters. Figure 4.32 shows the LiDAR over-laid on 0.69 meter spatial resolution ADAR imagery that was flown in 1999. One aspect of LiDAR is its precise geolocational attributes. The LiDAR elevation data over-laid on the ADAR imagery shows good alignment with the LiDAR elevation TIN coverage (Figure 4.32). The utility of georectification of imagery within the estuary is problematic simple due to the lack of stable and recognizable ground control points within the estuary. Natural features tend to change over time and the number of permanent

anthropogenic features is limited. LiDAR data facilitates the capability of georectifying imagery with acceptable accuracy.

LiDAR imagery was first analyzed using the elevation returns at the BOB 4 study site for shellfish classification applicability. A good visualization tool is the creation of Triangulated Irregular Networks (TINs) from the point data. This product shows quite clearly the water, patch reefs, and vegetated areas. Figure 4.31 shows the elevation TINs that have been classified into nine groups based upon the data historgam. The highest elevation in the study area is the vegetated burm along the shore with the lowest areas being water. It is difficult to determine is the classified elevation data can show differences between shellfish or mud. Although the LiDAR data postings are very close, (0.25 m) there appears to be a lack of vertical displacement between the shellfish and mud in order to adequately differentiate between the two features. Based on this assessment, the utility of using either the first or last returns of the elevation data appears to not contain enough variation to effectively discriminate shellfish classes.

Figure 4.31 - LiDAR Elevation Last Returns TIN – BOB 4 Study Area

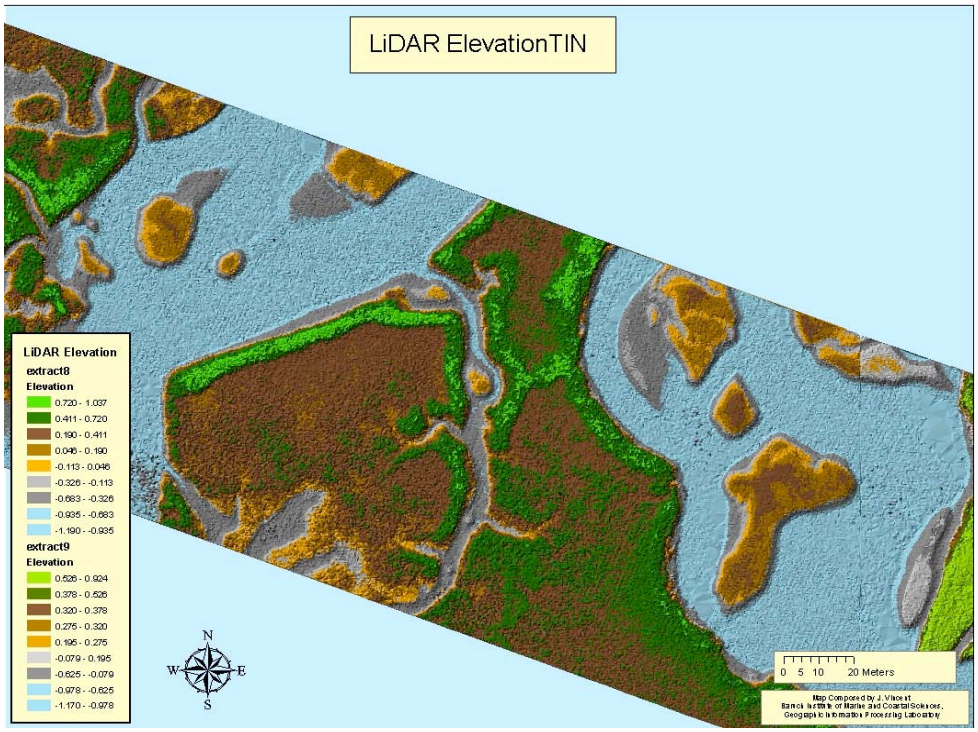

Figure 4.32 - LiDAR Last Return Elevation TIN Over-Laid on ADAR Imagery

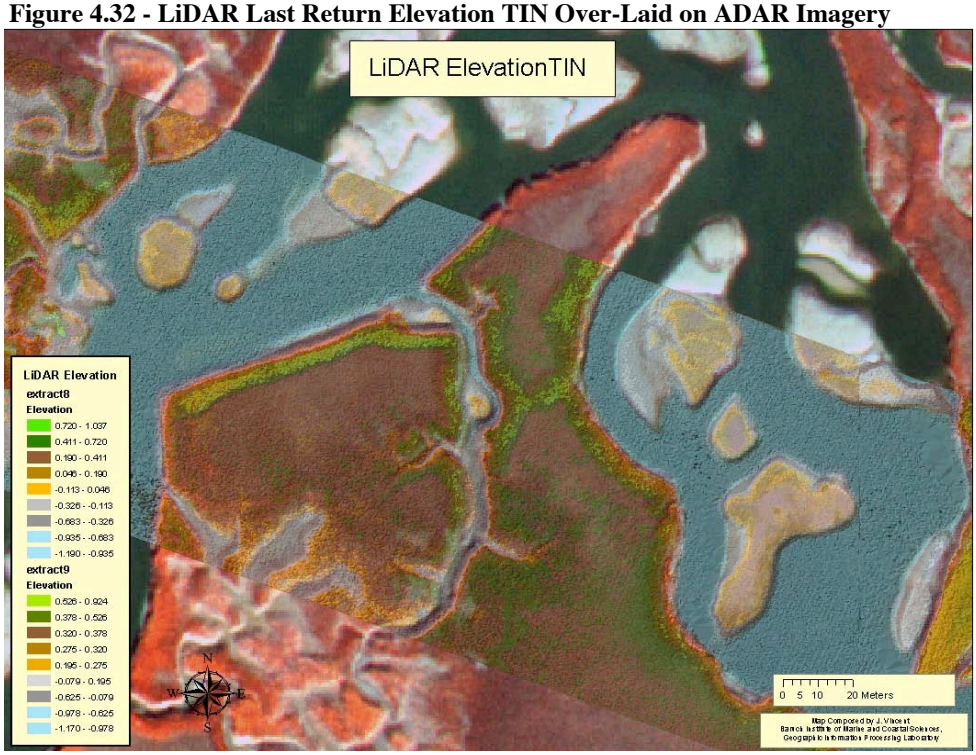

LiDAR intensity values were also assessed for their ability to discriminate between shellfish classes. The intensity of the last returns does not allow for a realistic classification of shellfish assemblages with the data in its original form after being transformed into TINs. As in the analysis of the AISA and HyMAP imagery, points within the patch reefs were isolated that contained both a combination of mud and shellfish areas. A statistical look at the data showed there to be a pronounced skewness to the data. Figure 4.33 shows the intensity of the last returns as a TIN file that was subset from the data. The image cohesion of the TIN intensity last returns is very poor and physiographic features within the study area are barely discernable. Statistics of the selected patch reefs show the highly skewed data. A logarithmic function was applied to the data to produce less skewed statistical data with the following results displayed in Figure 4.34.

Figure 4.33 – LiDAR Intensity Returns

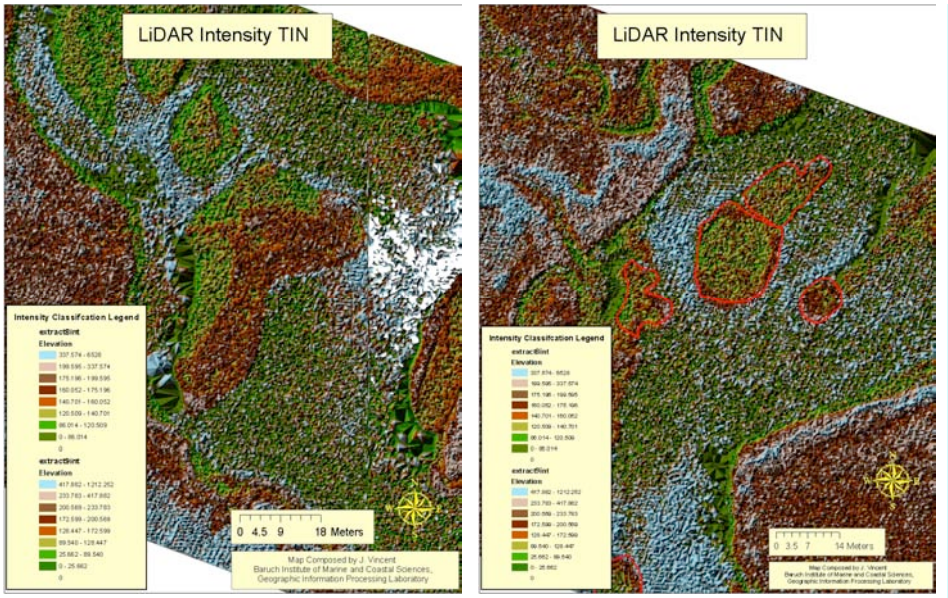

Figure 4.34 - LOG Transformed LiDAR Data

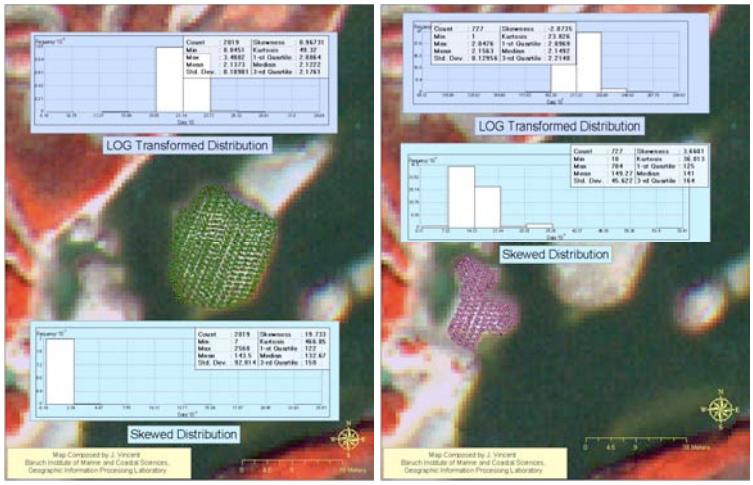

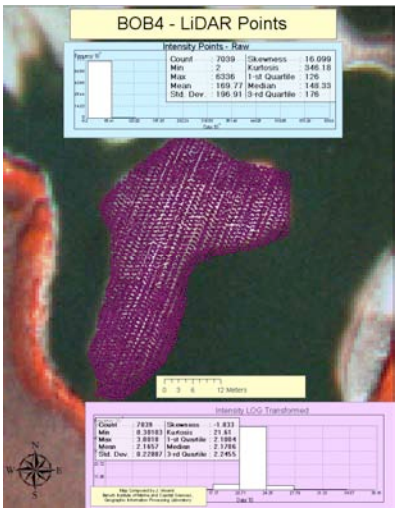

The creation of a raster continuous surface using the interpolation techniques known as Radial Basis Function interpolation was accomplished from the Log transformed points and classified into four classes. This surface is shown alongside the South Carolina Department of Natural Resources (SCDNR) shellfish survey for Bob's Garden in Figure 4.35. It is interesting to note that in the LiDAR log transformed classification there are only three classes of shellfish based primarily on the relative composition of shellfish and mud rather than differences within the shellfish population.

Figure 4.35 - Log Transformed Radial Basis Function of BOB 4 Study Site

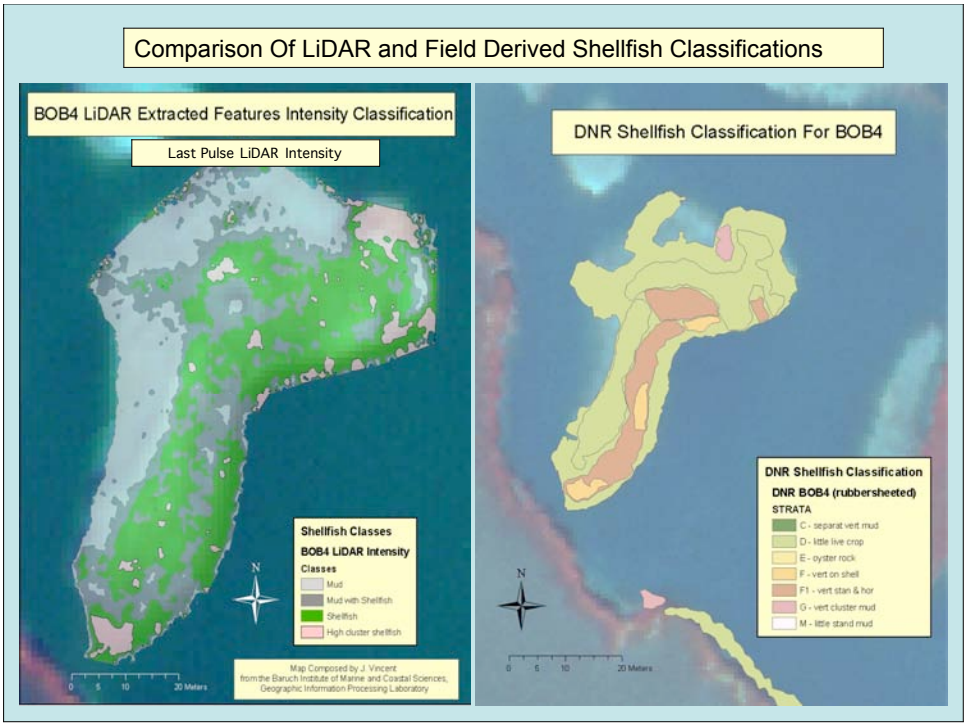

Figure 4.35 LiDAR shows only four classifications, mud, mud and shellfish, shellfish, and higher density shellfish. It should be noted that the pink class of higher density classification (in the upper right portion of the sample site) is actually an area of dead washed shells that repose horizontally. The lower bottom portion the area consists mainly of higher density live shellfish that are vertically oriented.

Figure 4.36 - BOB 4 LiDAR Log Transformed Last Return Using RBF

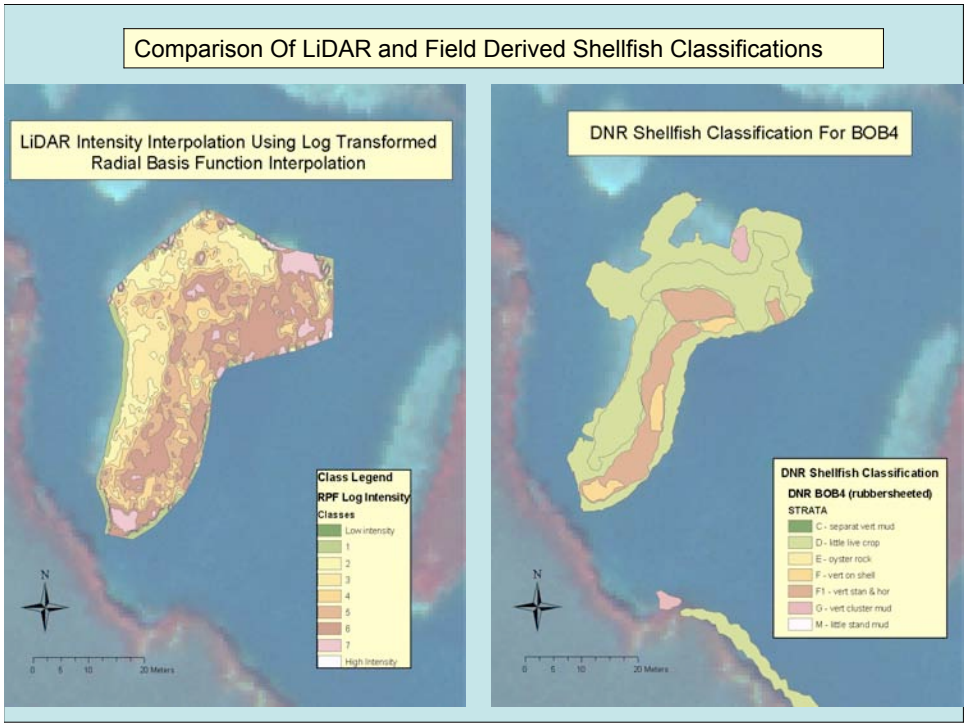

Using the same log transformed data points for the BOB4 sample site, the continuous raster surface was interpolated using the Radial Basis Function (RBF). Using different parameters for the kernel functions and decreasing the neighborhood size, resulted in greater classification sensitivity. Figure 4.36 shows these classifications alongside the SCDNR's field survey for the same sample site. The last intensity returns have the ability to classify the shellfish with greater sensitivity. One downfall of the field sample site is the inability of the surveyor to adequately and objectively classify different shellfish classes. This is partly due to the inaccessibility of the shellfish and the presence of very soft mud that does not allow the surveyor to easily walk the outlines of the shellfish using a global positioning system.

The use of Kriging was applied to the same BOB 4 sample site using the log transformed last returns. As mentioned above Kriging is a geostatistical interpolator that utilizes the autocorrelation relationships of the measured points to fit the line around the predicted location (ESRI 2005). There are many variations of Kriging but the method that was found to have the best results was ordinary Kriging. Figure 4.37 shows the results of using ordinary Kriging with the same log transformed last returns LiDAR points that were utilized with the radial basis function interpolation.

Figure 4.37 - BOB 4 LiDAR Log Transformed Last Return Interpolation Using Kriging

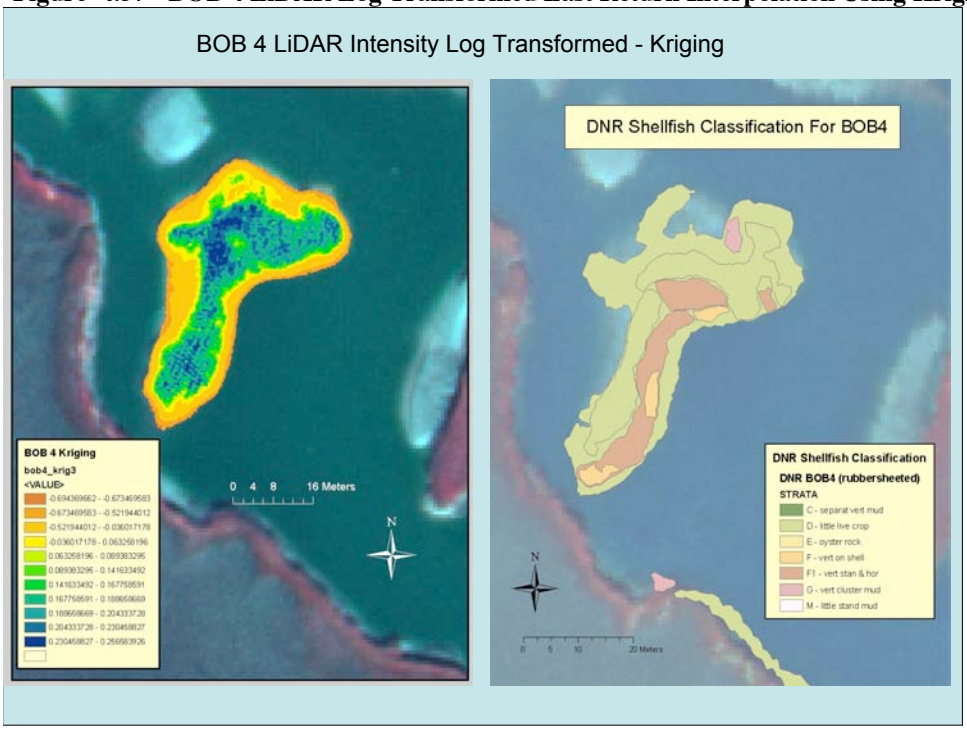

4.6 *In situ* Spectral Comparison of Cape Canaveral National Seashore

In May of 2003, a field excursion was initiated to Mosquito Lagoon within the Cape Canaveral National Seashore Park. The purpose of the excursion was the mapping, spectral sampling and specimen sampling of inter tidal shellfish. Mosquito Lagoon lies at the southern distribution of *Crassotrea virginica* and within the recent past experienced a surge of anthropogenic disturbances in the form of boat traffic through the lagoon and the adjacent Intercoastal Water Way (ICWW). Generally, shellfish mortality in Mosquito Lagoon was observed to be higher and density of live shellfish was less than observed in the North Inlet study areas. The tidal range is considerably narrower in Mosquito Lagoon than the North Inlet study area with vertical accumulation of shellfish reefs within Mosquito Lagoon no observed. Like North Inlet, Mosquito Lagoon displayed creek banks with dead shell piled above the high tide water mark. Presumably from boat traffic wakes washing shells onto the banks.

Since a majority of the shellfish observed at Mosquito Lagoon exhibited a low relief within a humid tropical environment it was observed there was a larger quantity of algal growth on both live and deceased shellfish. Coincident with this observation it was hypothesized the spectral results would indicate a larger shift in the red to infrared spectral regions indicative of active photosynthesis. Figure 4.38 shows a comparison between spectral signatures collected at Mosquito Lagoon and BOB4 and Jones Creek sample sites within North Inlet. The BOB4 sample sites are typical of vertically clustered live shellfish (F1 strata) and the Jones Creek 3 sample site is composed only of washed shell either dry or wet as noted. All samples were

collected in May of 2003. An examination of the chart (Figure 4.38) shows the highest overall reflection were the Jones Creek 3 washed shell both wet and dry.

Figure 4.38 - Spectral Comparison of Florida and South Carolina Shellfish

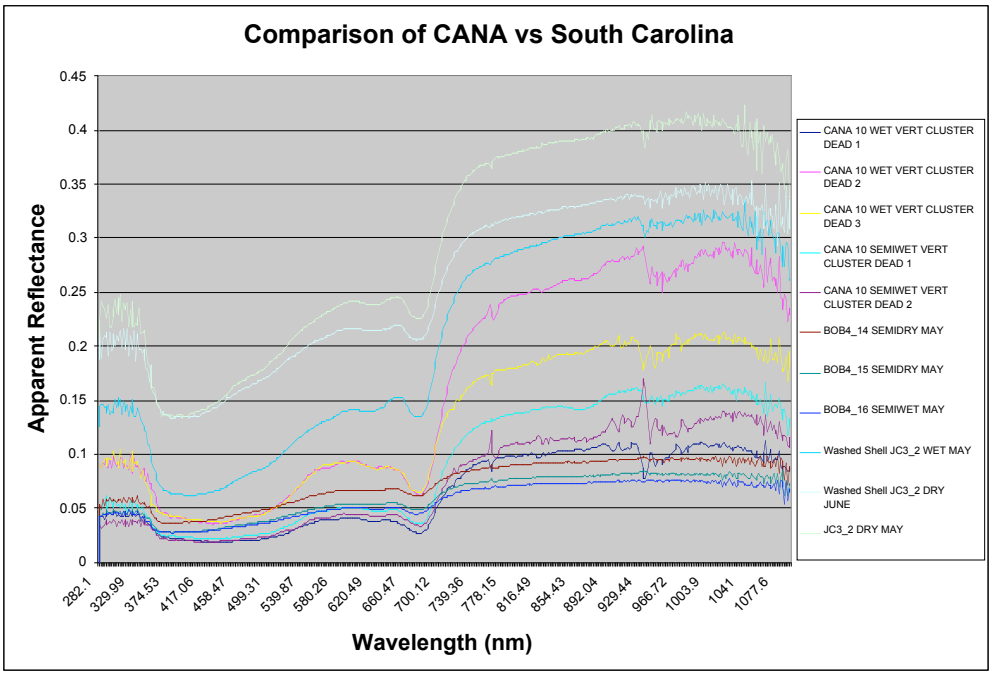

Examination of the chart in Figure 4.38 shows a slightly greater reflectance increase from the red to the infrared spectral regions from the Mosquito Lagoon sample site than from the North Inlet sample sites for either the washed or live vertically clustered shellfish. The spectral samples from Mosquito Lagoon with the vertically clustered dead shellfish followed by the live BOB4 vertically clustered shellfish having the lowest overall apparent reflectance. These results are consistent with the belief that the washed shell from North Inlet spends the majority of time out of water and thus exposed to more of the bleaching effects of the sun and less algal growth. Even live shellfish from North Inlet (BOB4 samples) did not have as large an increase in the red to infrared region as the shellfish from Mosquito Lagoon. This is presumed due to the BOB4 shellfish having a higher vertical relief. BOB4_11 and 12 sample points are from predominately washed shellfish that are situated lowest in the tidal stage and thus spend most of the tidal cycle submerged. It was also observed at these sample points to have the most abundant algal growth within the annual sample period thus providing a close environmental similarity with the Mosquito Lagoon shellfish than any of the remaining sample points within North Inlet. A May spectral sample for BOB4_12 does not exist due to being submerged at the time of sampling so the June dry sample is substituted. The May BOB4_11 sample that is represented was taken while the shellfish were wet. Figure 4.39 shows the chart of the Mosquito Lagoon samples and the North Inlet Samples of similar shellfish strata.

Figure 4.39 – Mosquito Lagoon and North Inlet Shellfish: Lowest Lying

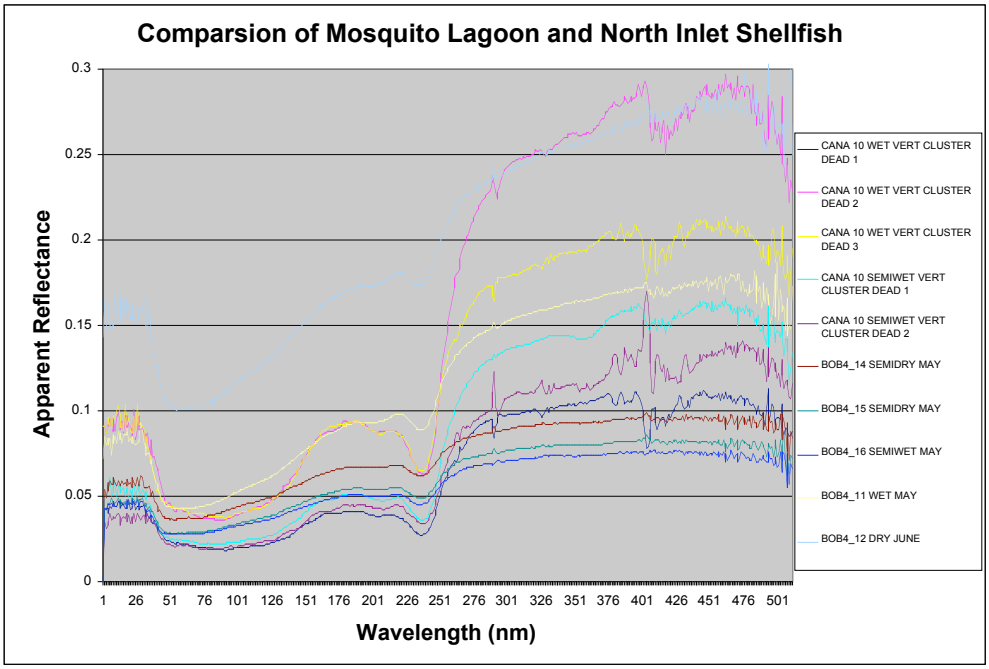

Examining Figure 4.39 shows the shellfish from North Inlet having a lower reflectance with the exception of the June BOB4_12 dry sample but the Mosquito Lagoon shellfish exhibit a greater red to infrared spectral region shift and the presence of a deepening "photosynthesis well" that occurs approximately at 690 nm that is synonymous with photosynthesis activity.

5.0 Discussion

Creation of a spectral library from a year of field sampling has provided the research community the ability to classify imagery with *in situ* endmember sets that have a wide spectral range of environmental conditions and oysters strata. There is the ability to also match field spectral data with remotely sensed data for a specific calendar month to attempt to match any seasonal variations. Statistical or remote sensing software allows the user to convolve the field data to match the remotely sensed imagery from the visible region through the shortwave infrared regions is a useful for using the field data with any remotely sensed platform. Problems occur when dates or seasonal variables do not match the variables inherent in the remotely sensed data. Additionally, *in situ* data provided a statistical inference to describe the huge spectral variability that occurs in and around the sample sites and the ability to compare this data with the statistical variability found in the image shellfish. Discrepancies occur between the *in situ* data and the remotely sensed data due to differences between the sensors, radiometric correction, atmospheric correction, time of day (sun angle), and even changes over time that occur to the habitat being sensed. Even when seasonal variables are kept constant, obtaining similarity between data sets can be problematical. Best results for spectral analysis have been found from utilizing image derived endmembers for the above reasons.

When using remote sensing techniques, to effectively detect and map objects, the sensor and platform must be appropriate to object being sensed (Jensen 2000). The spectral analysis portion of this research utilized HyMAP (4.0 x 4.0 m and 126 bands) and AISA (0.5 x 0.5 m and 7 bands) imagery. The object of interest was individually quite small (~15cm long) which required higher spatial resolution imagery to effectively detect and map the feature. However, the areal aggregation of oysters provides a greater target for detection, identification and mapping using HyMAP imagery. Within the larger areal aggregation, there is a much higher spectral variability so deriving image or *in situ* endmember bundles (that adequately encompasses all the spectral variability) becomes much more difficult. For the purposes of detecting, identifying and mapping oysters, the idea of a spectrally "pure" endmember that resides at the extreme point area of the data cloud is not practical or feasible. Instead, the utilization of higher spectral resolution imagery with as many spectral bands as possible is optimum for identification, detection and mapping of oysters. Our research showed that the AISA imagery was able to identify, detect, and map individual oyster clusters more accurately than the HyMAP imagery. Although the HyMAP pixel contains a greater degree of spectral information, the larger pixel size makes it more difficult to map individual groups of oyster strata within the pixel. Using the Linear Mixture Analysis, we can derive the fractional abundances of each of the endmembers within a pixel, but it does not delimit the oyster strata within the pixel. Using remotely sensed imagery with high spatial resolution, allows the visual discrimination of groups of oysters and to a small extent the oyster strata. Oyster health was initially tied to the ability to derive oyster strata. This research to date has been unable to classify oyster strata beyond the extreme ends of the spectrum. Bright shell (washed shell) with mostly dead oysters and few live standing oysters ("D" strata) and higher density live oysters that are vertically oriented ("A" or "E" strata).

The use of LiDAR data for classification purposes by itself has limited utility using elevation data. The LiDAR data was acquired with a high level of point densities that permitted close point spacing with the intent to infer "roughness" or "smoothness" in differences between oysters (rough) and mud (smooth). The level of vertical accuracy between points was not sufficient enough to adequately derive an index of roughness with a degree of known confidence. The use of the intensity returns has proved to be useful in delimiting areas on the patch reefs that have discernable differences in their reflective properties. As shown in the LiDAR Results section, there is a correlation of types of materials present in the scene and the level of returned LiDAR intensity. Due to the angles of light incidence bright washed shells tend to have higher level of reflectance than mud or live oysters. Vertical oysters show a more diffuse or scattered light effect and thus a lower intensity return than either of the washed shells or smooth mud surfaces. Future research should explore utilizing the classification of oysters from the LiDAR intensity returns as training inputs for Visual Learning System's Feature Analyst to classify AISA or high spatial resolution imagery.

A major aspect of utilizing either spectral analysis with hyperspectral imagery or LiDAR datasets is a substantial investment in computer, software and technical expertise. The amount of time for human and field collection of data for training purposes can be a substantial portion of costs that are dedicated solely to the analysis of hyperspectral

imagery. The integration of GIS into the process adds further expense to the investment. An advantage of the Automated Feature Extraction techniques is the time required for a user to become relatively proficient at extracting objects of interest within remotely sensed imagery. Additionally, the software is embedded within many popular GIS software packages, thereby making the results more fully integrated. It does not preclude the time and expense of having to acquire remotely sensed data for analysis but high spatial resolution imagery is becoming more commonly found for multiple uses within county and urban planning.

Adequate masking of the remotely sensed data is an important step in the mapping process. Masking of the of the BOB4 study site in the AISA imagery was needed to eliminate the presence of sun-glint and shadow. The imagery was acquired in the earlier portion of the morning so portions of stream bank areas on the west sides showed a pronounced sun glare, while portions of stream banks on the east side were in shadow. To address this problem, the areas of highest glare and shadow were masked out. This was done, rather than normalizing the data, since it becomes a question of what the values in the areas of shadow and glare should be, without knowing if the areas in question are mud, shellfish or water. The spectral value of those pixels can only be determined if a spectral reading is obtained at the location at the time of image acquisition. Figure 5.1 shows a horizontal spectral profile within the BOB4 study area and identifies spectrally and spatially areas of glare and shadow.

Figure 5.1 - Horizontal Spectral Profile of BOB4 Study Area – Shadow and Sun Glare

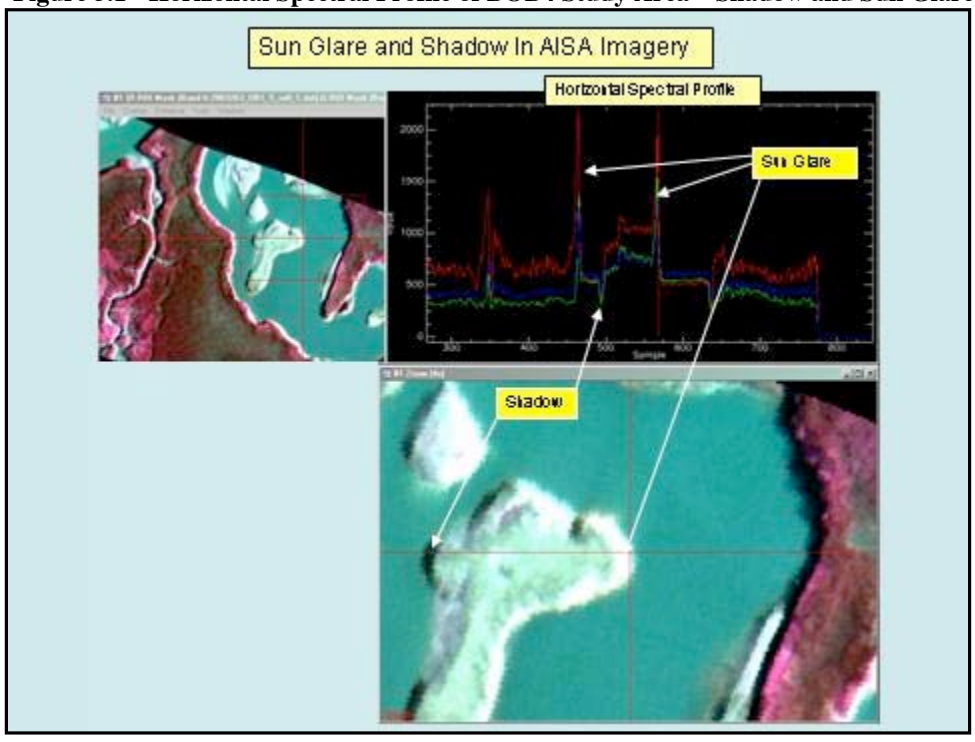

The horizontal spectral profile shows the x-axis of the cross-hairs which identify spectral characteristics that associate with certain types of earth materials. In this spectral profile, one can see to the right of the cross-hairs, water is visible in the image and a lower flat line is associated with the spectral characteristics. To the left of the cross-hairs the spectral profile dips significantly, showing areas that are in shadow. One can assume the material surrounding the sun glare or shadows are similar to the material within the shadow or sun glare but within an environment that exhibits a high degree of spectral variability, this is a large assumption. For this analysis, it was decided to err on the conservative side and mask out the affected areas.

Finally, an inherent limitation of ENVI and Leica Geosystem's ERDAS Imagine digital image processing software is the ability to statistically analyze spectral endmembers that are not image derived. One of the criterions imposed on selection of image endmembers is that they are statistically distinct and separate. In ENVI, the use of the Jeffries-Matusita Transformed Divergence test is usually applied to the ROI's that are to be used in mapping. There is not a mechanism to import library endmembers that were *in situ* derived to test if spectral endmembers from sample points in close proximity are spectrally distinct. This is especially critical when utilizing *in situ* endmembers because the same bench mark test that is applied to image endmembers cannot be applied to *in situ* endmember bundles to ensure they are distinct and separable in the context of the image to be analyzed. The digital image software are designed primarily to derive and map imagery using either image derived or *in situ* endmembers but there is a lack of tools that are specific to spectra per se for analysis and comparison of spectra.

6.0 Technology Transfer and Management Application

This is the first scientific investigation into the use of hyperspectral imagery and LiDAR data for mapping shellfish resources. This research will lead to an increasing number of scientists to recognize the great potential that hyperspectral and LiDAR remote sensing offer to the shellfish mapping community. Traditional broadband, medium-resolution sensors (Landsat ETM+, IRS-C, etc.) have largely failed in their ability to map and separate spectral differences in shellfish habitat. High-resolution digital frame cameras show promising results for producing quality imagery that can be photointerpreted to delineate oyster strata. When combined with hyperspectral and LiDAR technology, scientists have the ability to detect not only where different shellfish strata exist, but discriminate between shellfish beds and mud and detect subtle important health indicators which contribute to establishing better management strategies for these resources.

The development of these new mapping techniques that utilizes the unique spectral features found in oyster reefs will enhance coastal managers' access to up-to-date estuarine environmental data and information. The establishment of a web-based library of shellfish habitat spectral profiles and the identification of the ideal precise hyperspectral bands needed for matching these spectra will assist other resource managers in applying the same mapping techniques to map and monitor shellfish resources. These digital image processing routines have been transferred to other resource managers, through workshops, published articles, and internet dissemination in hopes of

using these tools to produce more accurate shellfish baseline maps that can then be used for designing better biological inventories and management strategies. It is hoped that the results from this study will be combined with tidal circulation models which have been developed in order to determine what effects, if any, water velocity and salinity regimes have on current shellfish distributions.

Hyperspectral applications are expanding rapidly as access to this type of data is becoming increasing available and more affordable. The Baruch Institute will continue to work with the NOAA Coastal Services Center and the NOAA National Estuarine Research Reserve System (NERRS) to further integrate the results of this research and to provide information to coastal managers as new mapping techniques become available. Resource managers will be able to apply these newly developed procedures using commercial off-the-shelf hyperspectral digital image processing software and research techniques and finding that have been published. New maps that are generated using these new techniques can be used to calculate commercial harvesting lease acreages and look for signs of over-harvesting, reef building, and monitoring oyster population changes.

In summary, technology transfer and management applications of this research include:

- The identification of optimal hyperspectral remote sensing bands for classifying shellfish habitat and a series of analytical digital image processing procedures for creating baseline maps of shellfish resources;
- Broad implications for new efforts in south-eastern states to assess status and trends of these critical EFH (essential fish habitats) and to direct new restoration/enhancement efforts;
- Rapid assessment techniques to monitor the status and thereby trends of oysters and associated habitats for coastal managers to be able to understand how environmental factors impact intertidal oyster reefs;
- Improvement of oyster reef management and restoration efforts in the southeastern U.S.
- Development of GIS-based predictive models generated through automated hyperspectral recognition for evaluating the productivity of various management strategies including shellfish restoration plans and identifying water quality problem areas.

7.0 Achievement and Dissemination

It is anticipated that the results of this work will be used to improve the effectiveness of coastal management measures by creating cost-effective and accurate baseline maps as well as improving evaluation/enhancement restoration efforts. Results are being made available to NERRS Managers and state and federal coastal agencies through web access, presentations and publications, and the NERRS Coastal Training Program. Information has been disseminated to user groups by:

- direct interactions with NERRS site Educational Coordinators;
- consultations with SCDNR's Office of Fisheries Management personnel;

- an Internet website linked to the web-based data and metadata dissemination server maintained by the NERR Centralized Data Management Office;
- oral and poster presentations at professional meetings; and
- peer-reviewed scientific publications.

The significant scientific contribution of this effort has been to the remote sensing and image processing communities through multiple presentations at national and international scientific meetings and a forthcoming peer-reviewed journal article. Equally important is the significance of this research to the marine and estuarine resource management and research communities. The research team has worked in partnership with both the staff of the North Inlet – Winyah Bay NERR, the ACE Basin NERR, NOAA's Coastal Services Center, and the South Carolina Sea Grant Consortium to host a Coastal Training Workshop. The focus of this workshop was to introduce local and state coastal resource managers and estuarine scientists to the potential role of remote sensing, image processing and data fusion for applied shellfish management. In addition, the workshop has been a mechanism to provide feedback to project researchers as to the perceived benefits and issues associated with the use of remote sensing for resource management. The workshop was held on June 27-28, 2003 in Georgetown, SC at the North Inlet – Winyah Bay NERR.

The private-sector participants in this research are GeoMetrics, Inc., a privately owned environmental engineering company with offices in Columbia and Myrtle Beach, SC., and The Nature Conservancy, the world's largest non-profit environmental company. Both are using the findings of this work to further promote the development of more accurate shellfish maps. Each organization has a long working relationship with academia and government entities and understands that resource managers need better and smarter tools for managing coastal resources. Both have successfully implemented advanced mapping technologies for protecting critical estuarine habitat and will continue to disseminate the results of this research through education and the training of environmental and conservation partners.

Selected Papers and Publications:

Vincent, J.S., D.E. Porter, L.D. Coen, D. Bushek and S. Schill. 2003. Using hyperspectral remote sensing to map and assess intertidal shellfish resources in the southeastern US. *Journal of Shellfish Research*. Vol. 2(1):359. Reviewed abstract

Proceedings and Posters Presented at Conferences:

Vincent, J., D. Porter, L. Coen, D. Bushek, and S. Schill, 2005, *"Using Automated Feature Extraction To Classify Shellfish Resources In South Carolina"* 2005 North Carolina Geographic Information Systems Conference, March 3-4, Winston-Salem, North Carolina

Vincent, J., D. Porter, L. Coen, D. Bushek, and S. Schill, 2004, *"Using Automated Feature Extraction for Mapping intertidal Shellfish RESOURCES Using Feature*

Analyst® for ArcGIS®," 2004 Feature Analyst User Conference, September 14-15, Missoula, Montana

Vincent, J., D. Porter, L. Coen, D. Bushek, and S. Schill, 2003, "*Assessing and Mapping Shellfish Resources Using Spectral Mixture Analysis,*" Proceedings from the 2003 *American Society of Photogrammetry and Remote Sensing Annual Convention and Exposition*, May 3-9, Anchorage, AK

Vincent, J.S., D.E. Porter, L.D. Coen, D. Bushek, S. Schill and J. Jensen. 2003. Mapping intertidal shellfish resources using remote sensing. 17th International Biennial ERF Conference. Seattle, WA. September 2003.

Vincent, J.S., D.E. Porter, L. Coen, D. Bushek and S. Schill. 2003. Using hyperspectral remote sensing to map and assess intertidal shellfish resources in the southeastern USA. National Shellfish Association Annual Meeting. New Orleans, LA. April 2003.

Vincent, J., D. Porter, L. Coen, D. Bushek, and S. Schill, 2003 *"Assessing and Mapping Shellfish Resources Using Hyperspectral Remote Sensing."*. Presented at the NOAA Coastal Services Center GEOTOOLS 03 Conference, Charleston South Carolina, 2003.

Vincent, J., D. Porter, L. Coen, D. Bushek, and S. Schill, 2002, *"Developing Hyperspectral Remote Sensing Methods to Rapidly Map and Assess Intertidal Shellfish Resources*," (Poster). Presented at the 6th International Conference on Shellfish Restoration. Charleston, South Carolina, 2002.

Vincent, J., D. Porter, L. Coen, D. Bushek, and S. Schill, 2003, *"Assessing and Mapping Intertidal Shellfish Resources Using Remote Sensing*," Presented at fall meeting of the Southeastern Estuary Research Society, Conway, South Carolina, 2002.

Vincent, J., Cutter, S. 2001*, "Dimensions of Social Vulnerability*," Presented at the Annual Conference of the Association of American Geographers, New York, New York, 2001.

Workshop Presentations:

"Deriving Shellfish Endmembers From Hyperspectral Imagery and Shellfish Spectral Variability," Workshop on Remote Sensing of Intertidal Shellfish Habitats, Sponsored by North Inlet-Winyah Bay and ACE Basin National Estuarine Reserve, June 27-28, 2003 Georgetown, SC

Honors and Awards:

Best presentation award at the fall meeting of the Southeastern Estuary Research Society, Conway, South Carolina, 2002.

8.0 Literature Cited

Adams, J. B., Smith, M. O., and Gillespie, A. R. 1993 Imaging spectroscopy: interpretation based on spectral mixture analysis. In *Remote Geochemical Analysis: Elemental and Mineralogical Composition.* Eds. Pieters, C. A. and Englert, P. A. Cambridge University Press, New York, New York. U.S.A.

Anderson, D. W., and Yianopoulos, G. M, 2001. Using GIS, GPS and Digital Phtography in Shellfish Management. *Proceedings of the 2nd Biennial Coastal GeoTools Conference*, Charleston, SC, January 8-11.

Bateson, A. and Curtiss. 1996. A method for manual endmember selection and spectral unmixing. *Remote Sensing of Environment.* 55:229-243.

Bezdek, J. C. 1981. *Pattern Recognition with Fuzzy Objective Function Algorithms*. Plenum, New York, New York U.S.A.

Bierwirth, P. N. 1990. Mineral mapping and vegetation removal via data-calibrated pixel unmixing, using multispectral images. *International Journal of Remote Sensing*. (11)11:1999-2017.

Breitburg, D., L.D. Coen, M.W. Luckenbach, R. Mann, M. Posey, and J.A. Wesson, 2000. Oyster reef restoration: convergence of harvest and conservation strategies. *Journal of Shellfish Research,* 19:371-377.

Chauvaud, S., C. Bouchon, and R. Maniere. 1998. Remote Sensing Techniques Adapted to High Resolution Mapping of Tropical Coastal Marine Ecosystems (coral reefs, seagrass beds and mangrove). *International Journal of Remote Sensing,* 19(18):3625-3639.

Chose, J.R. 1999. *Factors influencing bank erosion in tidal salt marshes of Murrells Inlet and North Inlet, South Carolina*. M.S. Thesis, University of Charleston and MUSC. 98 pp.

Coen, L.D., and A. Fischer, 2002. Managing the future of South Carolina's oysters: an experimental approach evaluating current harvesting practices and boat wake impacts. *Journal of Shellfish Research*, In press. Abstract from ICSR meeting, 2000 and in prep.

Coen, L. D. and Mark W. Luckenbach. 2000. Developing success criteria and goals for evaluating oyster reef restoration: Ecological function or resource exploitation? *Ecological Engineering* 15:323-343.

Coen, L.D., D.M. Knott, E.L. Wenner, N.H. Hadley, and A.H. Ringwood. 1999a. Intertidal oyster reef studies in South Carolina: Design, sampling and experimental focus for evaluating habitat value and function. Pp. 131-156, In: M.W. Luckenbach, R. Mann, J.A. Wesson (eds.), *Oyster Reef Habitat Restoration: A Synopsis and Synthesis of Approaches*. Virginia Institute of Marine Science Press, Gloucester Point, VA.

Coen, L.D., M.W. Luckenbach, and D.L. Breitburg. 1999b. The role of oyster reefs as essential fish habitat: a review of current knowledge and some new perspectives. Pp. 438-454, in L.R. Benaka, (ed.). Fish habitat: essential fish habitat and rehabilitation. *American Fisheries Society, Symposium 22*, Bethesda, MD.

Commito, John A. and Brian R. Rusignuolo. 2000. Structural complexity in mussel beds: the fractal geometry of surface topography. *Journal of Experimental Marine Biology and Ecology* 255:133-152.

Cracknell, A. P. 1999. Remote sensing techniques in estuaries and coastal zones – an update. *International Journal of Remote Sensing*. (19)3:485-496.

Dame, R. F. and P. D. Kenny, 1986, "Variability of *Spartina alterniflora* Primary Production in the Euhaline North Inlet Estuary," *Marine Ecology* 32:71-80.

Full, W. E., Ehrlich, R., and Klovan, J. E.. 1981. Extended Q model- objective definition of external endmembers in the analysis of mixtures. *Mathematical Geology*. 13:331-344.

Garci¬a-Haro, F.J., Gilabert, M. A., and Meli¬a, J. 1999. Extraction of endmembers from spectral mixtures. *Remote Sensing of Environment.* 68:237-253.

Grizzle, R.E. 1990. Distribution and abundance of (*Crassostrea virginica*) (Gmelin, 1791) (Eastern oyster) and (*Mercenaria* spp. (Quahogs) in a coastal lagoon. Journal of Shellfish Research 9:347-358.

Holden, H and E. Ledrew. 1999. Hyperspectral Identification of Coral Reef Features. *International Journal of Remote Sensing* 20(13):2545-2563.

Huete, A.R. 1986. Separation of soil-plant spectral mixtures by factor analysis. *Remote Sensing of Environment*. 19:237-251.

Jefferson, W. H., Michener, W.K., Karinshak, D. A., Anderson, W., and Porter, D. 1991. Developing GIS Data Layers for Estuarine Resource Management. *Proceedings, GIS/LIS 91*, pp. 331-341.

Johnson, P. E., Smith, M. O., and Adams, J. B. 1985. Quantitative analysis of planetary reflectance spectra with principle component analysis. In *Proceedings of 15th Lunar and Planetary Science Conference Pt. 2, Journal of Geophysical Research*. pp. C805-C810.

Kracker, Laura. 1999. The Geography of Fish: The Use of Remote Sensing and Spatial Analysis Tools in Fisheries Research. *The Professional Geographer* 51(3):440-450.

Lefsky, Michael A., Warren B. Cohen, Geoffrey G. Parker, and David J. Harding. 2002. LiDAR Remote Sensing for Ecosystem Studies. *BioScience* 52(1):19-30.

Lenihan, H.S., C.H. Peterson, 1998. How habitat degradation through fishery disturbance enhances impacts of hypoxia on oyster reefs. *Ecological Applications* 8,128-140.

Luckenbach, M.W., R. Mann and J.A. Wesson (eds.) 1999. *Oyster Reef Habitat Restoration. A Synopsis and Synthesis of Approaches*. Virginia Institute of Marine Science Press. Virginia Institute of Marine Science Press, Gloucester Point, VA, 358 pp.

Meyer,D.L., E.C. Townsend; 2000. Faunal utilization of created intertidal eastern oyster (*Crassostrea virginica*) reefs in the southeastern United States. *Estuaries* 23:33-45.

Meyer, D.L., E.C. Townsend; G.W. Thayer, 1997. Stabilization and erosion control value of oyster cultch for intertidal marsh. *Restoration Ecology* 5, 93-99.

Meyer,D.L., E.C. Townsend; P. L. Murphy, 1996. Final report for the project "*The Evaluation of restored wetlands and enhancement methods for existing restorations*". NMFS, SEFSC, Beaufort Lab, NC., 115 pp + append.

NOAA, 2003. Pilot Investigation of Remote Sensing for Intertidal Oyster Mapping in Coastal South Carolina: A Comparison of Methods, NOAA Coastal Services Center, NOAA/CSC/20514-PUB.

O'Brian, M. 2002. Feature Extraction with the VLS Feature Analyst System, White Paper for VLS, Inc.

Opitz, D., 1999. An Intelligent User Interface for Feature Extraction From Remotely Sensed Images. American Society for Photogrammetry and Remote Sensing, 171 – 177.

Pinn, E. H., M. R. Robertson, C. W. Shand and F. Armstrong. 1998. Broad-Scale Benthic Community Analysis in the Greater Minch Area (Scottish West Coast) Using Remote And Nondestructive Techniques. *International Journal of Remote Sensing* 19(16):3039-3054.

Sabol, D. E., Adams, J. B., and Smith, M.O. 1992. Quantitative subpixel spectral detection of targets in multispectral images. *Journal of Geophysical Research*. 97:2659-2672

Schmidt, L. 2000. Classifying oyster reefs using high-resolution multispectral imagery. Unpublished graduate research. University of South Carolina.

Shippert, P. 2002. Spotlight on Hyperspectral. *GeoSpatial Solutions*, 12(2): 40-45.

Smith, G. F.; D. G. Bruce, E. B. Roach. 2001. Remote Acoustic Habitat Assessment Techniques Used to Characterize the Quality and Extent of Oyster Bottom in the Chesapeake Bay. *Marine Geodesy* 24(3):171-189.

Strahler, A.H., Woodcock, C. E., and Smith, J. A. 1986. On the nature models in remote sensing. *Remote Sensing of Environment.* 20:121-139.

Tompkins, S., Mustard, J. F., Pieters, C. M., and Forsyth, D. W. 1997. Optimization of endmembers for spectral miture analysis. *Remote Sensing of Environment*. 59:472-489.

Turner, M. G., Gardner, R. H., and O'Neill, R. V. 2001. *Landscape ecology in theory and practice*. Springer-Verlag New York, Inc. New York, New York. U.S.A.

U.S.E.S., 1997, Urbanization and Southeastern Estuarine Systems (USES) Study Areas, http://www.baruch.sc.edu/usesweb/useshome.html.

Vernberg, F.J., W.B. Vernberg, D.E. Porter, G.T. Chandler, H.N. McKellar, D. Tufford, T. Siewicki, M. Fulton, G. Scott, D. Bushek and M. Wahl. 1999. Impact of coastal development on land-coastal waters. In *Land-Ocean Interactions: Managing Coastal Ecosystems.* E. Ozhan (ed.) MEDCOAST, Middle East Technical University, Ankara, Turkey. pp. 613-622.

Williams, S.L., and K.L. Heck, Jr., 2001. *Seagrass community ecology*, pp. 317-337, In: Marine community ecology, eds., M.D. Bertness, S.D. Gaines, and M.E.Hay, Sinauer Press, MA.

Cited in Garci¯a-Haro, F.J., Gilabert, M. A., and Meli¯a, J. 1999. Extraction of endmembers from spectral mixtures. *Remote Sensing of Environment.* 68:237-253.

9. Appendices

9.1 Secondary Spectral Signature Aggregation

***IN SITU* SPECTRORADIOMETIC DATA**
2ND LEVEL AGGREGATION

CLUSTER	DESCRIPTION	SAMPLE POINTS
	(BOB A-C are aggregated from BOB 1-3 sample sites)	
BOB A		BOB1_1 BOB1_2 BOB2_1 BOB3_1
BOB B		BOB1_3 BOB1_4 BOB2_2 BOB3_2
BOB C		BOB1_5 BOB1_6 BOB2_3 BOB2_4 BOB3_3 BOB3_4
	(BOB D- G are aggregated from BOB4 sample site)	
BOB D		BOB4_1 BOB4_2 BOB4_3 BOB4_4
BOB E		BOB4_7 BOB4_8 BOB4_11 BOB4_12 BOB4_17 BOB4_18 BOB4_20 BOB4_22
BOB F		BOB4_9 BOB4_10
BOB G		BOB4_5 BOB4_14 BOB4_15 BOB4_16 BOB4_19 BOB4_21

9.2 Field Sampling Collection Dates

Sampling Schedule for 2002-2003			
Month	**Date**	**Time**	**Height**
July, 2002	9th & 10th	1:34 PM / 2:21 PM	-.01 / -0.03
August, 2002	20th & 21st	12:29 PM	0.3
September	19th & 20th	12:10 PM / 12:55 PM	0.6 / 0.5
October	2nd & 3rd	10:35 AM/11:36 AM	0.6 / 0.4
November	14th & 15th	09:21 AM /10:13 AM	1.1 / 1
December	30th & 31st	10:39 AM/11:36 AM	0 / -0.2
January, 2003	29th & February 1st	11:54 AM / 2:17 PM	-0.6 / -.04
February	March 3rd & 4th	2:29 PM / 3:05 PM	-0.2 /-0.2
March	31st & April 1st	1:19 PM / 1:55 PM	0.0 / -.01
April	14th & 15th	12:58 PM / 1:47 PM	-0.3 / -0.7
May	Monday, 12th	12:36 PM	0.2
June	24th & 25th	10:55 AM / 11:40 AM	0.3/ 0.3
July	9th & 27th	10:34 AM / 1:20 PM	-.03 / 0.2

9.3 Shellfish Strata Classification

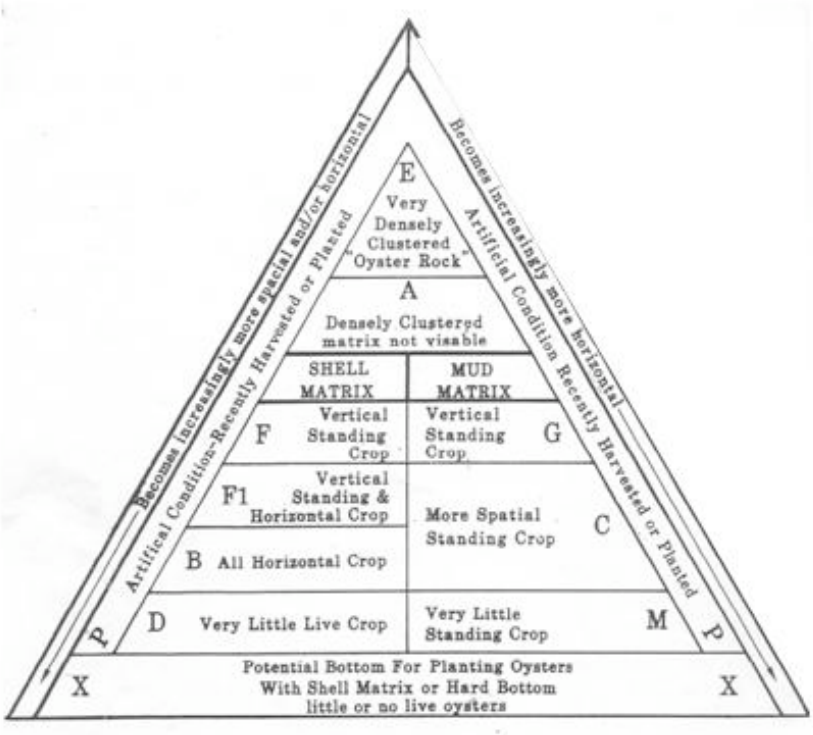

Strata A, SCDNR-OFM

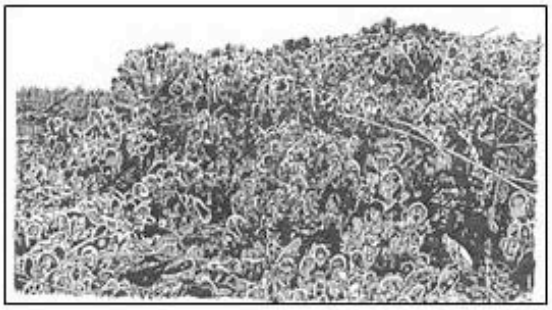

Strata E, SCDNR-OFM

Strata F, SCDNR-OFM

Strata F1, SCDNR-OFM

Strata G, SCDNR-OFM

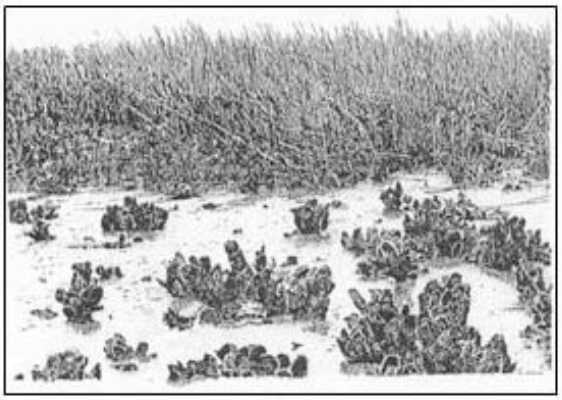

Strata C, SCDNR-OFM

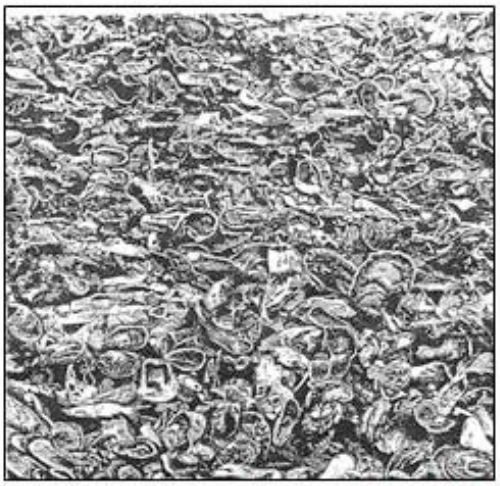

Strata B, SCDNR-OFM

Strata D, SCDNR-OFM